REFERENCE ONLY

UNIVERSITY OF LONDON THESIS

Degree PhD Year 2007 Name of Author BOSCHER, Nicolas

Atmospheric Pressure Chemical Vapour Deposition of Transition Metal Selenide Thin Films

A thesis presented to the University of London in partial fulfilment of the requirements for the Degree of Doctor of Philosophy.

Nicolas D. Boscher

Supervised by Dr. C. J. Carmalt and Professor Ivan P. Parkin

2007

I, Nicolas D. Boscher, confirm that the work presented in this thesis is my own. Where information has been derived from other sources, I confirm that this has been indicated in the thesis.

Abstract

This thesis investigates the formation of thin films of metal selenides *via* atmospheric pressure chemical vapour deposition (APCVD). The films and powders produced were characterised by SEM, EDAX/WDX, XPS, XRD, Raman, SQUID, reflectance and absorbance measurements.

The APCVD reaction of $TiCl_4$, $[V(NMe_2)_4]$ and $NbCl_5$ with $^tBu_2Se$ were respectively found to be a convenient route to stable and crystalline titanium, vanadium and niobium diselenide films. The use of VCl_4 and $VOCl_3$ showed that they were both found unsuitable for producing VSe_2 from the APCVD reaction with $^tBu_2Se$. Molybdenum and tungsten diselenide films were respectively synthesised using $MoCl_5$ and WCl_6 with Et_2Se. The WSe_2 films produced were highly hydrophobic with contact angles for water droplets in the range of 135 – 145°. Furthermore these surfaces were highly adherent for water droplets — that did not roll or slide even at a tilt angle of 90°. The deposition of tin monoselenide and tin diselenide films was achieved by the reaction of $SnCl_4$ with Et_2Se. The deposition temperature, flow rates and position on the substrate determined whether mixed SnSe - $SnSe_2$, pure SnSe or pure $SnSe_2$ thin films could be obtained.

The characterisation of the films and powders formed from the APCVD or gas phase reaction of CrO_2Cl_2 and Et_2Se confirmed the formation of an unknown solid solution of $Cr_2Se_{3-x}O_x$. $Cr_2Se_{3-x}O_x$ adopts the hexagonal Cr_2O_3 structure for a stoichiometry between Cr_2O_3 and $Cr_2Se_{0.2}O_{2.8}$, and the rhombohedral Cr_2Se_3 structure for a stoichiometry varying from $Cr_2Se_{0.3}O_{2.7}$ to $Cr_2Se_{2.15}O_{0.85}$. Magnetic studies showed that all the $Cr_2Se_{3-x}O_x$ compounds formed with the rhombohedral Cr_2Se_3 structure had an antiferromagnetic ordering with a Néel temperature lower than the expected one for Cr_2Se_3.

Acknowledgements

I wish to express my sincere thanks and appreciation to my supervisors, Dr. C. J. Carmalt and Professor Ivan Parkin, for their attention, guidance and support during my Ph.D. I would like to thank Dr. Christopher Blackman for constructive comments and suggestions. He has been abundantly helpful in numerous ways, including both my practical work and analysis. I would also like to thank Dr. Ana Garcia Prieto and Professor Quentin Pankurst for the SQUID analyses and related useful discussions. I am extremely grateful for the assistance of Kevin Reeves with EDAX, WDX and SEM, Dr. Robert Palgrave and Dr. Geoffrey Hyett for XPS, Steve Firth for Raman microscopy and TGA measurements and John Hill for mass spectrometry. In addition I would like to thank Dave Knapp, Joe Nolan and Dave Morphett for maintenance of my CVD rig.

I would like to express my gratitude to Dr. Siama Basharat, who has assisted me in the synthesis of my precursors and helped me to improve my English over these 3 years. In addition, special thanks are due to Caroline Knapp and Paolo Melgari for constructive comments and suggestions. It has been a pleasure to study at UCL during these 3 years. Dr. Jalpa Patel, Naima Narband, Dr. Uzma Qureshi, Dr. Clara Piccirillo, Stephen Potts, Dr. Jesus J. Gil-Tomas and Kristopher Page are cordially thanked for their friendship.

Most importantly I would like to thank my parents Pierrette and Daniel Boscher, my brothers Aurélien and Vincent Boscher, and Maryline Corbin. It is to them that I dedicate this work.

Table of Contents

List of Figures and Tables

Chapter 1
Introduction

1.1 Introduction

The aim of this work was to investigate the chemical vapour deposition (CVD) of a range of metal selenides. The films were synthesised using conventional atmospheric pressure (AP) CVD using a range of commercially available precursors. This introductory chapter describes the structure and properties of the materials which have been produced in thin film form in this work. Chapter 2 describes the experimental techniques and procedures adopted in this thesis. The deposition of metal selenide films is reported in Chapter 3, 4 and 5. The synthesis and characterisation of a new ternary phase chromium oxyselenide is reported in chapter 6. The final chapter discusses the main findings of this work.

1.2 Titanium Diselenide

1.2.1 Structure and Properties of $TiSe_2$

Titanium diselenide ($TiSe_2$) belongs to the family of layered transition metal dichalcogenides (MX_2; M = Ti, Zr, V, Nb, Ta, Mo, W, Sn...). These compounds adopt a CdI_2-type crystal structure, which consists of two-dimensional covalently bound layers of the type X-M-X (Figure 1.1). The layers are bound to each other by weak van der Waals interactions leading to a stacking sequence X-M-X-□-X-M-X with highly anisotropic properties. The interface between the X-M-X layers has vacant sites that allow intercalation of foreign atoms or molecules. Depending on how the molecular layers stack up, layered transition metal dichalcogenides can have many different crystallographic polytypes.

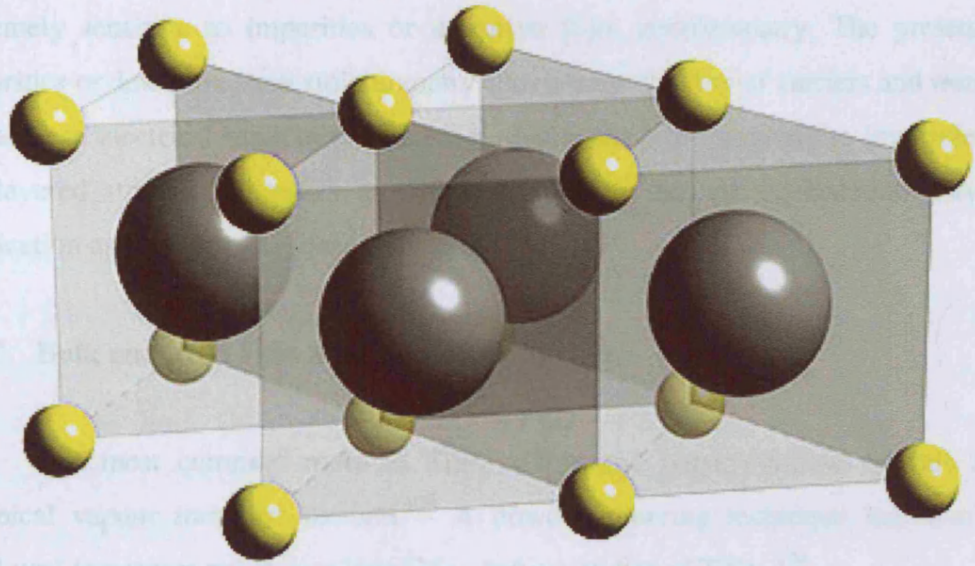

Figure 1.1 CdI_2-type crystal structure. Transition metal atoms are represented by grey spheres and chalcogenide atoms by yellow spheres.

There is only one known polytype of stoichiometric titanium diselenide (1T-$TiSe_2$), as in the Se-Ti-Se layers in $TiSe_2$ always stack without displacement. It crystallises in the P3ml space group with lattice parameters of a = 3.541 Å and c = 5.986 Å. $TiSe_2$ is known to exhibit a commensurate charge density wave (CDW) transition at T_c = 202 K, which is characteristics of low-dimensional materials. Low-temperature electron-diffraction studies have shown the second-order condensation at 202 K of a $2a_0$ x $2a_0$ x $2c_0$ superlattice. Titanium diselenide is semi-metallic at room temperature and turns into semiconductor after the CDW transitions at low temperature. Apart from $TiSe_2$, many forms of titanium selenide have been observed in the selenium-titanium system such as, Ti_5Se_8,[1] TiSe, Ti_8Se_9, Ti_3Se_4, Ti_2Se_3, Ti_5Se_8, $TiSe_3$ and Ti_2Se_9.[2,3]

1.2.2 Applications of $TiSe_2$

Due to its layered structure and the weak van der Waals forces between each layer, $TiSe_2$ films have been suggested as lubricating coatings. Transition metal dichalcogenides (MX_2) constitute an important class of inorganic layered compounds; they are good intercalation hosts - intercalation of gas molecules results in a change in

electrical resistance. Due to its small band overlap and low number of carriers, $TiSe_2$ is extremely sensitive to impurities or deviation from stoichiometry. The presence of impurities or deviation from stoichiometry adds a large number of carriers and results in a change in electrical resistance. Therefore, due to the high sensivity to impurities and the layered structure, titanium diselenide films with the right orientation may find application as hosts for gas sensors materials.

1.2.3 Bulk and Thin Film Synthesis of $TiSe_2$

The most common route to $TiSe_2$ single and polycrystalline crystals is the chemical vapour transport method.[136] A powder sintering technique has also been employed to prepare polycrystalline $TiSe_2$ and nanotubes of $TiSe_2$.[134]

Several reports detail the deposition of $TiSe_2$ thin films. Molecular beam epitaxy in a ultrahight vacuum (UHV) chamber has been reported to lead to $TiSe_2$ films.[4] Epitaxial growth of the films was achieved on Se-terminated GaAs (111)B substrates. However, the films produced were found to be titanium rich, with the titanium atoms filling the octahedral sites between the Se-Ti-Se sheets.

1.2.4 Chemical Vapour Deposition of $TiSe_2$ Thin Films

There is only one report of chemical vapour deposited titanium diselenide thin films.[5] McKarns et al. have prepared a series of potential $TiSe_2$ single-source precursors from titanium tetrachloride and dialkyl diselenides or dialkyl selenides. Treatment of $TiCl_4$ with dimethyl selenide and diethyl selenide in hexane at 0 °C led to the crystallisation of pure red air stable solids of $[TiCl_4(Se(CH_3)_2)_2]$ and $[TiCl_4(Se(CH_2CH_3)_2)_2]$ respectively. The CVD reaction of the dimethyl selenide adduct was found to be poorly reproducible and only produced titanium selenide films with a poor quality. However, the use of $[TiCl_4(Se(CH_2CH_3)_2)_2]$ as a single-source precursor produced a rose bronze coloured thin film of $TiSe_2$ at substrate temperatures of 500-600°C. However, after 30 days storage in air, the films became translucent with a very pale orange colour. These $TiSe_2$ films appeared to be unstable to ambient moisture and slowly degraded to give amorphous Ti-O-Se materials.

1.3 Vanadium Diselenide

1.3.1 Structure and Properties of VSe_2

Vanadium diselenide (VSe_2), which crystallises in the CdI_2-type, is known to be practically impossible to obtain in a perfectly stoichiometric form. It is known that in VSe_2 a small amount of vanadium atoms occupy the octahedral sites between the Se-V-Se sheets. Although the amount x of additional vanadium atoms can be very small, it seems almost impossible to produce a sample without interstitial intercalation of vanadium atoms. The exact formula is thus $V_{1+x}Se_2$ and the real stacking sequence is Se-V-Se-$V_{(x)}$-Se-V-Se.

1T-VSe_2 is the only polytype known for vanadium diselenide. It crystallises in the P3ml space group with lattice parameters of a = 3.35 Å and c = 6.12 Å. 1T-VSe_2 is metallic and is known to display remarkable properties, such as an incommensurate charge density wave (ICDW) phase (80 - 112 K) and a commensurate charge density wave (CCDW) phase of $4a_0 \times 4a_0$ (< 80 K). The lattice distortion of 1T-VSe_2 is not free of complications and near the transition temperature the 1T-VSe_2 shows sharp discontinuities in its electrical and magnetic properties. Various superstructures and structural transitions that are probably connected with the non-stoichiometry have also been reported. The phase diagram of the vanadium-selenium system has been fully investigated by Overbay and co-workers,[135] and apart from the paramagnetic metal VSe_2, many forms of vanadium selenide have been observed such as V_5Se_4, VSe, V_3Se_4, V_5Se_8 and V_2Se_9.

1.3.2 Applications of VSe_2

Like all transition metal dichalcogenides, 1T-VSe_2 has the ability to form intercalation complexes with foreign atoms or molecules incorporated between the VSe_2 layers. 1T-VSe_2 has already been widely studied as a host lattice in chemical and electrochemical intercalation reactions. Electrochemical cells using alkali-metal intercalated VSe_2 as a cathode material have been reported to show good reaction rates.

1.3.3 Bulk and Thin Films Synthesis of VSe_2

Despite a lot of studies that have focused on VSe_2 due to its CDW transition and intercalation properties, the synthesis of VSe_2 thin films or crystals is poorly described in the literature. This is probably due to the fact that stoichiometrically pure VSe_2 is difficult to prepare and the substance is usually metal-rich. VSe_2 single crystals have been prepared by chemical vapor transport, obtained from the elements in an evacuated quartz or silica ampoule heated at 800 °C for 7 days.[6,7] No chemical vapour deposition route to VSe_2 has been reported to date.

1.4 Niobium Diselenide

1.4.1 Structure and Properties of $NbSe_2$

Niobium diselenide ($NbSe_2$) has attracted attention due to its wide range of interesting physical properties, such as the presence of both a charge density wave transition and a superconducting transition. $NbSe_2$ has many different crystallographic polytypes, for example $2H_a$-, $2H_b$-, 3R-, $4H_a$-, $4H_{d1}$- and $4H_{d2}$-$NbSe_2$, the most common being $2H_b$-$NbSe_2$, which crystallises in the $P6_3/mmc$ space group with lattice parameters of a = 3.44 Å and c = 12.55 Å. Depending on the polytype, $NbSe_2$ shows different physical properties. The polytypes $2H_a$- or $2H_b$-, and $4H_a$-$NbSe_2$ are superconducting with a transition temperature of T_c = 7.2 K and T_c = 6.3 K, respectively.[8,9] A charge-density wave is present in all the $NbSe_2$ polytypes and an incommensurate charge-density wave is present in 2H-$NbSe_2$ below T_c = 33.3 K. In 2H-$NbSe_2$, the structure remains incommensurate through the superconducting transition.[10] Even though the phase diagram of the niobium – selenium system is not fully known, many forms of niobium selenide, apart from $NbSe_2$, have been observed, such as Nb_5Se_4, Nb_3Se_4, $NbSe_3$ and $NbSe_4$.[11,12,13]

1.4.2 Applications of $NbSe_2$

Similar to most of the transition-metal dichalcogenides, $NbSe_2$ has been cited for use as an electrical conductor and as a solid lubricant at high temperature. $NbSe_2$ is also

a good intercalation host. It has been shown that the growth of hydrogen intercalated in H_xNbSe_2 results in changes in the conductivity type from metallic to semiconducting.[14,15] Therefore, due to this sensitivity to intercalated molecules, niobium diselenide films may find application as hosts for sensor materials.

1.4.3 Bulk and Thin Films Synthesis of $NbSe_2$

The most common method to grow large single crystals of $NbSe_2$ is the chemical vapor transport (CVT)[11,16] of pre-reacted polycrystalline $NbSe_2$ with iodine as a transport agent. $NbSe_2$ thin films have been grown using van der Waals epitaxy (VDWE)[17] and pulsed-laser deposition (PLD).[18,19] No CVD route to $NbSe_2$ has been reported to date.

1.5 Molybdenum Diselenide

1.5.1 Structure and Properties of $MoSe_2$

Molybdenum diselenide ($MoSe_2$), which is isomorphous with MoS_2, crystallises in the $P6_3/mmc$ space group. Two polytypes are known for $MoSe_2$; hexagonal $2H_b$ and rhombohedral 3R. These polytypes have identical interlayer structures but different repeat distances between corresponding positions, with the $2H_b$ form having a doubling, and the 3R form a trebling, of the unit cell *c*-axis. The difference between each polytype is subtle and often mixtures of both can be found in the same crystal. The reported lattice parameters for $MoSe_2$ are a = 3.296 Å, c = 6.464 Å (× 2) for $2H_b$ and a = 3.296 Å, c = 6.464 Å (× 3) for 3R. Several other forms of molybdenum selenide have been observed, such as amorphous $MoSe_3$,[20] MoSe nanowires,[21] Chevrel phase (Mo_6Se_8),[22] as well as many cluster compounds such as Mo_9Se_{11}.[23]

1.5.2 Applications of $MoSe_2$

Semiconductor $MoSe_2$, has attracted attention because it is good at absorbing visible light, whilst being transparent at longer wavelengths.[24,25] Other applications include use as a solid-state lubricant, a cathode material for high energy density

batteries, and as an intercalation host.[24,26] It has also been reported as one of the most efficient systems for electrochemical solar energy conversion.[27,28,29] However, due to the difficulties in growing large single crystals, $MoSe_2$ has not yet found applications in electronic instruments or solar cells. Polycrystalline thin films of $MoSe_2$, though crystallographically less perfect than a single crystal, do show promising semiconductor properties.[24]

1.5.3 Bulk and Thin Films Synthesis of $MoSe_2$

The most common method of growing crystals of $MoSe_2$ is a solid-state reaction between stoichiometric amounts of elemental molybdenum and selenium. Molybdenum diselenide polycrystalline thin films have been grown by electrodeposition,[30,31] or pulsed electrodeposition, by chemical transport using bromine as a transport agent, and by molecular beam epitaxy,[32,33] but no CVD route to $MoSe_2$ has ever been reported.

1.6 Tungsten Diselenide

1.6.1 Structure and Properties of WSe_2

Tungsten diselenide (WSe_2) has been reported as a black or grey odourless material with good stability. As for many of the layered transition-metal dichalcogenides, WSe_2 crystallises with the CdI_2-type structure. Only one polytype of stoichiometric WSe_2 has been reported: 2H-WSe_2 (Figure 1.2). 2H-WSe_2 is a semiconductor with a band gap of 1.2 eV. Apart from WSe_2, only the X-ray amorphous WSe_3 has been reported.

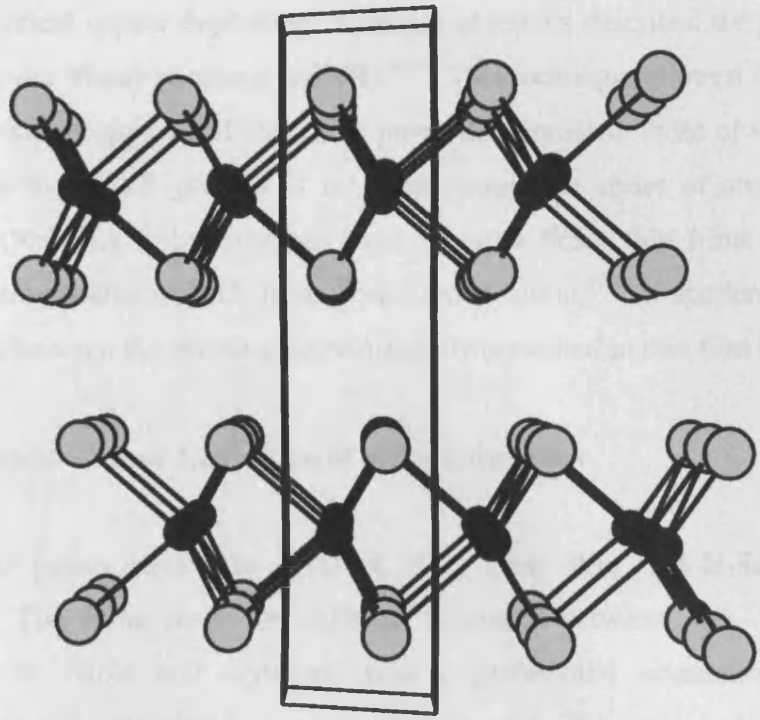

Figure 1.2 Crystal structure of 2H-WSe_2. Tungsten atoms are represented by black spheres and selenium atoms by grey spheres.

1.6.2 Applications of WSe_2

Due to its high optical absorption, high resistance against photocorrosion and its band gap near the optimum value (1.6 eV) for high efficiency photoelectrochemical solar cells, tungsten diselenide is an important material in photoelectrochemical conversion and photovoltaic solar energy conversion. Single crystals of WSe_2 have shown a good efficiency in photovoltaic application.[34] However, WSe_2 thin films are usually poorly photoconductive and unsuitable for photovoltaic application. The use of nickel coated substrate has allowed the growth of photoconductive WSe_2 thin films.[35] Tungsten diselenide has also been cited as a high temperature solid lubricant and as an electrode for rechargeable batteries.[137]

1.6.3 Bulk and Thin Films Synthesis of WSe_2

A number of routes to the growth of tungsten diselenide single crystals have been investigated. The most common being the chemical vapour transport (CVT) technique. Tungsten diselenide thin films can also be obtained by many processes,

including chemical vapour deposition. A couple of reports described the preparation of WSe_2 by van der Waals rheotaxy (vdWR).[36,37] This technique allowed textured WSe_2 films which exhibit optical and electronic properties similar to those of single crystals. Unfortunately the vdWR process is long and requires a series of steps using high temperature (950 °C). Other methods used to grow WSe_2 thin films include high-temperature selenisation of WO_3 films,[38] electrodeposition,[39,40] rf sputtering[41] and solid state reaction between the constituents sequentially deposited in thin film form.[42]

1.6.4 Chemical Vapour Deposition of WSe_2 Thin Films

A few papers report the CVD of WSe_2 using WF_6 and H_2Se as precursor agents.[43,44,45] The films grown on different substrates between 300 - 700 °C were reported to be stable and crytalline with a preferential orientation. A platelet microstructure with crystallites of 1 μm was observed. The optical absorption of the CVD film closely matched that of single-crystal WSe_2.

1.7 Tin Monoselenide

1.7.1 Structure and Properties of SnSe

Tin monoselenide (SnSe) is laminar IV-VI compound, which crystallises with an orthorhombic structure (space group Pbnm) and lattice parameters of a = 4.19 Å, b = 4.46 Å and c = 11.57 Å. Its structure (Figure 1.3) can be described as a distorted NaCl structure where tightly bound double layers of Sn and Se atoms are stacked along the c-axis. Each atom is strongly bonded to its three neighbours within its own double layer and only weakly bonded to its three more distant neighbours. The adjacent SnSe double layers are bound by weak van der Waals interactions, giving rise to an intermediate structure between three-dimensional and two-dimensional. This gives to SnSe anisotropic properties such as a lower hole mobility along the c-axis. SnSe is a p-type semiconductor with a narrow direct band gap close to 1.0 eV.[46] It melts at 860 °C and it has a phase transition from the orthorhombic to the cubic at 540 °C.

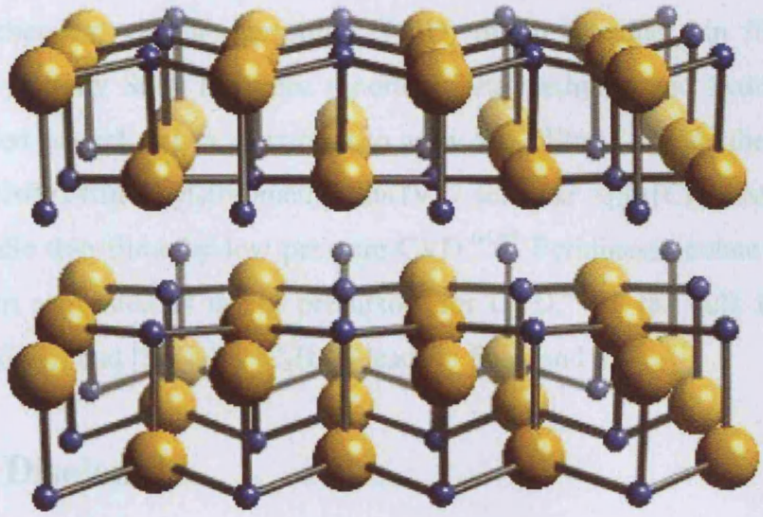

Figure 1.3 SnSe crystal structure. Tin atoms are represented by blue spheres and selenium atoms by yellow spheres.

1.7.2 Applications of SnSe

SnSe has attracted widespread attention due to its electronic and optical properties.[47,48,49] It is a promising candidate for solar cell applications.[50,51] SnSe has also been reported to have numerous applications in memory switching devices,[52] in holographic recording systems, as an anode material to improve lithium diffusivity or as a cathode in a lithium battery.[53]

1.7.3 Bulk and Thin Films Synthesis of SnSe

Bulk powders of tin monoselenide have been mostly synthesised by mixing and melting tin and selenium in the required stoichiometric ratio.[48] Other routes to bulk SnSe material include chemical vapor transport,[54] solvothermal process[55] and the Bridgman technique.[56] Thin film deposition of SnSe has been widely described in the literature. Chemical bath deposition,[57] electro-deposition,[58] solid state reaction,[59] solvothermal technique,[60] molecular beam epitaxy,[61] vacuum evaporation[48] and pulsed laser deposition[62] have been used to grow SnSe thin films.

1.7.4 Chemical Vapour Deposition of SnSe Thin Films

The chemical vapour deposition (CVD) of tin selenide thin films has been investigated yet only SnSe has been reported. Tetramethyltin and hydrogen selenide have been used as dual-source precursors to grow SnSe films.[63] While the single-source precursor bis(bis(trimethylsilyl)methyl)tin(IV) selenide $[Sn\{CH(SiMe_3)_2\}_2(\mu\text{-}Se)]_2$ deposited SnSe thin films by low pressure CVD.[64,65] Pyridineselenolate complexes of tin have been suggested as useful precursors for CVD,[66] as the bulk thermolysis of $[Sn(2\text{-}SeNC_5H_4)_2]$ and $[Sn(2\text{-}SeNC_5H_4)_4]$ leads to SnSe and $SnSe_2$.

1.8 Tin Diselenide

1.8.1 Structure and Properties of $SnSe_2$

Tin diselenide is an n-type semiconductor and its band gap is near 0.9 eV. $SnSe_2$ presents a hexagonal CdI_2-type crystal structure characterized by strongly bound two-dimensional Sn-Se-Sn sandwiches, which are weakly coupled by van der Waals forces. $SnSe_2$ has many different crystallographic polytypes the most common being the 2H and 18R.[67,68]

1.8.2 Applications of $SnSe_2$

Due to its electronic and optical properties,[48,69,70] $SnSe_2$ is a promising candidate for solar cell applications.[48,71]

1.8.3 Bulk and Thin Films Synthesis of $SnSe_2$

$SnSe_2$ crystals have been grown by vapour phase transport using iodine as a transporting medium.[72,73] However the iodine phase transport incorporates iodine, which affects the structure and properties of the $SnSe_2$ crystals. $SnSe_2$ polycrystalline thin films have been prepared using a conventional thermal evaporation of Sn and Se, or $SnSe_2$ powder[74] or van der Waals epitaxy.[75] Layered thin film p/n multi-junctions of SnSe and $SnSe_2$ have been produced by eutectic transformation.[76]

1.8.4 Chemical Vapour Deposition of $SnSe_2$ Thin Films

Pyridineselenolate complexes of tin have been suggested as possible precursors for the chemical vapour deposition of $SnSe_2$ thin films.[66] $[Sn(2\text{-}SeNC_5H_4)_2]$ and $[Sn(2\text{-}SeNC_5H_4)_4]$ are reported to sublime intact and decompose to $SnSe_2$ at elevated temperature. However, there is no report of the CVD of $SnSe_2$ thin films.

1.9 Chromium Sesquiselenide

1.9.1 Structure and Properties of Cr_2Se_3

Chromium sesquiselenide (Cr_2Se_3) has a rhombohedral-type superstructure,[77] which leads to complex antiferromagnetic arrangements below the Néel temperature T_N = 43 K. At transition temperature T_t = 38 K, Cr_2Se_3 exhibits an interesting order-order magnetic transition. These complex arrangements in the high-temperature antiferromagnetic AF (H) phase between T_N and T_t, and in the low-temperature antiferromagnetic AF (L) phase below T_t have been studied by neutron diffraction (Figure 1.4).[78,79,80]

A large number of phases have been reported in the chromium-selenium system and comprise Cr_5Se_8,[81] $CrSe_2$,[82,83] $CrSe_3$[84,85] and a series of compounds CrSe,[86,87] Cr_7Se_8,[88] Cr_5Se_6,[89] Cr_3Se_4,[90] and Cr_2Se_3 with the NiAs-type crystal structure, in which chromium vacancies are ordered.

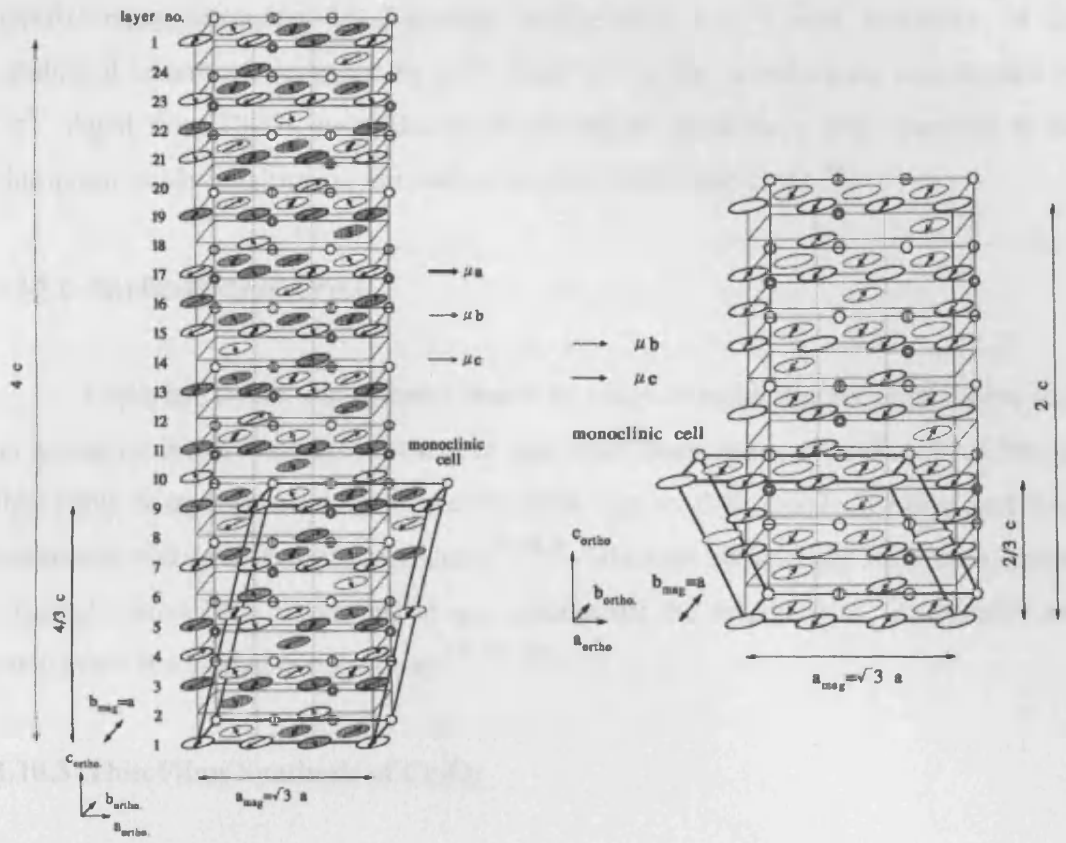

a) AF (L) phase **b) AF (H) phase**

Figure 1.4 Magnetic structure of Cr_2Se_3 in the low-temperature and high-temperature antiferromagnetic phases as drawn by Y. Adachi and co.[79] The arrows show the direction of magnetic moments of the Cr-atoms.

1.9.2 Bulk Synthesis of Cr_2Se_3

Cr_2Se_3 crystals have been grown by the solid reaction of elemental chromium and selenium in an evacuated quartz or silica tube state at 1000 - 1100 °C[79] and by the chemical vapour transport technique using iodine as a transport agent.[91,92]

1.10 Chromium Sesquioxide

1.10.1 Structure and Properties of Cr_2O_3

The insulating chromium sesquioxide (Cr_2O_3) is antiferromagnetic with a Néel temperature of 307.5 K.[93,94] It has the corundum structure, which consists of an

approximately hexagonal close-packed arrangement of O^{2-}, with two-thirds of the octahedral interstices occupied by Cr^{3+}. Each O^{2-} is thus tetrahedrally coordinated by Cr^{3+}. Apart from Cr_2O_3, many forms of chromium oxide have been observed in the chormium-oxide-titanium system such as Cr_3O_8, CrO_2[95] and Cr_2O_5.[96]

1.10.2 Applications of Cr_2O_3

Cr_2O_3 has drawn wide interest due to its range of technological applications such as a catalyst in polymerization reactions and solar thermal energy collectors. Chromia thin films have been used as protective films due to their good chemical and wear resistance, and low friction coefficient.[97,98,99] Titanium substituted chromium oxides, $Cr_{2-x}Ti_xO_3$ have been developed as gas sensors for the detection of combustible and toxic gases at elevated temperatures.[100,101,102]

1.10.3 Thin Films Synthesis of Cr_2O_3

Thin films of Cr_2O_3 have been prepared using by a large number of methods including sol-gel deposition,[103] sputtering,[104] oxidation of chromium metal,[105] electrochemical deposition,[106] dip coating[107] and chemical vapour deposition.

1.10.4 Chemical Vapour Deposition of Cr_2O_3 Thin Films

Cr_2O_3 thin films have been grown by metal-organic and atmospheric pressure CVD using a range of different precursors. The MOCVD of $Cr(acac)_3$,[108] Cr(III) (hexafluoroacetylacetonate), tris(2,2,6,6-tetra-methyl-3,5-heptanedionato) Cr(III)[97] and the APCVD of $Cr(CO)_6$[109,110] and chromyl chloride[111,112] have been reported to lead successfully to the formation of Cr_2O_3 thin films.

1.11 Chemical Vapour Deposition of Metal Selenides

1.11.1 Hydrogen Selenide

Hydrogen selenide (H_2Se) has been for a long time the most popular selenium precursor for the chemical vapour deposition of numerous selenides. It allows growth at temperatures as low as 300 °C or lower, and has already been successfully used to grow ZnSe,[113,114] $GeSe_y$,[115] Ga_2Se_3,[116,117] FeSe,[118] In_2Se_3[119] WSe_2 and $CuInSe_2$ thin films.[120] However, the use of H_2Se in a CVD process is not free of complications. Hydrogen selenide is a very toxic and hazardous gas, its time-weighted average threshold limit value (TLV-TWA) is 0.05 ppm. Moreover the CVD reaction of H_2Se, which is stored in high-pressure cylinder and often mixed with H_2, produces toxic and flammable products.[121] H_2Se starts to decompose above 100 °C and growth using H_2Se includes a serious problem, as a severe gas phase pre-reaction can occur with H_2Se, compromising the compositional uniformity and surface morphology of the films.

	Melting point	Boiling point	Appearance
H_2Se	-66 °C	-41 °C	Colourless gas

Table 1.1 Physical properties of hydrogen selenium.

1.11.2 Dialkylselenides

Dialkylselenides are employed primarily in the deposition of ZnSe based alloys[122,123] although they are also successfully used in other systems such as ZnMgSe,[124] CdSe,[125] $CuAlSe_2$,[126] $CuInGaSe_2$ [127] and Bi_2Se_3.[128,129] They are liquid at room temperature (Table 1.2) and are usually stored at atmospheric pressure in small stainless-steel bubblers, which involves less danger of widespread leakage compared with H_2Se. Because of this, metalorganic selenides including, dimethylselenide, diethylselenide, diisopropylselenide and ditertiarybutylselenide have attracted considerable attention as alternative candidates as selenium sources.

	Boiling point	Appearance	V.P. equation
$Se(CH_3)_2$	57 °C	Clear colourless liquid	$Log_{10}P = 9.872-2224/T(K)$
$Se(C_2H_5)_2$	108 °C	Pale yellow liquid	$Log_{10}P = 8.20-2020/T(K)$
$Se(i-C_3H_7)_2$	-	Pale yellow liquid	$Log_{10}P = 7.88-2074/T(K)$
$Se(t-C_4H_9)_2$	164 °C	Clear colourless liquid	$Log_{10}P = 7.87-2040/T(K)$

Table 1.2 Physical properties of some dialkylselenides.

Due to the thermal stability of dimethylselenide and diethylselenide, high growth temperatures are required (> 450 °C). In contrast, the relatively low thermal stability of the diisopropylselenide, and the low thermal stability ditertiarybutylselenide (onset of decomposition at 150 °C) allow access to very high quality layers at growth temperatures as low as 330 °C.

1.11.3 Dialkyldiselenides

Most of the dialkyldiselenides (Table 1.3) such as dimethyldiselenide and diethyldiselenide have been employed in the deposition of ZnSe based materials.[130,131] However, they are mainly used in a hydrogen radical enhanced CVD process and their use in common CVD processes is limited.

	Melting point	Boiling point	Appearance
$Se_2(CH_3)_2$	-	156 °C	Clear colourless liquid
$Se_2(C_2H_5)_2$	-	186 °C	Pale yellow liquid
$Se_2(C_6H_5)_2$	60 °C	-	Yellow powder

Table 1.3 Physical properties of some dialkyldiselenides.

1.11.4 Selenols

Tertiarybutylselenol has also been successfully used for the metalorganic vapour phase epitaxy growth of high quality ZnSe layers.[132] Growth temperature as low as 280 °C were reported using this volatile selenol. A few other volatile selenols (Table 1.4),

such as methylselenol or ethylselenol, could also be suitable precursors for the CVD of transition-metal selenides, but their growth temperature is usually higher than with the tertiarybutylselenol. A growth temperature of 400 °C is typically required for the MOVPE growth of ZnSe using methylselenol or ethylselenol.

	Boiling point	Appearance	V.P. equation
$(CH_3)SeH$	12 °C	Clear colourless liquid	$Log_{10}P = 6.95-1060/(T(K)+38)$
$(C_2H_5)SeH$	54 °C	Clear colourless liquid	-
$(t\text{-}C_4H_9)SeH$	-	Clear colourless liquid	-

Table 1.4 Physical properties of some selenols.

1.11.5 Selenium halides

The selenium halides (Table 1.5) could possibly be used for the growth of thin film of selenides by CVD. Germanium selenide thin films have already been synthesised by plasma enhanced CVD using Se_2Cl_2 and $GeCl_4$ in presence of H_2.[133]

	Melting point	Boiling point	Appearance
$SeCl_4$	205 °C	288 °C	White-yellow crystals
Se_2Cl_2	-85 °C	130 °C	Yellow-brown liquid

Table 1.5 Physical properties of some selenium halides.

1.12 Conclusion

Despite the attention drawn by the metal selenides, only little has been done about the chemical vapour deposition of transition metal diselenides films. In this chapter, the structure and properties of these materials have been summarised. In the next chapter the experimental and analytical methodology is outlined. The APCVD of group IV, V (Ti, V, Nb) and VI (Mo, W) diselenides are described in chapter 3 and 4. Chapter 5 investigates the deposition of tin selenides thin films, while chapter 6 reports the synthesis and characterisation of a new ternary phase chromium oxyselenide.

1.13 References

[1] M. He, A. Simon, V. Duppel, *Z. Anorg. Allg. Chem.*, **2004**, *630*, 535.

[2] T. Hirota, Y. Ueda, K. Kosuge, *Mater. Res. Bull.*, **1988**, *23*, 1641.

[3] J. L. Murray, *Bull. Alloy Phase Diag.*, **1986**, *7*, 163.

[4] H. Nishikawa, T. Shimada, A. Koma, *J. Vac. Sci, Technol. A*, **1996**, *14*, 2893.

[5] P. J. McKarns, T. S. Lewkebandara, G. P. A. Yap, L. M. Liable-sands, A. L. Rheingold, C. H. Winter, *Inorg. Chem.*, **1998**, *37*, 418.

[6] R. Guzman, P. Lavela, J. Morales, J. L. Tirado, *J. Appl. Electrochem.*, **1997**, *27*, 1207.

[7] F. J. Disalvo, J. V. Waszczak, *Phys. Rev. B*, **1981**, *23*, 457.

[8] D. H. Galvan, S. Li, W. M. Yuhasz, J. H. Kim, M. B. Maple, E. Adem, *Phys. C*, **2003**, *398*, 147.

[9] T. Shimada, H. Nishikawa, A. Koma, Y. Furukawa, E. Arakawa, K. Takeshita, T. Matsushita, *Surf. Sci.*, **1996**, *369*, 379.

[10] B. M. Murphy, J. Stettner, M. Traving, M. Sprung, I. Grotkopp, M. Muller, C. S. Oglesby, M. Tolan, W. Press, *Phys. B*, **2003**, *336*, 103.

[11] C. H. Du, W. J. Lin, Y. Su, B. K. Tanner, P. D. Hatton, D. Casa, B. Keimer, J. P. Hill, C. S. Oglesby, H. Hohl, *J. Phys.: Condens. Matter*, **2000**, *12*, 5361.

[12] H. Haraldsen, *Angew. Chem. Int. Ed. Engl.*, **1966**, *5*, 51.

[13] W. W. Fuller, T. M. Tritt, H. A. Hoff, *Phys. Rev. B*, **1990**, *41*, 1671.

[14] L. M. Kulikov, A. A. Semjonov-Kobzar, M. M. Antonova, A. A. Chechovsky, L. G. Akselrud, R. V. Skolozdra, D. Fruchart, J. L. Soubeyroux, *J. Alloys Compd.*, **1996**, *244*, 11.

[15] V. A. Makara, N. G. Babich, N. I. Zakharenko, V. A. Pasechny, O. V. Rudenko, V. F. Surzhko, L. M. Kulikov, A. A. Semenov-Kobzar, M. M. Antonova, A. A. Chekhovsky, L. G. Askel-Rud, L. P. Romaka, *Int. J. Hydrogen Energy*, **1997**, *2*, 233.

[16] R. Vaidya, M. Dave, S. G. Patel, A. R. Jani, *Indian J. Phys.*, **2005**, *79*, 85.

[17] A. Koma, *Kotai Butsuri*, **1986**, *21*, 620.

[18] H. Lee, M. Kanai, T. Kawai, *Thin Solid Films*, **1996**, *277*, 98.

[19] A. E. Day, J. S. Zabinski, *AIP Conf. Proc.*, **1993**, *288*, 601.

[20] S. P. Cramer, K. S. Liang, A. J. Jacobson, C. H. Chang, R. R. Chianelli, *Inorg. Chem.*, **1984**, *23*, 1215.

[21] F. J. Ribeiro, D. J .Roundy, M. L. Cohen, *Phys. Rev. B*, **2002**, *65*, 153401.

[22] M. Sergent, R. Chevrel, *J. Solid State Chem.*, **1973**, *6*, 433.

[23] A. Gruettner, K. Yvon, R. Chevrel, M. Potel, M. Sergent, B. Seeber, *Acta Crystallogr. B*, **1979**, *B35*, 285.

[24] W. Sienicki, *Mater. Chem. Phys.*, **2003**, *68*, 119.

[25] T. J. S. Anand, C. Sanjeeviraja, M. Jayachandran, *Vacuum*, **2001**, *60*, 431.

[26] M. Kristl, M. Drofenik, *Inorg. Chem. Commun.*, **2003**, *6*, 68.

[27] H. Tributsch, *J. Electrochem. Soc.*, **1978**, *125*, 1086.

[28] S. Chandra, D. P. Singh, P. C. Srivastava, S. N. Sahu, *J. Phys D: Appl. Phys.*, **1984**, *17*, 2125.

[29] J. Morales, J. Santos, J. L. Tirado, *Solid State Ionics*, **1996**, *83*, 57.

[30] S. M. Delphine, M. Jayachandran, C. Sanjeeviraja, *Mater. Res. Bull.*, **2005** *40*, 135.

[31] S. Chandra, S. N. Sahu, *J. Phys D: Appl. Phys.*, **1984**, *17*, 2115.

[32] T. J. Sahaya Anand, C.Sanjeeviraja, M. Jayachandran, *Vacuum*, **2001**, *60*, 431.

[33] C. Hammond, A. Back, M. Lawrence, K. Nebesny, P. Lee, R. Schlaf, N. R. Amstrong, *J. Vac. Sci. Technol. A*, **1995**, *13*, 1768.

[34 G. Prasad, O. N. Srivasta, *J. Phys. D: Appl. Phys.*, **1988**, *21*, 1028.

[35] N. Guetari, J. Ouerfelli, J. C. Bernede, A. Khelil, J. Pouzet, A. Conan, *Mater. Chem. Phys.*, **1998**, *52*, 83.

[36] T. Tsirlina, S. Cohen, H. Cohen, L. Sapir, M. Peisach, R. Tenne, A. Matthaeus, S. Tiefenbacher, W. Jaegermann, E. A. Ponomarev, C. Levy-Clement, *Sol. Energy Mater. Sol. Cells*, **1996**, *44*, 457.

[37] R. Tenne, E. Galun, A. Ennaoui, S. Fiechter, K. Ellmer, M. Kunst, C. Koelzow, C. Pettenkofer, S. Tiefenbacher, R. Scheer, H. Jungblt, W. Jaegermann, *Thin Solids Films*, **1996**, *272*, 38.

[38] G. Salitra, G. Hodes, E. Klein, R. Tenne, *Thin Solids Films*, **1994**, *245*, 180.

[39] S. M. Delphine, M. Jayachandran, C. Sanjeeviraja, *Mater. Chem. Phys.*, **2003**, *81*, 78.

[40] J. Jebaraj Devadasan, C. Sanjeeviraja, M. Jayachandran, *Mater. Chem. Phys.*, **2002**, *77*, 397.

[41] J. Pouzet, J. C. Bernede, A. Khellil, H. Essaidi, S. Benhida, *Thin Solids Films*, **1992**, *208*, 252.

[42] N. Guettari, J. Ouerfelli, J. C. Bernede, A. Khelil, J. Pouzet, A. Conan, *Mater. Chem. Phys.*, **1998**, *52*, 83.

[43] D. E. Miller, *Energy Res. Abstr.*, 1986, 11, 29.

[44] R. Bourezg, G. Couturier, J. Salardenne, *J. Chim. Phys. Physico-Chim Biol.*, **1991**, *88*, 2021.

[45] W.Sienicki, *Polish J. of Chem.*, **1992**, *66*, 1139.

[46] Z. Nabi, A. Kellou, S. Méçabih, A. Khalfi, N. Benosman, *Mater. Sci. Eng. B,* **2003**, *98*, 104.

[47] Y. Bertrand, G. Leveque, C. Raisin, F. Levy, *J. Phys. C: Solid St. Phys.*, **1979**, *12*, 2907.

[48] D. Pathinettam Padiyan, A. Marikani, K.R. Murali, *Cryst. Res. Technol.*, **2000**, *35*, 949.

[49] N. Ganesan, V. Sivaramakrishnan, *Semicond. Sci. Technol.*, **1987**, *2*, 519.

[50] W. Jaegermann, C. Pettenkofer, O. Lang, R. Schlaf, S. Tiefenbacher, Y. Tomm, *First WCPEC*, **1994**.

[51] M. R. Aguiar, R. Caram, M. F. Oliveira, C. S. Kiminami, *J. Mat. Sci.*, **1999**, *34*, 4607.

[52] Z. Zainal, S. Nagalingam, A. Kassim, M. Z. Hussein, W. M. M. Yunus, *Sol. Energy Mater. Sol. Cells*, **2004**, *81* 261.

[53] M. Z. Xue, J. Yao, S. C. Cheng, Z. W. Fu, *J. Electrochem. Soc.*, **2006**, *153*, 270.

[54] A. Agarwal, M. N. Vashi, D. Lakshminarayana, N. M. Batra, *J. Mater. Sci.: Mater. Electro.*, **2000**, *11*, 67.

[55] B. Li, Y. Xie, J. Huang, Y. Qian, *Inorg. Chem.*, **2000**, *39*, 2062.

[56] A. M. Elkorashy, *J. Phys. III*, **1991**, *1*, 1169.

[57] Z. Zainal, N. Saravanan, K. Anuar, M.Z. Hussein, W.M.M. Yunus, *Mater. Sci. Eng., B: Solid-State Mater. Adv. Tech.*, **2004**, *B107*, 181.

[58] B. Subramanian, T. Mahalingam, C. Sanjeeviraja, M. Jayachandran and M. J. Chockalingam, *Thin Solid Films*, **1999**, *357*, 119.

[59] D. Tran Quan, *Thin Solid Films*, **1987**, *149*, 197.

[60] Y. Xie, H. Su, B. Li, Y. Qian, *Mater. Res. Bull.*, **2000**, *35*, 459.

[61] I. R. Nuriev, E. Y. Salaev, A. K. Sharifova, *Ser. Fiz.-Tekh. Mat. Nauk.*, **1982**, *3*, 91.

[62] R. Teghil, A. Santagata, V. Marotta, S. Orlando, G. Pizzella, A. Giardini-Guidoni, A. Mele, *Appl. Surf. Sci.*, **1995**, *90*, 505.

[63] H. M. Manasevit, W. I. J. Simpson, *J. Electrochem. Soc.*, **1975**, *122*, 444.

[64] I. S. Chuprakov, K. H. Dahmen, J. J. Schneider, J. Hagen, *Chem. Mater.*, **1998**, *10*, 3467.

[65] I. S. Chuprakov, K. H. Dahmen, *J. Phys. IV: Proc.*, **1999**, *9*, 313.

[66] Y. Cheng, T. J. Emge, J. G. Brennan, *Inorg. Chem.*, **1996**, *35*, 342.

[67] B. Palosz, S. Gierlotka, F. Levy, *Acta Cryst.*, **1985**, *C41*, 1404.

[68] B. Palosz, E. Salje, *J. Appl. Cryst.*, **1989**, *22*, 622.

[69] Y. Bertrand, G. Leveque, C. Raisin, F. Levy, *J. Phys. C: Solid St. Phys.*, **1979**, *12*, 2907.

[70] N. Ganesan, V. Sivaramakrishnan, *Semicond. Sci. Technol.*, **1987**, *2*, 519.

[71] M. R. Aguiar, R. Caram, M. F. Oliveira, C. S. Kiminami, *J. Mat. Sci.*, **1999**, *34*, 4607.

[72] G. Domingo, R. S. Itoga, C. R. Kannewurf, *Phys. Rev.*, **1966**, *143*.

[73] J. George, C. Valsala-Kumari, *Cryst. Res. Technol.*, **1986**, *21*, 273.

[74] D. A. Hady, H. Soliman, A. El-Shazly, M. S. Mahmoud, *Vacuum*, **1999**, 52, 375.

[75] R. Schlaf, N. R. Armstrong, B. A. Parkinson, C. Pettenkofer, W. Jaegermann, *Surf. Sci.*, **1997**, *385*, 1.

[76] M. F. De Oliveira, R. Caram, C. S. Kiminami, *J. Alloys Compd.*, **2004**, *375*, 142.

[77] M. Chevreton, E. F. Bertaut, S. Brunie, *Bull. Soc. Sci. Bretagne*, **1964**, *39*, 77.

[78] Y. Adachi, M. Yuzuri, T. Kaneko, S. Abe, H. Yoshida, *J. Phys. Soc. Jap.*, **1994**, *63*, 369.

[79] Y. Adachi, M. Ohashi, T. Kaneko, M. Yuzuri, Y. Yamaguchi, S. Funahashi, Y. Morii, *J. Phys. Soc. Jap.*, **1994**, *63*, 1548.

[80] S. Ohta, Y. Adachi, T. Kaneko, M. Yuzuri, H. Yoshida, *J. Phys. Soc. Jap.*, **1994**, *6*, 2225.

[81] A. W. Sleight, T. A. Bither, *Inorg. Chem.*, **1969**, *8*, 566.

[82] C. M. Fang, C. F. van Bruggen, R. A. de Groot, G. A. Wiegers, C. Haas, *J. Phys.: Condens. Matt.*, **1997**, *9*, 10173.

[83] Y. Yoshida, K. Motizuki, *J. Phys. Soc. Jap.*,**1982**, *51*, 2107.

[84] S. J. Hibble, D. A. Rice, M. J. Almond, K. A. Hassan Mohammad, S. P. Pearse, J. R. Sagar, *J. Mater. Chem.*, **1992**, *2*, 1237.

[85] S. J. Hibble, R. I. Walton, D. M. Pickup, J. Chem. Soc., Dalton Trans.: *Inorg. Chem.*, **1996**, *11*, 2245.

[86] M. Koyama, N. Happo, M. Tamura, J. Harada, T. Mihara, A. Furuta, M. Nakatake, H. Sato, M. Taniguchi, Y. Ueda, *J. Electron Spectrosc. Relat. Phenom.*, **1996**, *78*, 83.

[87] L.M. Corliss, N. Elliott, J.M. Hastings, R.L. Sass, *Phys. Rev.*, **1961**, *5*, 1402.

[88] T. Kaneko, J. Sugawara, K. Kamigaki, S. Abe, H. Yoshida, *J. Appl. Phys.*, **1982**, *53*, 2223.

[89] H. Sato, M. Koyama, K. Takada, H. Okuda, K. Shimada, Y. Ueda, J. Ghijsen, M. Taniguchi, *J. Electron Spectrosc. Relat. Phenom.*, **1998**, *88*, 333.

[90] M. Behrens, R. Kiebach, W. Bensch, D. Haeussler, W. Jaeger, *Inorg. Chem.*, **2006**, *45*, 2704.

[91] K. Sato, Y. Aman, M. Hirai, M. Fujisawa, *J. Phys. Soc. Jpn.*, **1990**, *59*, 435.

[92] H. D. Lutz, K. H. Bertram, M. Sreckovic, W. Molls, *Z. Naturforsch.*, **1973**, *28*, 685.

[93] T. R. McGuire, E. J. Scott, F. H. Grannis, *Phys. Rev.*, **1956**, *102*, 1000.

[94] G. W. Pratt, P. T. Hailey, *Phys. Rev.*, **1963**, *131*, 1923.

[95] M. N. Iliev, A. P. Litvinchuk, H. G. Lee, C. W. Chu, A. Barry, J. M. D. Coey, *Phys. Stat. Sol.*, **1999**, *215*, 643.

[96] J. E. Maslar, W. S. Hurst, T. A. Vanderah, I. Levin, *J. Raman Spectrosc.*, **2001**, *32*, 201.

[97] G. Carta, M. Natali, G. Rossetto, P. Zanella, G. Salmaso, S. Restello, V. Rigato, S. Kaciulis, A. Mezzi, *Chem. Vap. Dep.*, **2005**, *11*, 375.

[98] K. P. Lillerud, P. Kofstad, *J. Electrochem. Soc.*, **1980**, *127*, 2397.

[99] P. Kofstad, K. P. Lillerud, *J. Electrochem. Soc.*, **1980**, *127*, 2410.

[100] P. T. Moseley, D. E. Williams, *Sens. Actuators*, 1990, *B1*, 113.

[101] G. S. Henshaw, D. H. Dawson, D.E. Williams, *J. Mater. Chem.*, **1995**, *5*, 1791.

[102] D. E. Williams, Sens. *Actuators*, **1999**, *B57*, 1.

[103] S. Mukherjee, A. K. Pal, S. Bhattacharya, *J. Phys.: Condens. Matter*, **2005**, *17*, 3385.

[104] R. C. Ku, W. L. Winterbottom, *Thin Solid Films*, **1985**, *127*, 241.

[105] R. E. Kirby, E. L. Garwin, F. K. King, A. R. Nyaiesh, *J. Appl. Phys.*, **1987**, *62*, 1400.

[106] G. P. Halada, C. R. Clayton, *J. Electrochem. Soc.*, **1991**, *138*, 2921.

[107] T. S. Sudarshan, J. D. Cross, *IEEE Trans. Elect. Insul.*, **1976**, *EI-11*, 32.

[108] S. Chevalier, G. Bonnet, J. P. Larpin, *Appl. Surf. Sci.*, **2000**, *167*, 125.

[109] V. M. Bermudez, W. J. Desisto, *J. Vac. Sci. Technol. A*, **2001**, *19*, 576.

[110] T. Ivanova, M. Surtchev, K. Gesheva, *Phys. Stat. Sol.*, **2001**, *184*, 507.

[111] W. J. Desisto, P. R. Broussard, T. F. Ambrose, B. E. Nadgorny, M. S. Osofsky, *Appl. Phys. Lett.*, **2000**, *76*, 3789.

[112] Y. N. Cho, W. J. Desisto, *Chem. Vap. Dep.*, **2003**, *9*, 121.

[113] P. Miles, *Proc. Symp. Mater. Sci. Aspects Thin Film Syst. Sol. Energy Convers.*, **1974**, 402.

[114] S. Sritharan, K. Jones, K. M. Motyl, *J. Cryst. Growth*, **1984**, *68*, 656.

[115] B. Cros, Y. Brocheton, M. Ribes, *Mater. Manuf. Processes*, **1990**, *5*, 411.

[116] M. von der Emde, D. R. T. Zahn, T. Ng, N. Maung, G. H. Fan, I. B. Poole, J. O. Williams, A. C. Wright, *Appl. Surf. Sci.*, **1996**, *104*, 575.

[117] N. Maung, G. Fan, T. Tg, J. O. Williams, A. C. Wright, *J. Mater. Chem.*, **1999**, *9*, 2489.

[118] X. J. Wu, Z. Z. Zhang, J. Y. Zhang, Z. G. Ju, D. Z. Shen, B. H. Li, C. X. Shan, Y. M. Lu, *J. Cryst. Growth*, **2007**, *300*, 483.

[119] K. J. Chang, S. M. Lahn, J. Y. Chang, *Appl. Phys. Lett.*, **2006**, *89*, 182118.

[120] S. Duchemin, M. C. Artaud, F. Ouchen, J. Bougnot, A. M. Pougnet, *J. Mater. Sci. - Mater. Electron.*, **1996**, *7*, 201.

[121] M. C. Artaud, F. Ouchen, L. Martin, S. Duchemin, *Thin Solid Films*, **1998**, *324*, 115.

[122] H. Mitsuhashi, I. Mitsuishi, M. Mizuta, H Kukimoto, *Jpn. J. Appl. Phys.*, **1985**, *24*, 578.

[123] W. S. Kuhn, A. Naumov, H. Stanzl, S. Bauer, K. Wolf, H. P. Wagner, W. Gebhardt, U. W. Pohl, A. Krost, W. Richter, U. Dumichen, K. H. Thiele, *J. Cryst. Growth*, **1992**, *123*, 605.

[124] P. Prete, N. Lovergine, L. Tapfer, M. Berti, S. K. Sinsha, A. M, Mancini, *J. Cryst. Growth*, **2000**, *221*, 410.

[125] U. W. Pohl, R. Engelhardt, V. Turck, D. Bimberg, *J. Cryst. Growth*, **1998**, *195*, 569.

[126] S. Chichibu, S. Shirakata, R. Sudo, M. Uchida, Y. Harada, S. Matsumoto, H. Higuchi, S. Isomura, *Jpn. J. Appl. Phys.*, **1993**, *32*, 139.

[127] M. Sugiyama, F. B. Dejene, A. Kinoshita, M. Fukaya, Y. Maru, T. Nakagawa, H. Nakanishi, V. Alberts, S. F. Chichibu, *J. Cryst. Growth*, **2006**, *294*, 214.

[128] A. Al Bayaz, A. Giani, M. A. Khalfioui, A. Foucaran, F. Pascal-Delannoy, A. Boyer, *J. Cryst. Growth*, **2003**, *258*, 135.

[129] A. Al Bayaz, A. Giani, A. Foucaran, F. Pascal-Delannoy, A. Boyer, *Thin Solid Films*, **2003**, *441*, 1.

[130] J. Gotoh, H. Shirai, J. Hanna, I. Shimizu, *Jpn. J. Appl. Hys.*, **1991**, *30*, L1241.

[131] H. Fujiwara, J. Gotoh, I. Shimizu, *New Funct. Mater.*, **1993**, *A*, 163.

[132] K. Nishimura, Y. Nagao, K. Sakai, *Jpn. J. Appl. Phys.*, **1993**, *32*, L428.

[133] D. Blanc, J. I. B. Wilson, *Opt. Eng.*, **1988**, *27*, 917.

[134] J. Chen, Z. Tao, S. Li, X. Fan, S Chou, *Advanced Materials*, **2003**, *15*, 1379.

[135] M. Overbay, T. Novet, D. C. Johnson, *J. Solid State Chem.*, **1996**, *123*, 337.

[136] H. P. B. Rimmington, A. A. Balchin, *J. Crystal Growth*, **1974**, *21*, 171

[137] R. Bourezg, G. Couturier, J. Salardenne, F. Lévy, *Phys. Rev. B*, **1992**, *46*, 15404.

Chapter 2
Experimental Techniques

This chapter describes the experimental techniques and procedures reported in this thesis. The first section deals with the deposition technique employed in this work. While the second part describes the characterisation apparatus and techniques used.

2.1 Atmospheric Pressure Chemical Vapour Deposition

Chemical Vapor Deposition (CVD) involved chemical reactions which transform gaseous molecules, called precursors, into a solid material, in the form of thin film or powder, on the surface of a substrate.[1,2] A number of forms of CVD, such as low pressure (LP) CVD, plasma enhanced (PE) CVD, laser (L) CVD, metal-organic (MO) CVD and atmospheric pressure (AP) CVD, are in wide use. These processes differ in the means by which chemical reactions are initiated and progress. CVD has found applications in the areas of integrated circuits, optoelectronic devices, sensors, micromachines, fine metal and ceramic powders and protective coatings.

2.1.1 Description of the APCVD Apparatus

The apparatus and procedure described here was used for the production of all the films described in chapters 3, 4, 5 and 6. Atmospheric pressure chemical vapour deposition (APCVD) experiments were carried out under a nitrogen atmosphere on glass substrates using a horizontal-bed cold-wall APCVD reactor (Figure 2.1). The glass substrate, supplied by Pilkington, was SiO_2 coated to prevent the diffusion of ions from the glass into the film. It was heated by a graphite block containing a Whatman cartridge heater and the temperature of the substrate was monitored by a Pt-Rh thermocouple. The nitrogen (99.99 %) was obtained from BOC and used as supplied. The gas was preheated to 100 °C by being passed along 2 m lengths of coiled stainless steel tubing inside a tube furnace. The precursors were placed into different stainless steel bubblers, which were heated by an external jacket. They were then introduced into the gas streams by passing hot nitrogen through the bubblers. The flow rates of nitrogen

through the bubblers, was kept within 0.1 - 4.0 $L.min^{-1}$, and the flow rate through the mixing chamber were kept constant during all the deposition. The gases in the reaction were made to pass over the heated glass substrate and confined in position by a top plate that was ca. 4 mm above the substrate. After passage through the reaction chamber the gas stream was treated with bleach to destroy the possible presence of H_2Se and vented inside a fume cupboard.

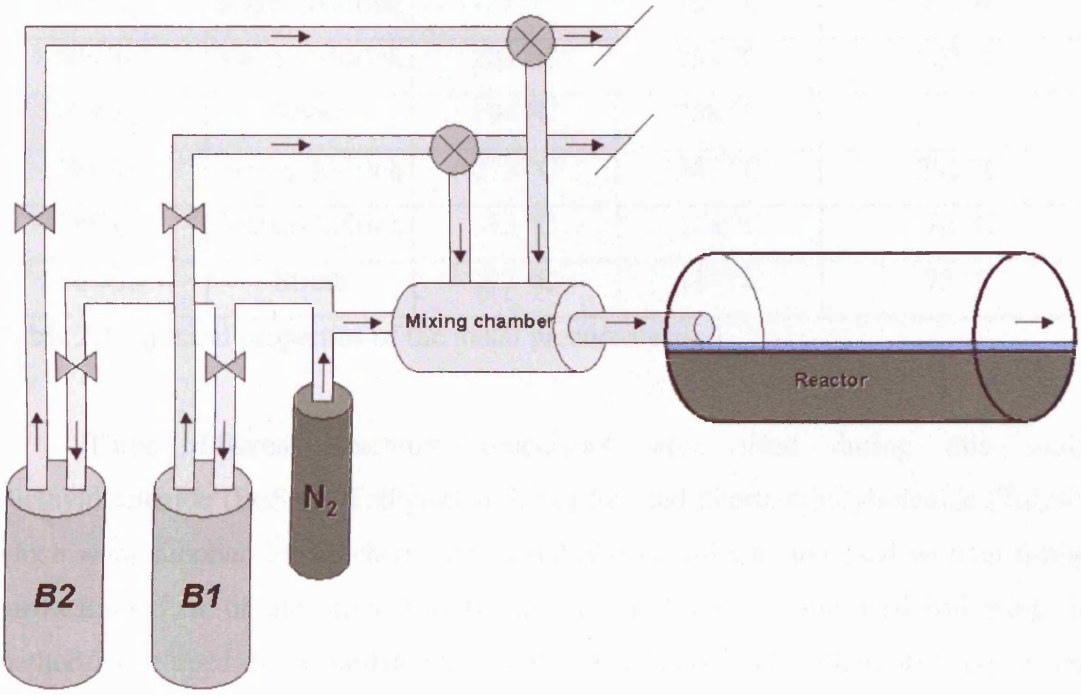

Figure 2.1 Schematic diagram of an atmospheric pressure chemical vapour deposition rig.

At the end of the deposition, the bubbler line was closed and the substrates were allowed to cool under nitrogen in the reactor. Then the substrates were handled briefly in air before storage in a dry oxygen-free nitrogen atmosphere in a glove box.

2.1.2 Precursors Used

Titanium chloride ($TiCl_4$), vanadium tetrachloride (VCl_4), vanadium oxychloride ($VOCl_3$), niobium pentachloride ($NbCl_5$), tungsten hexachloride (WCl_6), tin tetrachloride ($SnCl_4$) and Chromyl chloride (CrO_2Cl_2) were obtained from Strem or

Sigma-Aldrich. They were used as-supplied without further purification. The vanadium tetrakisdimethylamide [$V(NMe_2)_4$] was synthesized as described in the literature.[3]

	Supplier	Melting point	Boiling point	Temperature for V.P. = 200 mm Hg
$TiCl_4$	Sigma-Aldrich	-25 °C	135 °C	91 °C
VCl_4	Sigma-Aldrich	-28 °C	154 °C	104 °C
$VOCl_3$	Sigma-Aldrich	-77 °C	126 °C	82 °C
$NbCl_5$	Sigma-Aldrich	205 °C	254 °C	202 °C
$MoCl_5$	Strem	194 °C	268 °C	-
WCl_6	Sigma-Aldrich	275 °C	347 °C	282 °C
$SnCl_4$	Sigma-Aldrich	-33 °C	114 °C	72 °C
CrO_2Cl_2	Strem	-97 °C	117 °C	75 °C

Table 2.1 Physical properties of the metal precursors used.

Three different selenium precursors were used during this study. Diethyldiselenide (Et_2Se_2), diethylselenide (Et_2Se) and ditertiarybutylselenide ($^tBu_2Se$), which were supplied by Epichem, Strem and Sigma-Aldrich, and used without further purification. Part of the ditertiarybutylselenide used was synthesised following the method developed by Cole-Hamilton and co-workers.[4] The ditertiarybutylselenide produced showed no difference compared to the commercial sources in the quality and stoichiometry of the films deposited.

2.2 Sample Characterisation

After preparation, the samples were characterized with several techniques, including scanning electron microscopy, energy dispersive X-ray and wavelength dispersive X-ray analyses, X-ray photoelectron spectroscopy, X-ray diffraction, Raman microscopy and SQUID magnetometry.

2.2.1 Scanning Electron Microscopy

Scanning electron microscopy (SEM) functions by rastering an electron beam over a sample and collecting the secondary electrons emitted. The resulting image can give information about the morphology, uniformity and thickness of the films produced. To get film thickness measurements a fresh edge was made by cleaving the film. The film was then observed edge up. SEM was obtained on a JEOL 6301 instrument with a working distance of 15 mm. Accelerating voltages were between 10 eV and 20 eV depending on the sample. Magnification ranged from × 1 000 to × 100 000.

2.2.2 Energy Dispersive X-ray and Wavelength Dispersive X-ray Analyses

Energy dispersive X-ray (EDAX) and wavelength dispersive X-ray (WDX) analyses were used to obtained the stoichiometry and level of contamination within the films. EDAX and WDX were obtained on a Philips XL30ESEM instrument. An accelerating voltage of 20 keV and a working distance of 10 mm was used in EDAX. All elements were standardised relative to cobalt. An accelerating voltage of 7.5 keV and a working distance of 10 mm was used in WDX.

2.2.3 X-ray Photoelectron Spectroscopy

X-ray photoelectron spectroscopy (XPS) was used to determine the relative elemental abundances in the films and detect the level of contamination of the sample. It also provides information on the chemical environment of elements within the sample. In XPS, the sample is placed in the beam of an X-ray source in an Ultra-High Vacuum (UHV) chamber. The X-ray removes core level electrons from the surface of the sample. Ejected electrons from different elements have characteristic kinetic energies.

In this study, XPS was undertaken using a VG ESCALAB 220I XL instrument with using a focused (300 μm spot) monochromatic Al-K_α radiation at a pass energy of 20 eV. An electron flood gun was used to control charging. Scans were acquired with steps of 50 meV. Binding energies were referenced to an adventitious C 1s peak at 284.6 eV. Argon sputtering was used for approximately 1 min in a rastering mode in

order to remove surface contamination. Casa XPS software was used for data processing.

2.2.4 X-ray Diffraction

X-ray diffraction (XRD) was used to identify the crystal phase composition of the films deposited. It also allowed us to check the eventual formation of mixture or the presence of secondary phases within the film. The XRD equipment used in this study was a Brucker AX5 B8 diffractometer using monochromated Cu $K_{\alpha 1}$ radiation ($K_{\alpha 1}$ = 1.5406 Å) with a photon energy of 40 keV. The diffractometer used glancing incident radiation (5°). The samples were indexed using Unit Cell software and compared to database standards.

2.2.5 Raman Microscopy

The laser Raman spectrometer used in this study was a Renishaw 1000 Raman spectrometer. It used a 632.8 nm helium–neon laser. The Raman system was calibrated against the emission lines of neon.

2.2.6 Superconducting Quantum Interference Device Magnetometry

The magnetic properties of the films and powders formed were measured using a superconducting quantum interference device magnetometer (SQUID). The samples were ripped from their glass substrate using a ceramic spatula and inserted in gelatin capsule. Direct-current (DC) magnetic susceptibility measurements and hysteresis loops were performed using a commercial SQUID magnetometer (Quantum Design MPMS-XL). The DC magnetic susceptibilty was measured in a magnetic field of 10 Oe over a temperature range from 5 K to 350 K.

2.2.7 Thermal Gravimetric Analysis

Thermogravimetric analysis (TGA) continuously records changes in the mass of the materials heated and give indications on the stoichiometry and decomposition

pathway of the powders produced. TGA was performed on a Netzsch STA 449C instrument from room temperature up to 1600 °C with a heating rate of 10 °C.min^{-1}.

2.2.8 Transmittance and Reflectance Spectroscopy

Transmittance and reflectance spectroscopy was carried out to determined the optical properties of the coatings. Spectra were were recorded between 300 and 1200 nm by a Zeiss miniature spectrometer. Reflectance measurements were standardised relative to a rhodium mirror and transmission relative to air.

2.2.9 Contact Angle Measurements

Water contact angle of the films were calculated by measuring the diameter of a 1 μL droplet of water that had been dropped onto the surface of the film.

2.3 References

[1] K.L. Choy, *Prog. Mater. Sci.*, **2003**, *48*, 57.

[2] W. A. Bryant, *J. Mater. Sci.*, **1977**, *12*, 1285.

[3] A. Haaland, K. Rypdal, H.V. Volden, R.A. Andersen, *J. Chem. Soc., Dalton Trans.*, **1992**, 891.

[4] D.F. Foster, N.L. Pickett, D.J. Cole-Hamilton, *Polyhedron*, **1999**, *18*, 1329.

Chapter 3
APCVD of Group IV and V Selenides

3.1 Introduction

This chapter describes the APCVD of group IV and V metal selenides. In an attempt to produce titanium selenide thin films, the APCVD reactions of ditertiarybutylselenide, diethyldiselenide and diphenyldiselenide with titanium tetrachloride were investigated at substrate temperatures of 250 - 600 °C. The APCVD of vanadium selenide thin films using three different vanadium precursors, vanadium tetrachloride, vanadium oxychloride and vanadium tetrakisdimethylamide with ditertiarybutylselenide was also studied. Niobium selenide thin films were produced from niobium pentachloride and ditertiarybutylselenide via APCVD at 300 - 600 °C.

Reactions to produce mixed titanium-niobium selenide thin films from the APCVD reaction of titanium tetrachloride and niobium pentachloride with ditertiarybutylselenide were also performed. The APCVD reaction of these three precursors was studied at 550 °C over a wide range of different flow rate conditions.

3.2 Titanium Diselenide Films

A series of films were prepared using titanium tetrachloride $TiCl_4$ with different selenium sources; ditertiarybutylselenide $^tBu_2Se$ and diethyldiselenide Et_2Se_2. $TiCl_4$ has been used in a large number of CVD processes and is a good candidate of choice for growing titanium chalcogenides films.[1,2] The APCVD reaction of $TiCl_4$ and $[Ti(NMe_2)_4]$ with thiols (^tBuSH or $HS(CH_2)_2SH$) has led to the deposition of TiS_2 thin films. However, when using a sulfide $^tBu_2S_2$, $[Ti(NMe_2)_4]$ failed to produce TiS_2 films. Instead $[Ti(NMe_2)_4]$ was found to decompose to a titanium carbonitride rather than react with the sulfur precursor to form a titanium sulfide film. In contrast the reaction of $TiCl_4$ with $^tBu_2S_2$ resulted in the deposition of TiS_3 or TiS_2 films depending on the deposition temperature.[3]

3.2.1.1 Films from $TiCl_4$ and Et_2Se_2: Reaction Conditions

The APCVD reaction of titanium tetrachloride $TiCl_4$ with diethyldiselenide Et_2Se_2 was studied for the temperature range 450 – 600 °C. Deposition times for all experiments was one minute. The $TiCl_4$ and Et_2Se_2 bubblers were respectively heated to 80 °C and 140 °C. Flow rates of nitrogen through the $TiCl_4$ bubbler and the Et_2Se_2 bubbler were kept constant at 0.3 $L.min^{-1}$ and 0.6 $L.min^{-1}$ respectively, whereas the flow rate through the mixing chamber was 1 $L.min^{-1}$ for all depositions. These conditions corresponded to a $TiCl_4$ flow of 2.8 $mmol.min^{-1}$ and a Et_2Se_2 flow of 5.2 $mmol.min^{-1}$.

3.2.1.2 Appearance, Substrate Coverage and Adherence of the Films

Films produced from Et_2Se_2 and $TiCl_4$ between 450 and 600 °C had a powdery purple matt appearance, failed the Scotch tape test, and were easily scratched with a steel scalpel. The films were soluble in common organic solvents (eg. isopropanol, dichloromethane, acetone...) and quickly decomposed in nitric acid and bleach. At 450 °C, the films only covered the last 10 cm of the substrate. Whilst at a substrate temperature of 600 °C films were grown across the entire substrate. After two months storage in air, the films became slightly darker.

3.2.1.3 Scanning Electron Microscopy

Scanning electron microscopy of the films grown from Et_2Se_2 and $TiCl_4$ showed a series of plate-like crystallites orientated perpendicular to the substrate (Figure 3.1). The plates were observed to become longer and thicker with increasing deposition temperature.

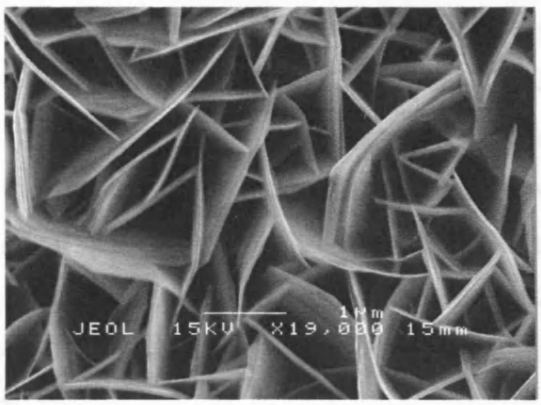

Figure 3.1 Scanning electron micrographs of a film produced from the APCVD reaction of $TiCl_4$ with Et_2Se_2 at 500 °C.

3.2.1.4 Energy Dispersive X-ray Analysis

Films produced from the APCVD reaction of $TiCl_4$ with Et_2Se_2 were all found to have a Ti : Se ratio slightly lower than that expected for $TiSe_2$. The overall stoichiometry of the films varied from $TiSe_{1.9}$ at 450 °C to $TiSe_{1.6}$ at 600 °C (Table 3.1). EDAX showed that there was no chlorine or carbon in the films deposited from the reaction of $TiCl_4$ with Et_2Se_2.

Table 3.1 EDAX, XRD and Raman data for the films produced by APCVD reaction of $TiCl_4$ with Et_2Se_2.

Deposition temperature	EDAX	XRD; lattice constants in Å	Raman
450 °C	$TiSe_{1.9}$	1T-$TiSe_2$; a = 3.49 Å, c = 6.00 Å	$TiSe_2$; 133 + 197 cm^{-1}
500 °C	$TiSe_{1.9}$	1T-$TiSe_2$; a = 3.50 Å, c = 5.95 Å	$TiSe_2$; 134 + 198 cm^{-1}
550 °C	$TiSe_{1.8}$	1T-$TiSe_2$; a = 3.51 Å, c = 5.99 Å	$TiSe_2$; 134 + 200 cm^{-1}
600 °C	$TiSe_{1.6}$	1T-$TiSe_2$; a = 3.50 Å, c = 5.93 Å	$TiSe_2$; 133 + 198 cm^{-1}

3.2.1.5 X-ray Photoelectron Spectroscopy

The XPS of a film deposited from the reaction of $TiCl_4$ and Et_2Se_2 at 500 °C revealed the presence of two titanium environments. The stronger peaks correspond to

Ti $2p_{1/2}$ = 463.6 eV and Ti $2p_{3/2}$ = 458.2 eV of $TiSe_2$, which compare well with the literature values reported for $TiSe_2$ (Ti $2p_{1/2}$ = 462.5 eV and Ti $2p_{3/2}$ = 457.5 eV).[4] The second titanium environment, with peaks at Ti $2p_{1/2}$ = 464.8 eV and Ti $2p_{3/2}$ = 459.1 eV, is due to oxide contamination and match the literature values reported for TiO_2 (Ti $2p_{1/2}$ = 464.7 eV and Ti $2p_{3/2}$ = 459.0 eV).[5] The oxygen content within the sample was found to decrease after etching the film, which suggests the partial oxidation of the surface of the titanium selenide films. XPS revealed the presence of only one selenium environment in the film.

3.2.1.6 X-ray Diffraction

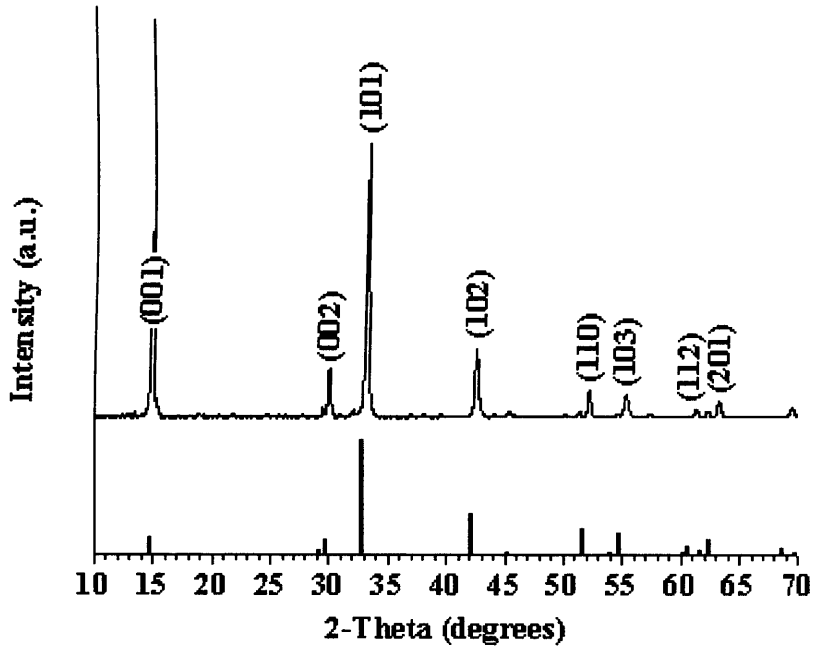

Figure 3.2 The XRD pattern obtained for a film deposited from the APCVD reaction of $TiCl_4$ with Et_2Se_2 at 500 °C. Literature stick pattern for $TiSe_2$ powder (JCPDS File No. 30-1383) is shown.

The XRD of the films grown from the APCVD reaction of Et_2Se_2 and $TiCl_4$ showed that the reflections matched the reference spectrum for $TiSe_2$ (JCPDS File No. 30-1383). At substrate temperature from 500 to 600 °C, the $TiSe_2$ films showed pronounced preferential orientation with the (001) direction perpendicular to the substrate (Figure 3.2). All the other films produced at lower temperature showed less

preferred orientation. The lattice parameters reported in Table 3.1, were all found to be slightly smaller than the literature lattice parameters for hexagonal $TiSe_2$ in both bulk and nanotube forms a = 3.54 Å; c = 6.00 Å.[6,7] Cell parameters have not been reported before for CVD produced $TiSe_2$, but the smaller cell parameters observed here could be due to the selenium deficiency of the films (Table 3.1). No additional phase, such as TiO_2, was observed by XRD.

3.2.1.7 Raman Microscopy

Raman analysis of the films formed from $TiCl_4$ and Et_2Se_2 gave the characteristic $TiSe_2$ Raman pattern, with peaks at 133 cm^{-1} and at 197 cm^{-1} (Table 3.1). No evidence of a secondary phase was observed in the as-prepared films (Figure 3.3). However, after two months of storage in air, the films showed the presence of $TiSe_2$ and TiO_2 (Figure 3.4).[8] The five well-resolved Raman peaks observed at 143 cm^{-1} (E_g), 197 cm^{-1} (E_g), 396 cm^{-1} (B_{1g}), 514 cm^{-1} (A_{1g}) and 636 cm^{-1} (E_g) were assigned to the anatase form of TiO_2.[9]

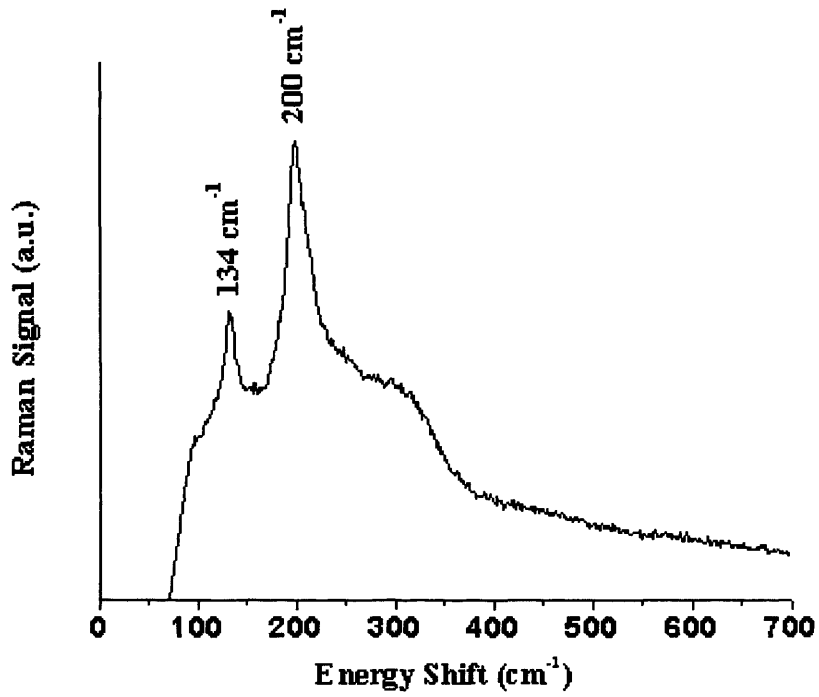

Figure 3.3 Raman pattern obtained for a film produced from the APCVD reaction of $TiCl_4$ with Et_2Se_2 at 550 °C.

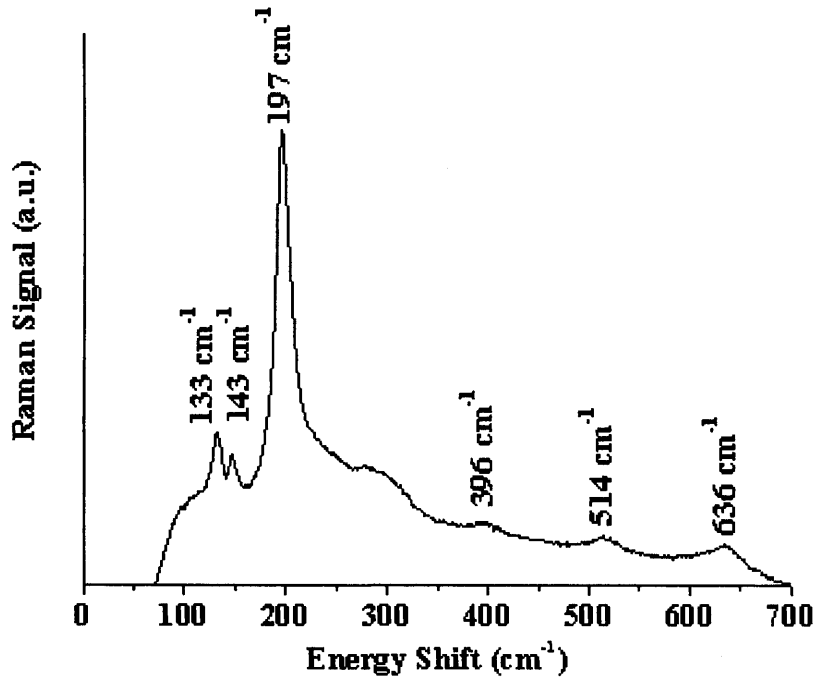

Figure 3.4 Raman pattern obtained for a film produced from the APCVD reaction of $TiCl_4$ with Et_2Se_2 at 550 °C after storage in air for two months.

3.2.1.8 Optical Properties

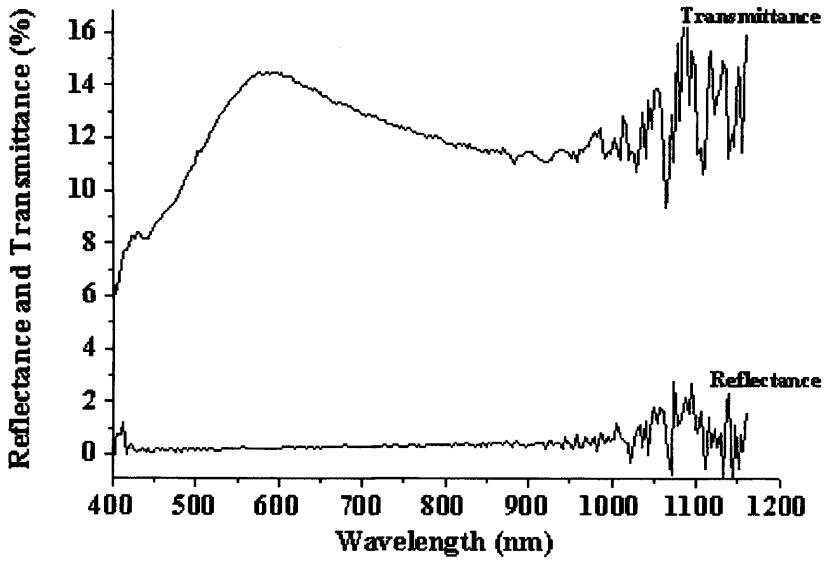

Figure 3.5 Transmittance and reflectance of a film deposited from $TiCl_4$ with Et_2Se_2 at 550 °C.

The optical transmittance of all the films from 400-1200 nm produced was fairly low with a maximum of 15 % at ca. 600 nm (Figure 3.5). The films showed no reflectivity over the entire wavelength range studied.

3.2.2.1 Films from $TiCl_4$ and $^tBu_2Se$: Reaction Conditions

The APCVD reaction of titanium tetrachloride ($TiCl_4$) with ditertiarybutylselenide ($^tBu_2Se$) was investigated from 250 °C, the onset of deposition, up to 600 °C. Deposition times for all experiments was one minute. The $TiCl_4$ and $^tBu_2Se$ were both heated to 80 °C. Flow rates of nitrogen through the $TiCl_4$ bubbler and the $^tBu_2Se$ bubbler were kept constant at 0.3 $L.min^{-1}$ and 0.6 $L.min^{-1}$ respectively, and the flow rate through the mixing chamber was 1 $L.min^{-1}$ for all depositions. These conditions corresponded to a $TiCl_4$ flow of 2.8 $mmol.min^{-1}$ and a $^tBu_2Se$ flow of 5.2 $mmol.min^{-1}$.

3.2.2.2 Appearance, Substrate Coverage and Adherence of the Films

At deposition temperatures below 300 °C, the films produced from $^tBu_2Se$ and $TiCl_4$ were navy blue and highly reflective with a mirror-like appearance. The films had a dark-purple matt appearance at deposition temperatures above 300 °C. They passed the Scotch tape test, however were easily scratched with a steel scalpel. The films were found to be soluble in common organic solvents and were quickly decomposed in nitric acid and bleach. The extent of film coverage was dependent on the deposition temperature. For a deposition temperature between 250 °C and 400 °C, uniform thickness films were grown across the entire length of the substrate. With higher temperatures, the growth profile was concentrated closer towards the leading edge of the substrate such that at a deposition temperature of 600 °C only the first 6 cm of the substrate was coated.

3.2.2.3 Scanning Electron Microscopy

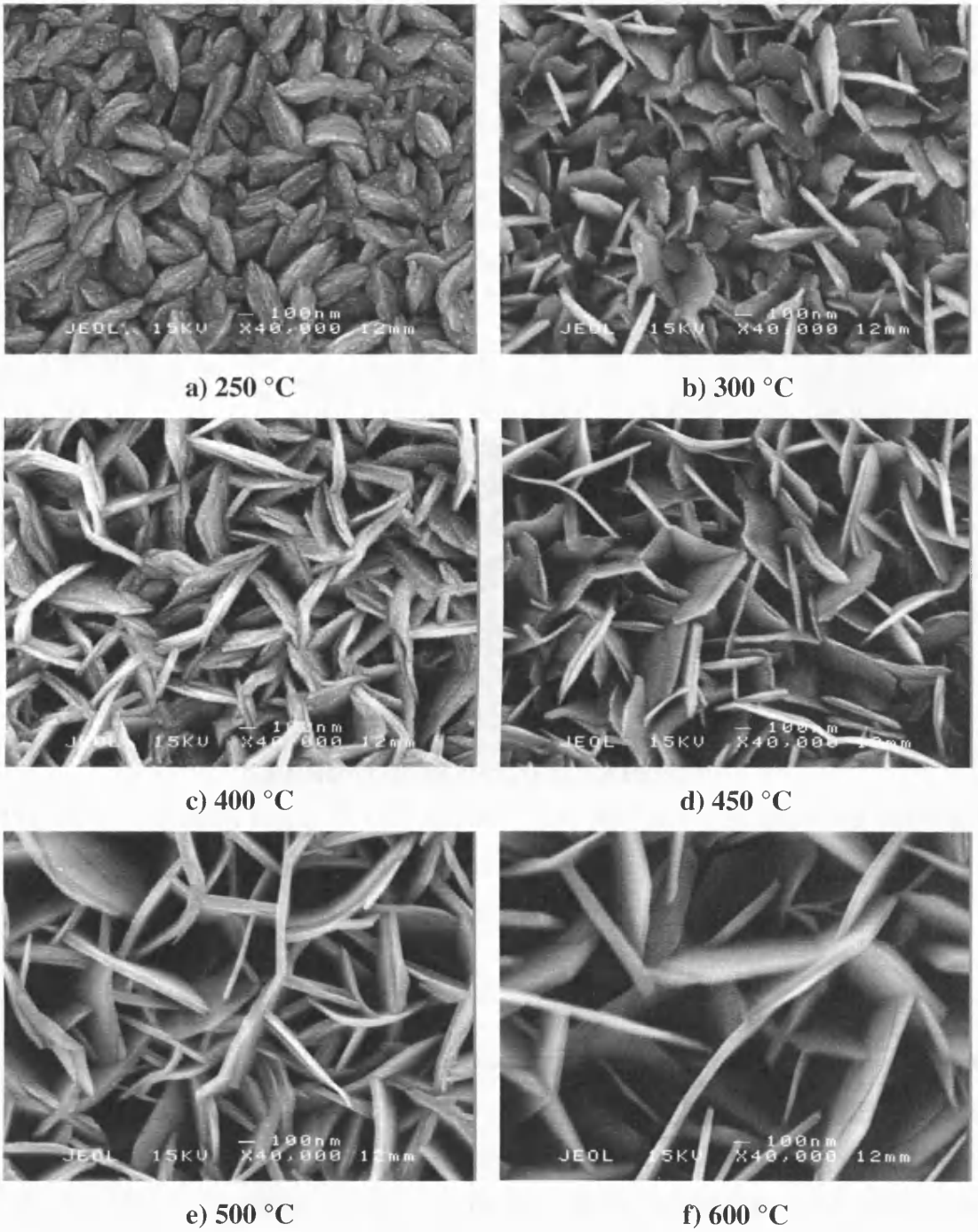

Figure 3.6 Scanning electron micrographs of the films produced from the APCVD reaction of $TiCl_4$ with $^tBu_2Se$ at 250 – 600 °C.

Scanning electron microscopy of the films grown from $^tBu_2Se$ and $TiCl_4$ showed a series of plate like crystallites (Figure 3.6). The plates were observed to become longer and thicker with increasing deposition temperature. Notably at deposition

temperatures of 300 °C and above the plates have a degree of texturing with some preferred growth perpendicular to the substrate. The films produced from the APCVD reaction of $TiCl_4$ with $^tBu_2Se$ showed the crystal size to increase from ca. 0.5 μm at 250 °C to 2 μm at 600 °C. The thickness of the films, determined using cross-sectional SEM, was between 0.3 μm (250 °C) and 0.7 μm (600 °C) (Figure 3.7). The faster growth rates and larger particles observed at the highest deposition temperatures are expected from a surface reaction rate limited process. Increase of the deposition temperature involves a faster growth kinetics and a smaller number of nucleation sites, which result in a smaller number of particles seen at the highest deposition temperatures.

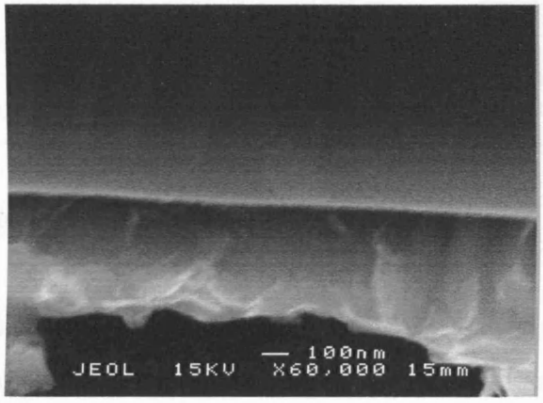

← **Glass substrate**

← **Film**

Figure 3.7 Scanning electron micrographs of the side of a film produced from the APCVD reaction of $TiCl_4$ with $^tBu_2Se$ at 400 °C.

3.2.2.4 Energy Dispersive X-ray Analysis

EDAX analysis of the films produced at a temperature below 550 °C from the APCVD reaction of $TiCl_4$ and $^tBu_2Se$ showed that they contained titanium and selenium with a ratio close to the one expected for $TiSe_2$, with a stoichiometry varying from $TiSe_{1.8}$ at 250 °C to $TiSe_{2.1}$ at 500 °C. Films produced at 600 °C were found to be substoichiometric with a selenium to titanium ratio of 1.5. No chlorine or carbon were detected in the films by the EDAX analysis (Table 3.2).

Table 3.2 EDAX, XRD and Raman data for the films produced by APCVD reaction of $TiCl_4$ with $^tBu_2Se$.

Deposition temperature	EDAX	XRD; lattice constant in Å	Raman
250 °C	$TiSe_{1.8}$	1T-$TiSe_2$; a = 3.49 Å, c = 5.95 Å	$TiSe_2$; 133 + 197 cm^{-1}
300 °C	$TiSe_{2.1}$	1T-$TiSe_2$; a = 3.52 Å, c = 5.99 Å	$TiSe_2$; 134 + 198 cm^{-1}
350 °C	$TiSe_{2.1}$	1T-$TiSe_2$; a = 3.49 Å, c = 6.02 Å	$TiSe_2$; 134 + 197 cm^{-1}
400 °C	$TiSe_{2.1}$	1T-$TiSe_2$; a = 3.52 Å, c = 5.98 Å	$TiSe_2$; 133 + 197 cm^{-1}
450 °C	$TiSe_{2.1}$	1T-$TiSe_2$; a = 3.51 Å, c = 6.01 Å	$TiSe_2$; 133 + 198 cm^{-1}
500 °C	$TiSe_{2.1}$	1T-$TiSe_2$; a = 3.51 Å, c = 6.00 Å	$TiSe_2$; 133 + 198 cm^{-1}
600 °C	$TiSe_{1.5}$	1T-$TiSe_2$; a = 3.47 Å, c = 5.92 Å	$TiSe_2$; 134 + 198 cm^{-1}

3.2.2.5 X-ray Photoelectron Spectroscopy

The XPS of the films deposited from $TiCl_4$ with $^tBu_2Se$ showed that the films were predominantly made of titanium diselenide with a small amount of titanium oxide present. The two strongest peaks observed at 458.5 eV and 463.9 eV correspond to Ti $2p_{3/2}$ and Ti $2p_{1/2}$ of $TiSe_2$, and the two peaks at 459.3 eV and 465.1 eV correspond to Ti $2p_{3/2}$ and Ti $2p_{1/2}$ of TiO_2. These values compare well with the literature values reported for $TiSe_2$ (Ti $2p_{1/2}$ = 462.5 eV and Ti $2p_{3/2}$ = 457.5 eV)[4] and TiO_2 (Ti $2p_{1/2}$ = 464.7 eV and Ti $2p_{3/2}$ = 459.0 eV).[5,10] Only one selenium environment was present in the films with peaks at 53.2 eV and 54.1 eV corresponding to Se $3d_{5/2}$ and Se $3d_{3/2}$ of $TiSe_2$ (Se $3d_{5/2}$ = 53.4 eV and Se $3d_{3/2}$ = 54.2 eV).[11] The oxygen 1s peak observed at 530.6 eV was observed to be less intense after etching into the film, suggesting that the surface is partially oxidised.

3.2.2.6 X-ray Diffraction

X-ray Diffraction analysis of the films from the APCVD reaction of $^tBu_2Se$ and $TiCl_4$ showed all the films to be crystalline and found to match the reference spectrum for $TiSe_2$ (JCPDS File No. 30-1383). The lattice parameters of all the films produced at

deposition temperature below 500 °C compare well with the literature lattice parameters (Table 3.2). However, the lattice parameters of the films produced at 600 °C (ca. a = 3.47 Å, c = 5.92 Å) were smaller than the one expected for hexagonal $TiSe_2$ (ca. a = 3.54 Å; c = 6.00 Å).[6] This could be due to the selenium deficient stoichiometry of the films which had a titanium to selenium ratio of 1 : 1.5.

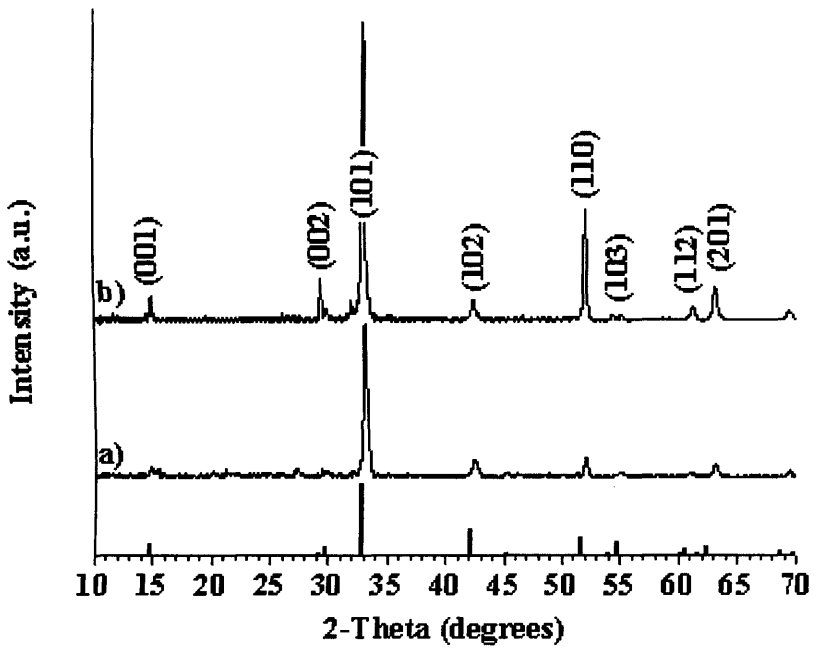

Figure 3.8 Scanning electron micrographs of a film produced from the APCVD reaction of $TiCl_4$ with $^tBu_2Se$ at 350 °C (a) and 500 °C (b). Literature stick pattern for $TiSe_2$ powder (JCPDS File No. 30-1383) is shown.

3.2.2.7 Raman Microscopy

Raman analysis of the films formed from $TiCl_4$ and $^tBu_2Se$, irrespective of the deposition temperature, showed the same pattern (Table 3.2). This was readily identified as the distinctive $TiSe_2$ Raman pattern reported in the literature for the bulk solid with peaks at 133 cm^{-1} and at 198 cm^{-1} (Figure 3.9).[8] No evidence was seen for a secondary phase, such as TiO_2, which in the anatase phase is an excellent Raman scatterer.[9]

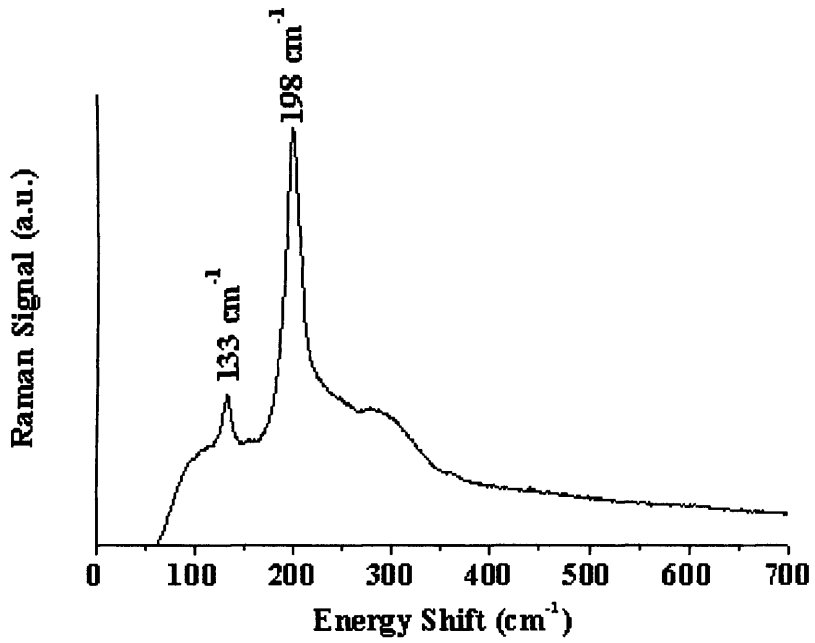

Figure 3.9 Raman pattern obtained for a film produced from the APCVD reaction of $TiCl_4$ with $^tBu_2Se$ at 500 °C after storage in air for two months.

3.2.2.8 Optical Properties

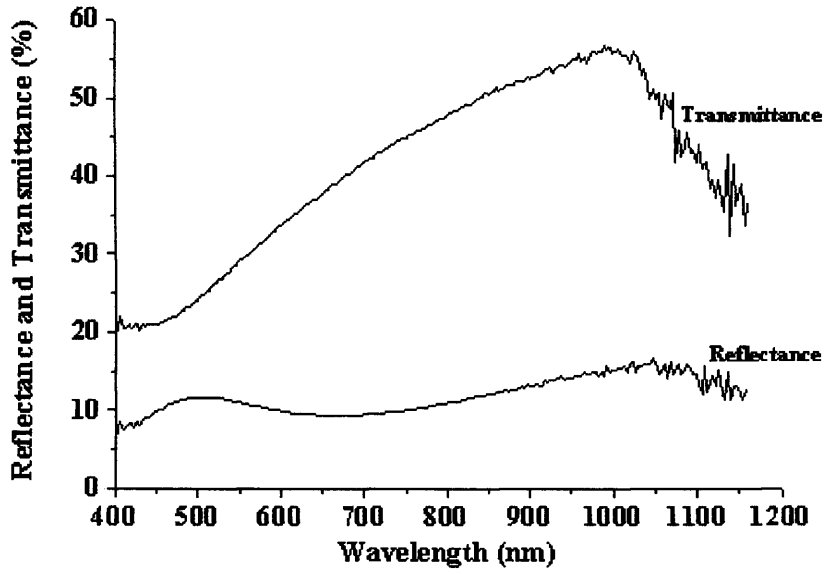

Figure 3.10 Transmittance and reflectance of a film deposited from $TiCl_4$ with $^tBu_2Se$ at 400 °C.

The reflectance of all the $TiSe_2$ films was fairly low over the entire wavelength range studied (ca. 10 %). The films showed a high transmittance in the near-IR region (ca. 50 %), while the transmittance measured at 400 nm was only 20 % (Figure 3.10).

3.2.3 Comparison and Discussion

The results show that the selenium precursor used in this work has an effect on the stoichiometry and quality of the films deposited. Films grown from the APCVD reaction of $TiCl_4$ with Et_2Se_2 were all found to be substoichiometric, with an overall stoichiometry varying from $TiSe_{1.9}$ at 450 °C to $TiSe_{1.6}$ at 600 °C. While the films deposited from $^tBu_2Se$ were slightly superstoichiometric at deposition temperature between 300 °C and 500 °C (ca. $TiSe_{2.1}$). The films from either precursor showed a series of plate like crystallites by SEM and gave the same XRD and Raman patterns identified as the 1T-$TiSe_2$ patterns. Due to their porous nature, the films grown from all different precursors and reaction temperature showed an exceptionally small (ca. 10°) water contact angle. The porous nature of the films also facilitates the hydrolysis of the films by allowing water to diffuse rapidly into the coating, and after a two months storage in air, the films growth from either precursor became slightly darker. No change was observed in the Raman and XRD spectra of the films produced from $^tBu_2Se$, indicating that the films are relatively air stable. However, the Raman spectra of the films produced from Et_2Se_2 revealed the formation of TiO_2.

$^tBu_2Se$ could be considered as a desirable precursor to grow $TiSe_2$ thin films. Despite Et_2Se_2 having one more selenium atom than $^tBu_2Se$, Et_2Se_2 led to the formation of substoichiometric films at identical flow rates and temperature conditions (ca. 5.2 $mmol.min^{-1}$) which oxidised in air. The use of Ph_2Se_2 with $TiCl_4$ was proved to be unsuccessful and did not deposit any films. The presence of the two phenyl groups in Ph_2Se_2 makes it an unsuitable precursor for a CVD process.

3.3 Vanadium Diselenide Films

In an attempt to deposit vanadium diselenide films, ditertiarybutylselenide and range of different vanadium precursors (vanadium tetrachloride, vanadium oxychloride and vanadium tetrakisdimethylamide) were used in an APCVD reaction.

3.3.1.1 Films from $VOCl_3$ and $^tBu_2Se$: Reaction Conditions

The reaction of vanadium oxychloride ($VOCl_3$) and ditertiarybutylselenide ($^tBu_2Se$) was investigated from 250 °C (the onset of deposition) up to 600 °C. The $VOCl_3$ and $^tBu_2Se$ bubblers were heated to 75 °C and 100 °C respectively. The flow rates of nitrogen through the $VOCl_3$ bubbler and the $^tBu_2Se$ bubbler were kept constant at 0.3 $L.min^{-1}$ (1.0 $mmol.L^{-1}$) and 0.6 $L.min^{-1}$ (5.5 $mmol.min^{-1}$), respectively, and the flow rate through the mixing chamber was 2 $L.min^{-1}$ for all depositions. Deposition time for all experiments was one minute.

3.3.1.2 Appearance, Substrate Coverage and Adherence of the Films

The extent of the film coverage was dependent on the deposition temperature. Only the four first centimeters of the substrate were coated at a substrate temperature of 600 °C, whilst the whole substrate was coated with uniform thickness at 250 °C. This indicates that the deposition is mass transport-limited at the highest temperature. The films produced were dark-blue and reflective. They all passed the Scotch tape test, however they were easily scratched with a steel scalpel. The films were insoluble in common organic solvents but were quickly decomposed in nitric acid and bleach. Moreover, the films were air sensitive and after a few days exposure to air they oxidised, becoming red-orange, to form a vanadium oxide.

3.3.1.3 Scanning Electron Microscopy

At deposition temperatures above 350 °C, the SEM images of the films prior to oxidation show a single type of plate-like crystallite that have grown in an orientation perpendicular to the substrate. This morphology is characteristic of an island growth

mechanism. The long-axis length of the plates varied from ca 50 nm at 350 °C to 200 nm at 600 °C. At 300 °C and below, the films produced were fairly featureless with less distinct islands.

3.3.1.4 Energy Dispersive X-ray Analysis

The EDAX results (Table 3.3) showed that all the films from the reaction of $VOCl_3$ and $^tBu_2Se$ contained vanadium and selenium with V : Se ratios close to 1 (ca. 0.9 – 1.2). Moreover, a substantial amount of chlorine was detected in the films (ca. 10-20 atom%). Due to the presence of oxygen in the substrate and subsequent electron breakthrough, the amount of oxygen in the film could not be accurately quantified, however the films do seem to contain significant oxygen-as made. The oxygen content was found to increase and chlorine and selenium content to decrease progressively on storage in air. However the films if handled in a N_2 glove box were indefinitely stable.

Table 3.3 Reaction temperatures, EDAX, X-ray diffraction and Raman data for the films produced by the APCVD reaction of $^tBu_2Se$ with $VOCl_3$.

Deposition Temperature	EDAX	XRD; lattice constants in Å	Raman
250 °C	$VSe_{0.7}Cl_{0.3}$	-	VO_x
300 °C	$VSe_{1.1}Cl_{0.2}$	-	VSe_2 / VO_x
350 °C	$VSe_{1.2}Cl_{0.1}$	1T-VSe_2; a = 3.32 Å, c = 6.04 Å	VSe_2 / VO_x
400 °C	$VSe_{1.1}Cl_{0.2}$	1T-VSe_2; a = 3.29 Å, c = 6.10 Å	VSe_2 / VO_x
450 °C	$VSe_{1.2}Cl_{0.1}$	1T-VSe_2; a = 3.31 Å, c = 6.08 Å	VSe_2 / VO_x
500 °C	$VSe_{1.1}Cl_{0.2}$	1T-VSe_2; a = 3.29 Å, c = 6.09 Å	VSe_2 / VO_x
550 °C	$VSe_{0.9}Cl_{0.2}$	1T-VSe_2; a = 3.29 Å, c = 6.08 Å	VSe_2 / VO_x
600 °C	$VSe_{0.8}Cl_{0.2}$	1T-VSe_2; a = 3.24 Å, c = 6.02 Å	VSe_2 / VO_x

3.3.1.5 X-ray Diffraction

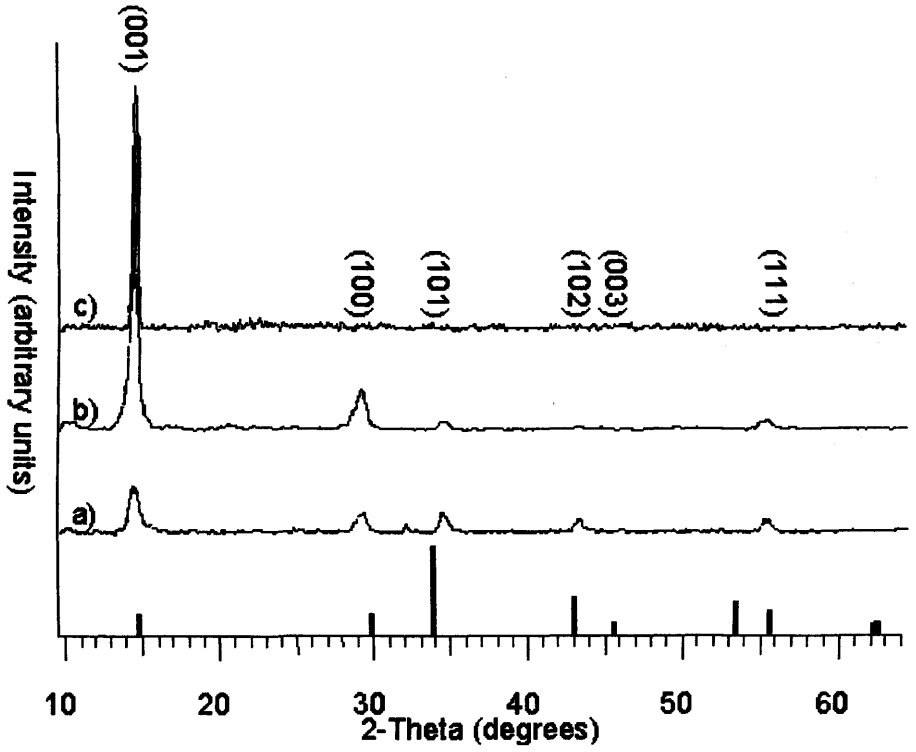

Figure 3.11 The XRD patterns obtained for the film formed on the glass from the APCVD of $VOCl_3$ and $^tBu_2Se$ at 350 °C (a), 450 °C (b) and 600 °C (c). Literature stick pattern for $V_{1+x}Se_2$ powder (JCPDS File No. 032-1415) is shown.

The films formed above 350 °C from the APCVD reaction of $VOCl_3$ with $^tBu_2Se$ were all found to be crystalline (Figure 3.11). X-ray diffraction showed that the reflections matched the reference spectrum for hexagonal phase $V_{1+x}Se_2$, with x between 0.02 and 0.13 (JCPDS Files No. 032–1415 and No. 002-0978).[12] A preferential growth orientation along the (001) direction was noticed in these films produced from $VOCl_3$ and $^tBu_2Se$. With an increase in the reactor temperature, the films become more crystalline and more preferentially orientated. At 600 °C, the films produced were highly crystalline with a strong preferential growth along the (001) direction. The indexed cell constants found for the films, a = 3.32 Å and c = 6.10 Å compare well with the literature for hexagonal $VSe_{1.96}$, a = 3.353 Å and c = 6.101 Å, while they did not match the reported cell constants for $VSe_{0.9\text{-}1.2}$, a = 3.525-3.721 Å and c = 5.979-5.998 Å.[12] This suggests that the vanadium selenide films show a stoichiometry close to VSe_2. No evidence of a secondary phase was observed in XRD. The presence of extra

vanadium from the EDAX analysis can be explained by the co-formation of an X-ray amorphous vanadium oxide or vanadium oxychloride phase.

3.3.1.6 Raman Microscopy

The Raman pattern shown in Figure 3.12 is representative of all films except those deposited at 250 °C. The Raman pattern showed the distinctive band at 205 cm^{-1} correspondenting to the A_{1g} mode of 1T-VSe_2. Raman analysis of the films also showed the presence of two additional peaks at 250 and 340 cm^{-1}. These two peaks could be assigned to the VO_x ($2.0 < x < 2.5$) phase.[13,14] This confirmed the co-formation of a vanadium oxide during the APCVD of the VSe_2 thin films. Raman analysis of the film deposited at 250 °C, did not show the formation of a vanadium selenide, only the presence of the two additional peaks assigned to VO_x were observed.

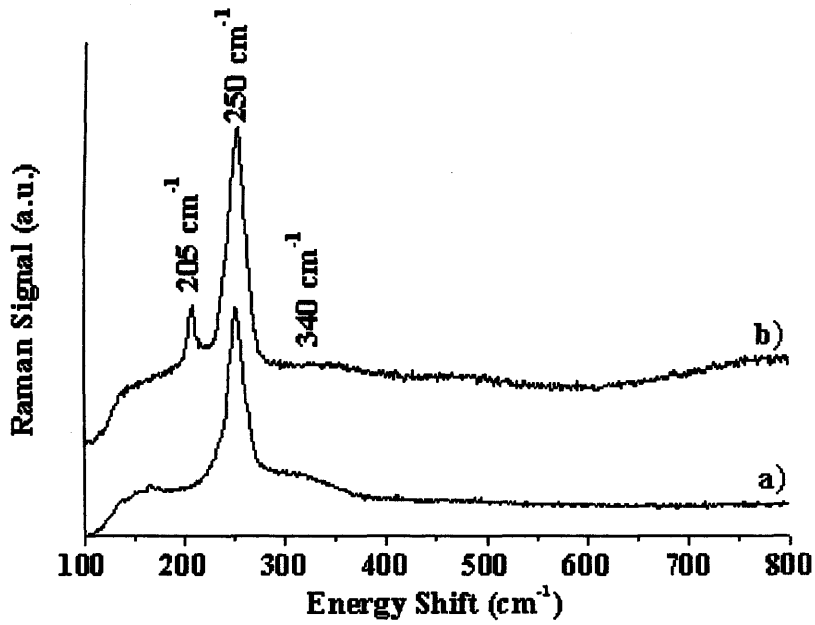

Figure 3.12 Raman pattern obtained for the film formed on glass from the APCVD of $VOCl_3$ and $^tBu_2Se$ at 250 °C (a) and 500 °C (b).

3.3.2.1 Films from [$V(NMe_2)_4$] and $^tBu_2Se$: Reaction Conditions

The reaction of vanadium tetrakisdimethylamide [$V(NMe_2)_4$] and ditertiarybutylselenide $^tBu_2Se$ were investigated at substrate temperatures between 250

and 500 °C. The $[V(NMe_2)_4]$ and $^tBu_2Se$ bubblers were heated to 130 °C and 90 °C respectively, with a flow rate of nitrogen of 0.5 $L.min^{-1}$ (vapour pressure data not available) and 2 $L.min^{-1}$ (8.3 $mmol.min^{-1}$) respectively. The flow rate through the mixing chamber was kept constant at 1 $L.min^{-1}$ and the deposition time for the experiments was ten minutes.

3.3.2.2 Appearance, Substrate Coverage and Adherence of the films

During the APCVD reaction of $[V(NMe_2)_4]$ with $^tBu_2Se$, deposition was observed on both the top guide plate and the heated substrate. The extent of the film coverage was dependent on the deposition temperature. Only the first ten centimetres of the substrate were coated at a deposition temperature of 500 °C, whereas the whole substrate was coated with uniform thickness at 250 °C. This indicates that the deposition is mass transport-limited at the highest temperature. The films produced from $^tBu_2Se$ and $[V(NMe_2)_4]$ were dark black matt in appearance. Optical experiments show that the films were highly absorbing in the visible and near IR regions. They passed the Scotch tape test but failed the scratch test (steel, brass). They were insoluble in the common organic solvents and quickly decomposed in diluted nitric acid or diluted bleach. After a one-year storage in air, the thinner parts of the films partially changed colour from black to dark-orange; thus indicating the formation of a vanadium oxide on the surface of the films. However, the films produced from $^tBu_2Se$ and $[V(NMe_2)_4]$ were found to be much more resistant to oxidation than the ones produced from $^tBu_2Se$ and $VOCl_3$. The films did not show any particular hydrophobicity or hydrophilicity, the contact-angle measurement for water droplets was 35°.

3.3.2.3 Scanning Electron Microscopy

The SEM images for the films deposited between 400 and 500 °C showed a series of hexagonal platelets oriented perpendicular to the substrate (Figure 3.13). The platelets became longer and thicker with increasing deposition temperature. The average length of the platelets was 0.2 μm for the films deposited at 400 °C and 1 μm for those formed at 500 °C. This change in platelet size can be related to faster growth kinetics and smaller numbers of nucleation sites at the higher temperatures. For deposition temperature below 300 °C, the SEM images of the films were featureless. Using cross-

sectional SEM, the thickness of the films was determined as being between 0.3 μm (300 °C) and 0.4 μm (500 °C).

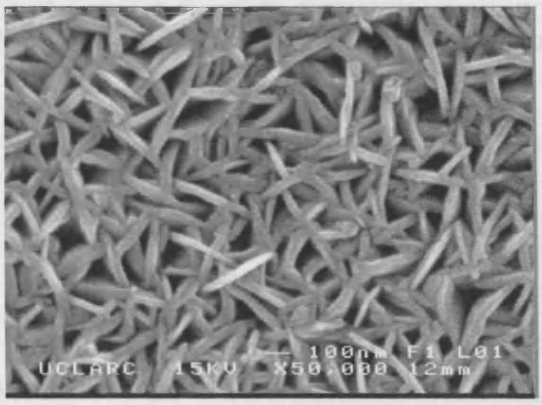

a) 400 °C

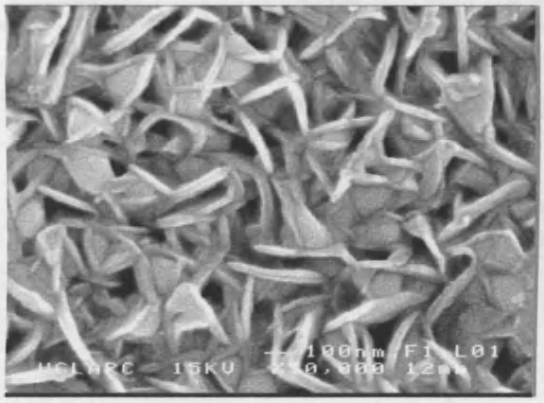

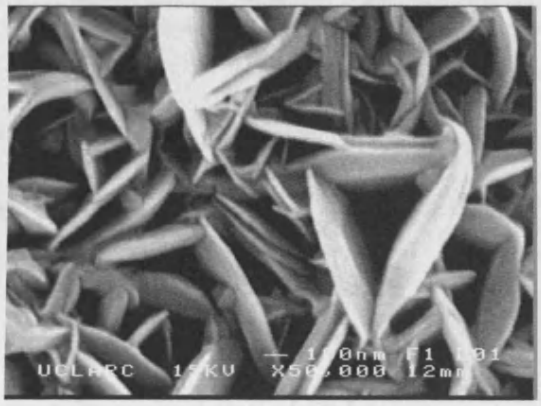

b) 450 °C **c) 500 °C**

Figure 3.13 Scanning electron micrographs of the films produced from the APCVD of $[V(NMe_2)_4]$ and $^tBu_2Se$ at 400 and 500 °C.

3.3.2.4 Energy Dispersive X-ray Analysis

EDAX showed that all the films contained vanadium and selenium with a V : Se ratio dependent on the deposition temperature and flow rate conditions. At higher deposition temperature, films with a stoichiometry $VSe_{1.96}$ were formed, whilst at lower temperature the films showed a V : Se ratio slightly higher than that expected for VSe_2 ($VSe_{2.08-2.10}$). The error limit for EDAX system used was ca. 3 atom%, this means that all of the films designated $VSe_{1.9-2.1}$ in Table 3.4 were essentially indistinguishable. The films showed uniformity in composition along the length of the substrate and across its width for any film. No nitrogen was detected in all the films produced, however a substantial amount of carbon was detected in the films (ca. 10 atom%).

Table 3.4 Reaction temperatures, EDAX, X-ray diffraction and Raman data for the films produced by the APCVD reaction of $^tBu_2Se$ with $[V(NMe_2)_4]$.

Deposition Temperature	EDAX	XRD; lattice constants in Å	Raman
250 °C	$VSe_{2.15}$	-	VSe_2
300 °C	$VSe_{2.10}$	1T-VSe_2; $a = 3.36$, $c = 6.14$	VSe_2
400 °C	$VSe_{2.08}$	1T-VSe_2; $a = 3.34$, $c = 6.14$	VSe_2
450 °C	$VSe_{2.10}$	1T-VSe_2; $a = 3.35$, $c = 6.14$	VSe_2
500 °C	$VSe_{1.96}$	1T-VSe_2; $a = 3.35$, $c = 6.13$	VSe_2

3.3.2.5 X-ray Photoelectron Spectroscopy

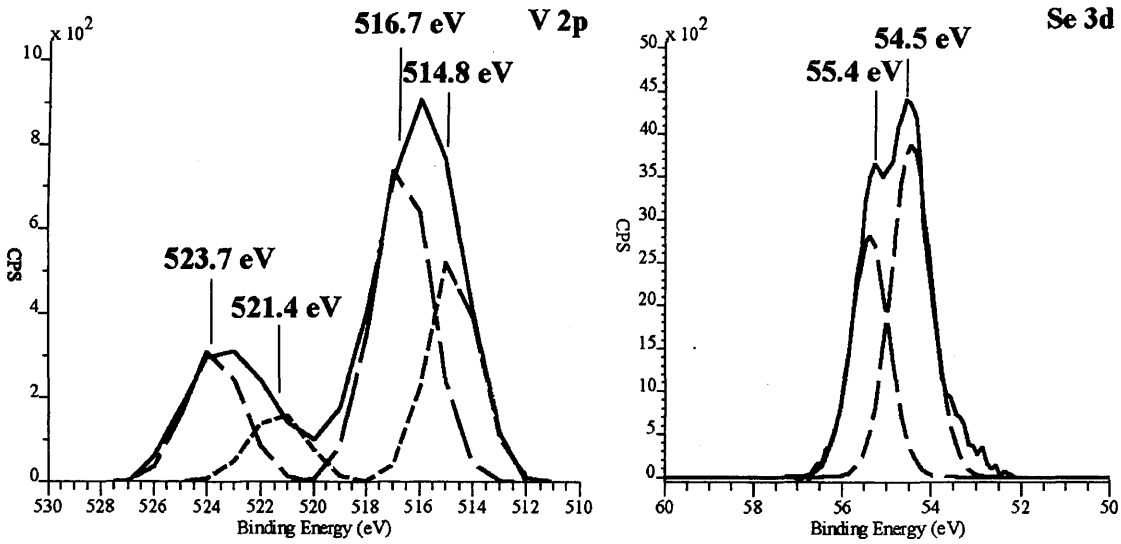

Figure 3.14 X-ray photoelectron spectrum of the V 2p and Se 3d peaks from the surface of a film formed on glass from the APCVD of $[V(NMe_2)_4]$ and $^tBu_2Se$ at 500 °C.

The XPS of a film deposited from $[V(NMe_2)_4]$ and $^tBu_2Se$ at 500 °C shows that there are two vanadium environments present in the film (Figure 3.14). The first environment corresponds to V $2p_{3/2}$ = 516.7 eV and V $2p_{1/2}$ = 523.7 eV of the vanadium diselenide (V $2p_{3/2}$ = 516.9 eV and V $2p_{1/2}$ = 524.3 eV).[4] The second doublet at V $2p_{3/2}$ = 514.8 eV and V $2p_{1/2}$ = 521.4 eV is due to oxide contamination and match the

reported peaks for the vanadium in V_2O_3 (V $2p_{3/2}$ = 514.9 eV and V $2p_{1/2}$ = 522.0 eV).[15] The selenium peak for the same film shows that there is only one selenium environment present in the films (Figure 3.14). The presence of the two peaks at 54.5 eV and 55.4 eV is due to Se in VSe_2 (Se $3d_{5/2}$ = 54.3 eV and Se $3d_{3/2}$ = 55.1 eV).[16]

3.3.2.6 X-ray Diffraction

The XRD data show that all the films grown from $[V(NMe_2)_4]$ and $^tBu_2Se$ above 300 °C (Figure 3.14), were crystalline and show a good match with the reported pattern for $VSe_{1.97}$ (JCPDS File No. 002-0978). The crystalline films produced show a preferred growth orientation along the (101) and (110) axis. The lattice parameters, calculated as a = 3.35 Å and c = 6.14 Å, were in good agreement with the reported values for VSe_2 , which are a = 3.35 Å and c = 6.12 Å.[17]

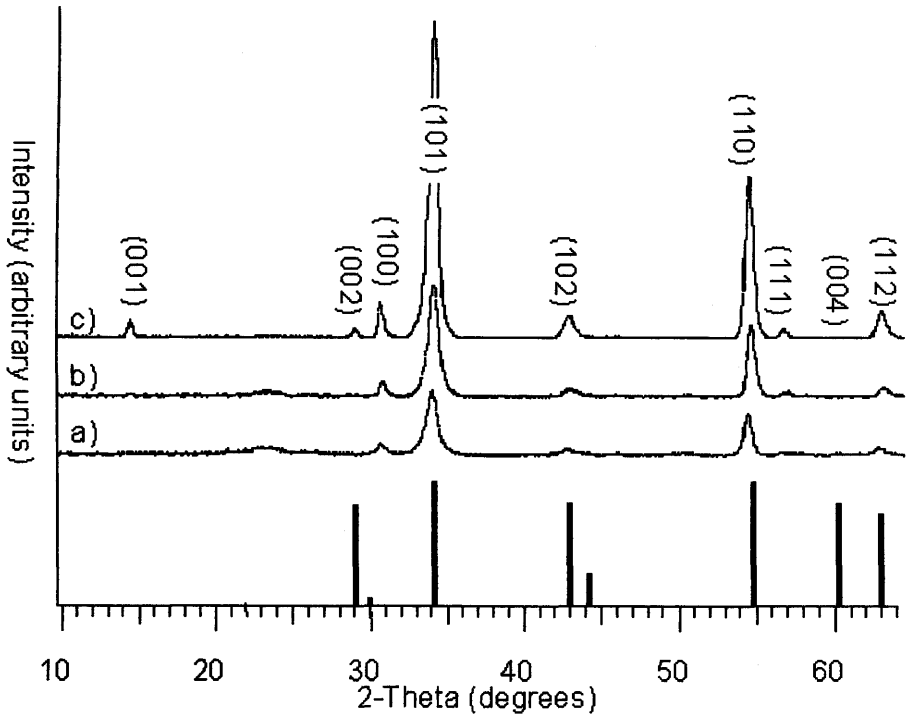

Figure 3.15 XRD patterns obtained for the film formed on glass from the APCVD of $[V(NMe_2)_4]$ and $^tBu_2Se$ at 300 °C (a), 400 °C (b) and 500 °C (c). Literature stick pattern for $VSe_{1.97}$ powder (JCPDS File No. 002-0978) is shown.

3.3.2.7 Raman Microscopy

Raman analysis of all films, irrespective of temperature, showed the same pattern. This was readily identified as the distinctive VSe_2 Raman pattern reported in the literature for the bulk solid, with a strong peak at 206 cm^{-1} (Figure 3.16). This band corresponds to the frequency of the Raman active A_{1g} modes of 1T-VSe_2.[18,19] The presence of two shoulders around 250 and 340 cm^{-1} could match the Raman spectra of the VO_x ($2.0 < x < 2.5$) phase.[14] After one year in air, no change was observed in the Raman spectra of these films indicating that these films are relatively air stable and only the upper layers of the films are oxidized.

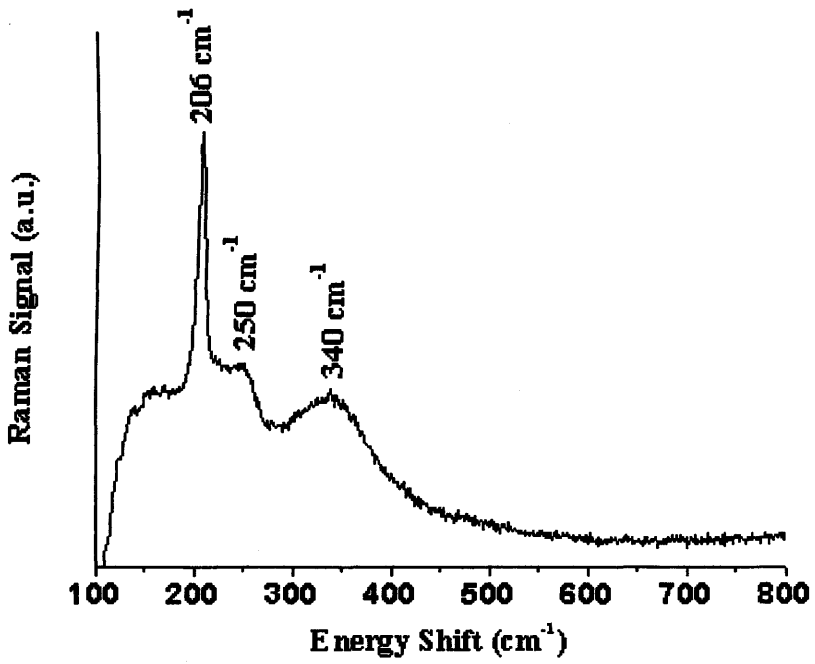

Figure 3.16 Raman pattern obtained for a film produced from the APCVD reaction of $[V(NMe_2)_4]$ with $^tBu_2Se$ at 400 °C.

3.3.2.8 SQUID

The magnetic susceptibility (χ) of a delaminated film produced from $[V(NMe_2)_4]$ and $^tBu_2Se$ at 500 °C shows the drop observed near 110 - 115 K in several magnetic studies of VSe_2 (Figure 3.17).[20,21,22] The drop in χ corresponds to the combination of the onset of the charge density wave (CDW) transition 1T-VSe_2 and the paramagnetic

contribution of the excess of vanadium in $V_{1+x}Se_2$. The shape of the Curie tail suggests that the vanadium species intercalated concentration x in 1T-VSe_2 is less than 0.1 %.[20,23]

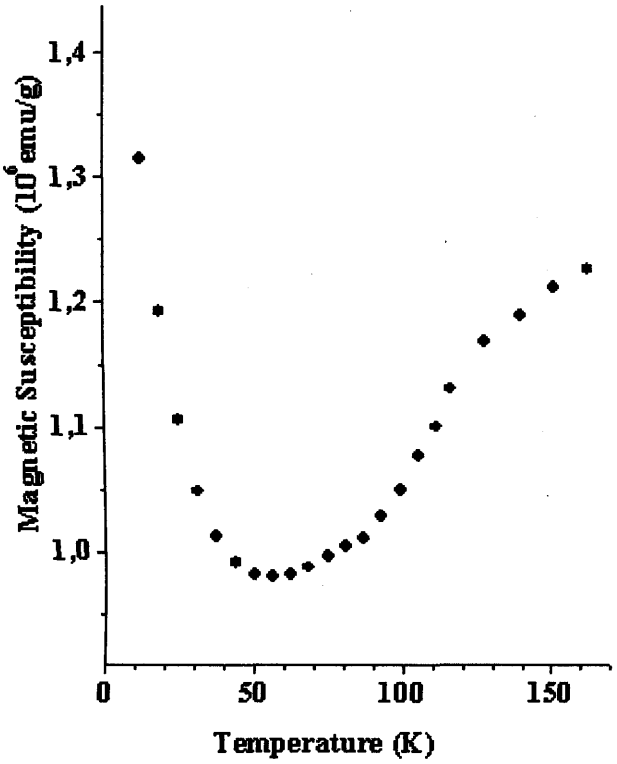

Figure 3.17 Magnetic susceptibility of a film VSe_2 formed from the APCVD of $[V(NMe_2)_4]$ and $^tBu_2Se$ at 500 °C.

3.3.3 Comparison and Discussion

The results show that the vanadium precursor used has a significant effect on the stoichiometry and quality of the films produced. APCVD experiments show that vanadium tetrachloride and vanadium oxychloride were unsuitable precursors for deposition of vanadium selenide thin films. The use of VCl_4 did not deposit a thin film, while $VOCl_3$ led to vanadium rich films with significant contamination by chlorine and the co-formation of a vanadium oxide. Vanadium tetrakisdimethylamide was found to be a better precursor for the APCVD of vanadium selenide thin films. The films produced from $[V(NMe_2)_4]$ and $^tBu_2Se$ had a selenium to vanadium ratio close to 2, and XRD and Raman analysis were consistent with the formation of VSe_2. These results can be compared to previous APCVD work on vanadium phosphide using these three

different precursors.[24,25] From a series of attempts using $Cy^{hex}PH_2$ or $(Me_3Si)_3P$, it was found that no reliable film could be produced using VCl_4 and very thin films with limited coverage were produced using $VOCl_3$. Moreover, the films could be obtained only at the highest temperature (ca. 600 °C) with a V to P ratio between 0.6 and 0.8. On the other hand, APCVD of $[V(NMe_2)_4]$ and $Cy^{hex}PH_2$ led to uniform reflective silver films with a stoichiometry close to the one expected for VP.

Vanadium tetrakisdimethylamide has been used as a precursor to vanadium nitride films. However no nitrogen was observed within the VSe_2 films formed by reaction of $^tBu_2Se$ and $[V(NMe_2)_4]$. This precursor along with other metal dialkylamides, has the advantage of volatility for CVD studies. It also readily loses the dimethylamide group in dual-source CVD reactions. In the reactions studied here it is tempting to write a simple equation for the process, in which $[V(NMe_2)_4]$ reacts with tertiarybutylselenol (^tBuSeH) to form gaseous dimethylamide ($HNMe_2$), isobutene ($^iC_4H_8$) and VSe_2. However, it has not been possible to gather direct evidence for this hypothesis:

$$^tBu_2Se \rightarrow {}^tBuSeH + {}^iC_4H_8 \qquad \textbf{(3.1)}$$

$$[V(NMe_2)_4] + 2\,{}^tBuSeH \rightarrow VSe_2 + 4\,HNMe_2 + 2\,{}^iC_4H_8 \qquad \textbf{(3.2)}$$

The $[V(NMe_2)_4]$ is a better precursor then $VOCl_3$ for the formation of VSe_2 films. Although $VOCl_3$ does function in this role, the product from the CVD seems to be a composite of VSe_2 and a VO_x or VO_xCl_y phase – hence the V=O bond is not completely lost in the process. The vanadium precursor $VOCl_3$ has been succesfully used in CVD, however, primarily for the formation of oxide films[14,26,27,28] and oxynitride films[29] at temperatures below 650 °C. Nevertheless, temperatures above 800 °C were required when using $VOCl_3$ to fully eliminate oxygen and produce pure vanadium nitride[30,31] or vanadium boride thin films.[32,33]

3.4 Niobium Diselenide Films

In an attempt to deposit niobium diselenide films, niobium pentachloride ($NbCl_5$) and ditertiarybutylselenide ($^tBu_2Se$) were used in an APCVD reaction. Previous studies have shown that despite its high melting point of 205 °C, $NbCl_5$ is an efficient CVD precursor and has been used to grow Nb_2O_5 and NbS_2 thin films.[34,35] Other successful uses of $NbCl_5$ in a CVD process comprise the deposition of niobium diboride,[36] niobium nitrides,[37] and niobium germanium.[38]

3.4.1.1 Films from $NbCl_5$ and $^tBu_2Se$: Reaction Conditions

Niobium selenide films were produced from the APCVD reaction of niobium pentachloride ($NbCl_5$) and ditertiarybutylselenide ($^tBu_2Se$) between 250 and 600 °C. During the reaction, the bubbler temperatures and the flow rates were kept constant to 90 °C and 0.5 $L.min^{-1}$ (67.4 $mmol.min^{-1}$) for the $^tBu_2Se$ bubbler and to 210 °C and 2.0 $L.min^{-1}$ (47.8 $mmol.min^{-1}$) for the $NbCl_5$ bubbler. The temperature of the mixing-chamber was kept constant at 275 °C and the deposition time was one minute for all the experiments.

3.4.1.2 Appearance, Substrate Coverage and Adherence of the Films

The APCVD reaction of $NbCl_5$ with $^tBu_2Se$ led to the deposition of films on both top plate and bottom substrate. The extent of the film coverage was dependent of the deposition temperature. Only the first six centimetres of the bottom substrate were coated at a deposition temperature of 600 °C, indicating a mass transport limited reaction, whilst the whole substrate was coated with uniform thickness at 300 °C. At a deposition temperature above 600 °C, the films produced from $^tBu_2Se$ and $NbCl_5$ were dark-green and powdery. They failed the Scotch tape test and the scratch test but were insoluble in the common organic solvents, only slowly decomposed in diluted nitric acid or diluted bleach, and were stable in air. At deposition temperatures below 550 °C, the films had a dark-black matt appearance; they passed the Scotch tape test, but were scratched with a steel scalpel. Due to their porous nature, the films grown from $NbCl_5$

and $^{t}Bu_2Se$ at all the different reaction temperatures showed an exceptionally small water contact angle (10°).

3.4.1.3 Scanning Electron Microscopy

The SEM images for the films deposited at the onset of deposition 300 °C, show *ca.* 0.2 μm plates in a perpendicular orientation to the substrate (Figure 3.18). The SEM images for the films deposited at substrate temperatures between 400 and 600 °C show a series of hexagonal platelets which become longer and thicker with increasing deposition temperature. The average length of the platelets was 0.2 μm for the films deposited at 400 °C, up to 0.6 μm at 600 °C. This change in platelet size can be related to faster growth kinetics and smaller numbers of nucleation sites at the higher temperatures.

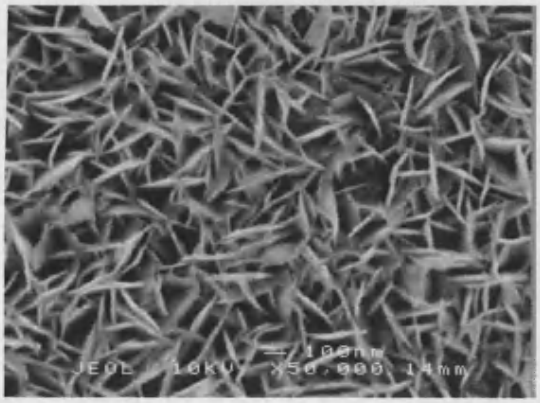

a) 300 °C

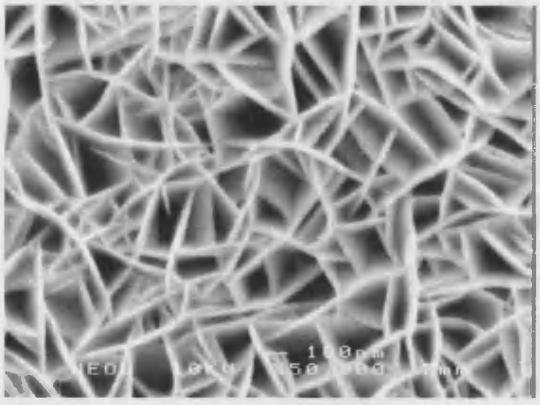

b) 500 °C

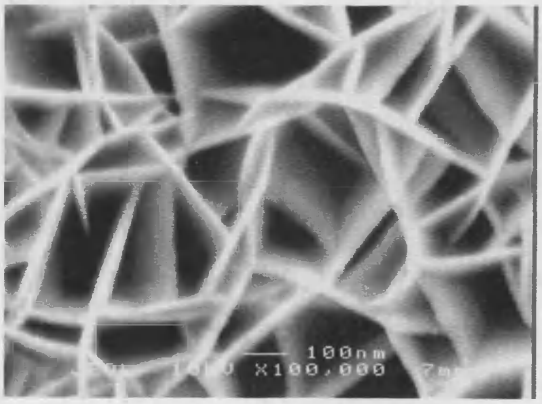

c) 600 °C

Figure 3.18 Scanning electron micrographs of the films produced from the APCVD reaction of $NbCl_5$ with $^{t}Bu_2Se$ at 300 and 500 °C.

3.4.1.4 Energy Dispersive X-ray Analysis

EDAX analysis of the films produced from the reaction of $NbCl_5$ and $^tBu_2Se$ at a deposition temperature of 600 °C showed the Nb : Se ratio expected for $NbSe_2$ (Table 3.5). No chlorine, carbon or other contamination was found in these films. The films deposited at substrate temperatures below 500 °C were selenium rich with a niobium to selenium ratio of 1 : 2.5 at 350, 450 and 500 °C. This could indicate the formation of $NbSe_3$ or $NbSe_4$, or the presence of elemental selenium. No chlorine contamination was found in the films except those produced at the very lowest deposition temperature (ca. 300 °C) - and then it was at trace levels ca. 1 atom%.

Table 3.5 EDAX, Raman and X-ray diffraction data for the films produced by APCVD reaction of ditertiarybutylselenide with $NbCl_5$.

Deposition Temperature	EDAX	XRD; lattice constant in Å	Raman
300 °C	$NbSe_{2.4}$	2H-$NbSe_2$; a = 3.36 Å, c = 12.47 Å	182 + 245 + 310 cm^{-1}
350 °C	$NbSe_{2.5}$	2H-$NbSe_2$; a = 3.37 Å, c = 12.59 Å	183 + 248 + 309 cm^{-1}
400 °C	$NbSe_{2.6}$	2H-$NbSe_2$; a = 3.42 Å, c = 12.56 Å	184 + 248 + 310 cm^{-1}
450 °C	$NbSe_{2.5}$	2H-$NbSe_2$; a = 3.36 Å, c = 12.63 Å	183 + 247 + 309 cm^{-1}
500 °C	$NbSe_{2.5}$	2H-$NbSe_2$; a = 3.41 Å, c = 12.63 Å	183 + 246 + 309 cm^{-1}
600 °C	$NbSe_2$	2H-$NbSe_2$; a = 3.44 Å, c = 12.58 Å	2H-$NbSe_2$

3.4.1.5 X-ray Photoelectron Spectroscopy

X-ray photoelectron spectroscopy of the film produced at 600 °C from $^tBu_2Se$ and $NbCl_5$ revealed the presence of two different niobium environments in the film (Figure 3.19). The peaks at 203.2 eV and 205.9 eV can be assigned to the Nb $3d_{5/2}$ and Nb $3d_{3/2}$ peaks respectively of niobium diselenide (Nb $3d_{5/2}$ = 203.4 eV and Nb $3d_{3/2}$ = 206.1 eV).[39] Whereas the peaks at 207.3 eV and 210.0 eV can be assigned to the Nb $3d_{5/2}$ and Nb $3d_{3/2}$ peaks of Nb_2O_5 (Nb $3d_{5/2}$ = 207.6 eV and Nb $3d_{3/2}$ = 210.2 eV).[40] This data suggest that the surface of the film is partially oxidised. The XPS of the

selenium 3d peak for the same $NbSe_2$ film shows that there are three selenium environments present (Figure 3.19). The peaks at 52.9 eV and 53.8 eV can be assigned to the Se $3d_{5/2}$ and Se $3d_{3/2}$ peaks respectively of the niobium diselenide. The two doublet peaks at 54.1 eV, 55.0 eV and 54.6 eV, 55.5 eV can be assigned to elemental selenium and selenium dioxide respectively.

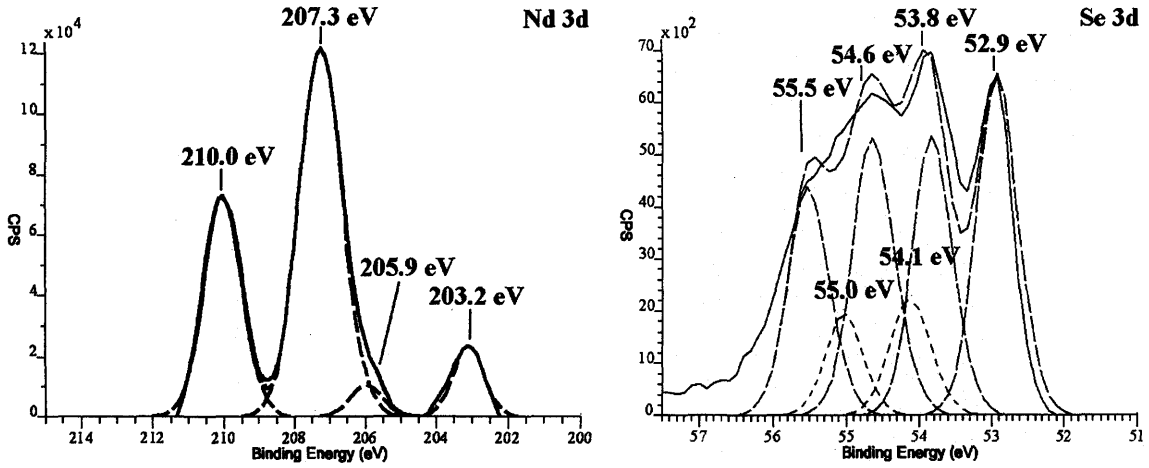

Figure 4.19 XPS spectra of the Nd 3d and Se 3d peaks from the surface of a film deposited from the APCVD of $NbCl_5$ and $^tBu_2Se$ at 600 °C. The uppermost solid curves show the experimental data and the dashed lines show a best fit.

3.4.1.6 X-ray Diffraction

XRD of the films showed the reflections to match the reference spectrum for 2H-$NbSe_2$ (JCPDS File No. 018-0923) (Figure 3.20). The films produced at 600 °C were highly crystalline. Interestingly measuring the XRD pattern sequentially from the leading edge of the film until the back of the film showed that the preferred orientation became significantly more pronounced with distance from the reactor inlet. No preferential orientation was noticed in the first centimetre of the coating, the diffraction peaks gave the literature intensity stick pattern. Very strong preferential growth along the (002) direction was shown in the next few centimetres. This preferred orientation effects suggest that depletion in reagents leads to a slightly altered growth mechanism. Notably no preferential orientation was noticed in the films grown at lower substrate temperature. The indexed cell constants found for the films grown at 600 °C, a = 3.44 Å and c = 12.58 Å, compare well with the literature for hexagonal $NbSe_2$ a = 3.44 Å and c = 12.55 Å. The films grown at lower substrate temperatures all matched the literature

diffraction patterns for 2H-$NbSe_2$ with the anticipated intensities and peak positions, however a detailed analysis of the cell constants indicated that they all tended to have slightly smaller *a* values than stochiometric $NbSe_2$.

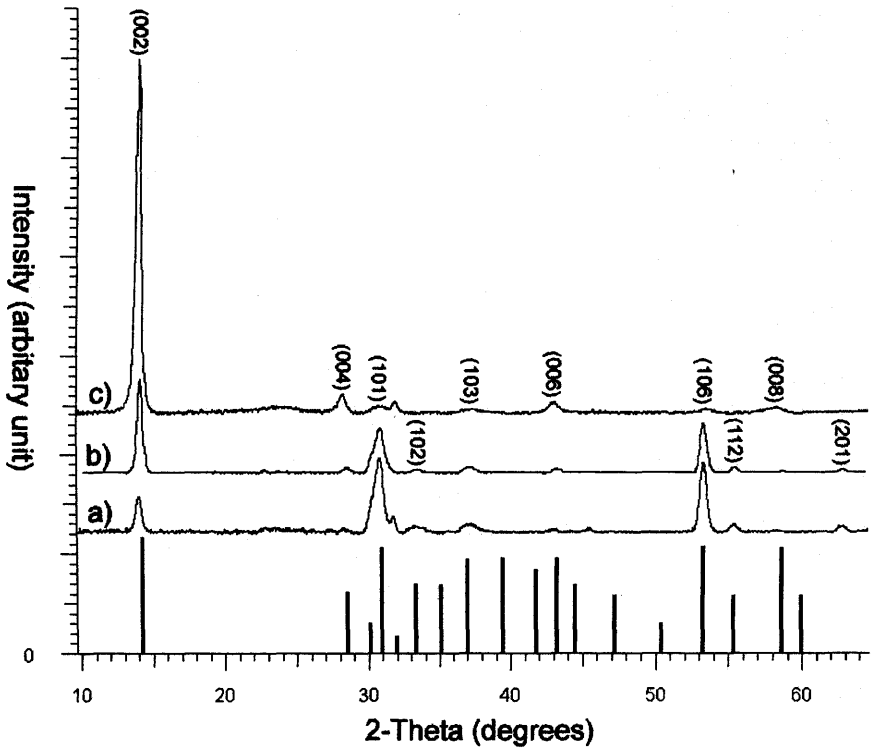

Figure 3.20 XRD patterns obtained for the film formed on glass from the APCVD of $NbCl_5$ and $^tBu_2Se$ at 300 °C (a), 400 °C (b) and 500 °C (c). Literature stick pattern for $NbSe_2$ powder (JCPDS File No. 018-0923) is shown.

3.4.1.7 Raman Microscopy

Raman analysis of the films produced from $NbCl_5$ and $^tBu_2Se$ at 600 °C was identified as the distinctive 2H-$NbSe_2$ Raman pattern from the literature with a wide peak at 182 cm^{-1} and a strong peak at 228 cm^{-1} with a shoulder at 238 cm^{-1} (Figure 3.21).[41,42,43]

Raman analysis of the films produced from $NbCl_5$ and $^tBu_2Se$ at 400 °C showed two strong bands around 182 cm^{-1} and 245 cm^{-1} and a smaller peak at 310 cm^{-1} (Figure 3.22). This is quite different to that seen for the films grown at higher temperature and could indicate the formation of a new phase. However as the XRD patterns match up to the 2H polytype the difference in the Raman pattern are probably attributable to the

excess selenium found by EDAX, which seems to be tolerated within the same structure type.

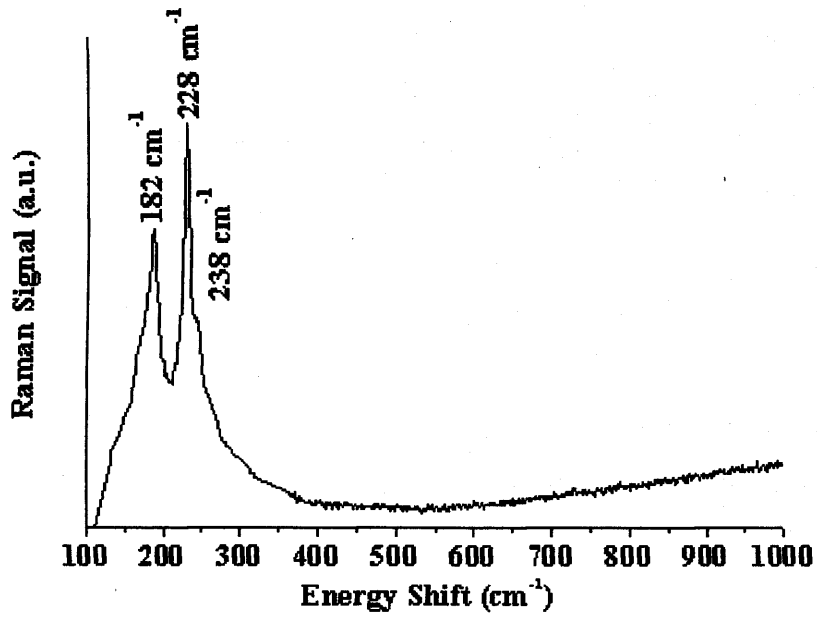

Figure 3.21 Raman pattern obtained for a film produced from the APCVD reaction $NbCl_5$ with $^tBu_2Se$ at 600 °C.

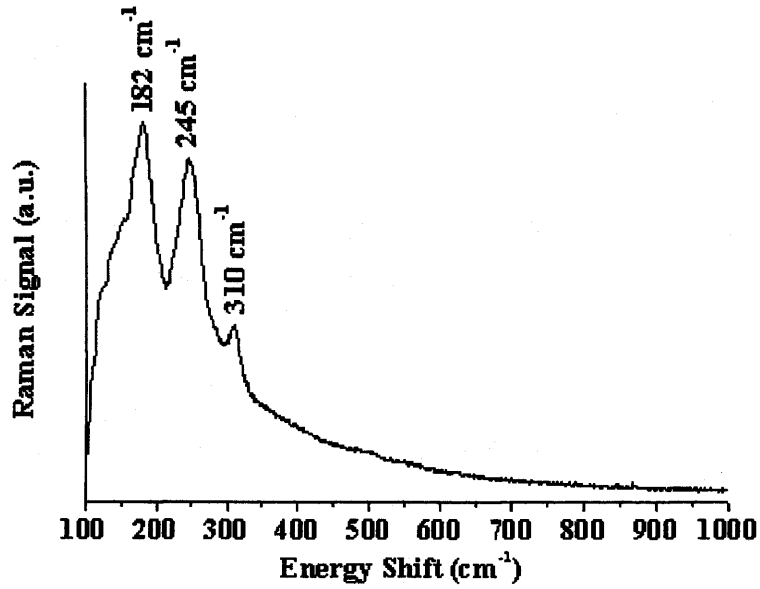

Figure 3.22 Raman pattern obtained for a film produced from the APCVD reaction of $NbCl_5$ with $^tBu_2Se$ at 400 °C.

3.4.1.8 Mass Spectrometry

The gaseous by-products of the APCVD reaction of $NbCl_5$ and $^tBu_2Se$ at 600 °C were analysed by mass-spectrometry. $^tBu_2Se$ is known to start to decompose at a temperature as low as 150 °C. The dissociation of $^tBu_2Se$ starts with a β-elimination mechanism forming the intermediate species tertiarybutylselenol (^tBuSeH) and isobutene ($^iC_4H_8$).

$$^tBu_2Se \rightarrow {}^tBuSeH + {}^iC_4H_8 \quad \textbf{(3.3)}$$

Then, ^tBuSeH can decompose to release elemental selenium and isobutane ($^iC_4H_{10}$) or a second β-elimination mechanism occurs to form H_2Se and $^iC_4H_8$.

$$^tBuSeH \rightarrow Se + {}^iC_4H_{10} \quad \textbf{(3.4)}$$

$$^tBuSeH \rightarrow H_2Se + {}^iC_4H_8 \quad \textbf{(3.5)}$$

A wide variety of fragments are produced during the ionisation of $^tBu_2Se$ in the mass-spectrometer. The predominant fragments appear at the *m/z* values 39, 41, 43, 56, 57, 78, 192 and 194. Many of these *m/z* values overlap with the *m/z* values of the possible decomposition products like $^iC_4H_8$: $m = 56$, $^iC_4H_{10}$: $m = 58$, Se: $m = 78$, H_2Se: $m = 80$ and ^tBuSeH: $m = 137$. However, some values such as $m/z = 42, 43$ ($^iC_4H_{10}$) and $m/z = 55, 56$ ($^iC_4H_8$) have a weak or no cross sensitivity. The products of the APCVD reaction of $NbCl_5$ with $^tBu_2Se$ give peaks at $m/z = 35, 36, 37, 38$ (HCl), $m/z = 70, 72, 74$ (Cl_2) and $m/z = 29, 50, 51, 92, 93, 94$ (^tBuCl).

Analysis of the gases after passing throught the mixing-chamber at 275 °C (Figure 3.23) revealed that the selenium precursor $^tBu_2Se$ has started to decompose before entering the reactor chamber. The peaks at $m/z = 55, 56$ ($^iC_4H_8$) indicate the dissociation of $^tBu_2Se$ into ^tBuSeH and $^iC_4H_8$. The presence of a peak at $m/z = 77$ (Se), also indicates that a small amount of the tertiarybutylselenol formed has started to

decompose to elemental selenium and $^{i}C_4H_{10}$. No indication of a pre-reaction between $NbCl_5$ and $^{t}Bu_2Se$ was observed.

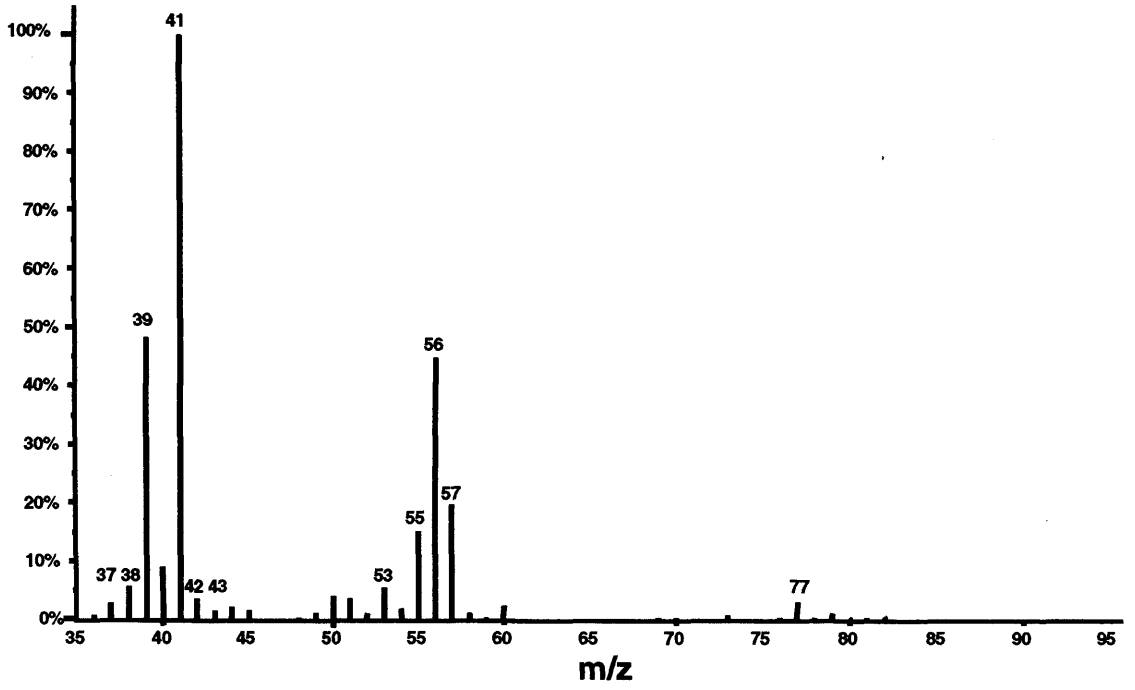

Figure 3.23 Mass spectrum of the gas produced from the reaction of $NbCl_5$ with $^{t}Bu_2Se$ in the mixing chamber at 275 °C.

The analysis of the by-products of the APCVD reaction of $NbCl_5$ and $^{t}Bu_2Se$ 600 °C confirmed the formation of $^{i}C_4H_8$ (*m/z* = 55, 56) and $^{i}C_4H_{10}$ (*m/z* = 42, 43) (Figure 3.24). The intensities of the peaks observed at *m/z* = 35, 36, 37, 38 (HCl), *m/z* = 70, 72, 74 (Cl_2) and *m/z* = 29, 50, 51, 92, 93, 94 ($^{t}BuCl$) indicate that the chlorine is more likely eliminated by forming $^{t}BuCl$ or HCl rather than Cl_2.

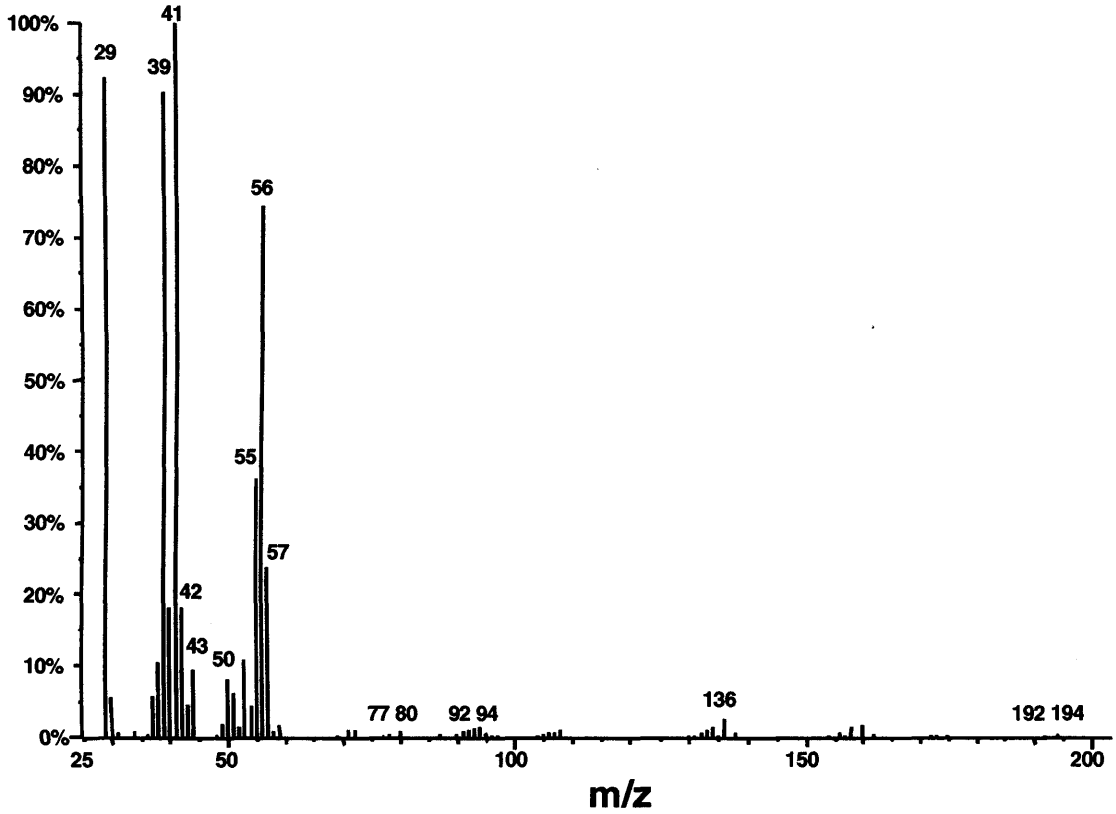

Figure 3.24 Mass spectrum of the gaseous by-product of the APCVD reaction of $NbCl_5$ with $^tBu_2Se$ at 600 °C.

3.4.2 Discussion

The results show that the APCVD reaction of $NbCl_5$ and $^tBu_2Se$ was a suitable route for the formation of niobium diselenide thin films when deposited above 550 °C. Below substrate temperatures of 550 °C, the films grown were all superstoichiometric, with a Nb to Se ratio between 1 : 2.4 and 1 : 2.6. X-ray diffraction, Raman and spot EDX analysis did not detect any free selenium metal in these films, despite this XPS showed the presence of elemental selenium in the films. Furthermore, none of these techniques showed the presence of other niobium selenide phases, such as $NbSe_3$ or $NbSe_4$. No other elements were found in the films except for a slight surface oxidation of the first few nanometres of the films. As the films grown at 300 – 550 °C were all exceptionally similar if not the same as the 2H-$NbSe_2$ polytype by X-ray diffraction, it is logical to assume that the excess selenium is embedded and intercalated within the structure. The interface between the Se-Nb-Se layers is known to have vacant sites that

allow intercalation of atoms, thus the formula of the films is $NbSe_{2+x}$ (x = 0.4 – 0.6). The films had a different unit cell size than the literature values with the *a* and *c* axis slightly smaller. Intuitively though one would expect a large increase in the cell parameters with excess selenium incorporation. A further explanation is that an amorphous phase is present with a higher selenium content that does not show up on the XRD, Raman or XPS analysis; however, given the breadth of analysis completed, this seems unlikely. Hence, the lower-temperature films were consistent with the formation of the 2H-$NbSe_2$ structure with some incorporated selenium. No evidence of any literature reference on this type of material has been reported previously.

Interestingly the Raman patterns were quite revealing and supportive of a similar structure type, having a slightly different pattern to that seen for the films grown at 600 °C, which exactly matched the literature pattern for 2H-$NbSe_2$. These results can be compared to previous APCVD work on niobium sulfide using niobium pentachloride and 1,2-ethanedithiol.[3,44] In this case, superstoichiometric $NbS_{2.4}$ films were formed at the lowest substrate temperature (ca. 350 °C and 400 °C). The Raman pattern of these films showed extra peaks at 240 and 544 cm^{-1}, while the peak corresponding to the A_{1g} Raman mode was absent.

3.5 Mixed Titanium-Niobium Diselenide Films

Following the successful use of titanium tetrachloride ($TiCl_4$) and niobium pentachloride ($NbCl_5$) with ditertiarybutylselenide ($^tBu_2Se$) to produce titanium diselenide ($TiSe_2$) and niobium diselenide ($NbSe_2$) thin films respectively, the APCVD reaction of $TiCl_4$, $NbCl_5$ and $^tBu_2Se$ was studied in an attempt to deposit mixed titanium-niobium diselenide films ($Ti_{1-x}Nb_xSe_2$).

3.5.1.1 Films from $TiCl_4$, $NbCl_5$ and $^tBu_2Se$: Reaction Conditions

Titanium-niobium selenide films were produced from the APCVD reaction of titanium tetrachloride $TiCl_4$, niobium pentachloride $NbCl_5$ and ditertiarybutylselenide ($^tBu_2Se$) for different flow rate conditions. During the APCVD reaction, the $TiCl_4$, $NbCl_5$ and $^tBu_2Se$ bubblers were respectively kept constant to 80 °C, 210 °C and 90 °C,

and the temperature of the reaction chamber was maintained at 550 °C. The flow rate through the $^{t}Bu_2Se$ bubbler was kept constant to 2.0 L min^{-1} (29.3 $mmol.min^{-1}$), while the range of flow rates of nitrogen through the $TiCl_4$ and $NbCl_5$ bubblers was between 0 – 2.0 L min^{-1}. These conditions correspond to a $TiCl_4$ molar-flow of up to 18.3 $mmol.min^{-1}$ and a maximum $NbCl_5$ molar-flow of 48.1 $mmol.min^{-1}$ (Table 3.6). Deposition times for all experiments was one minute.

3.5.1.2 Appearance, Substrate Coverage and Adherence of the films

The APCVD reaction of $TiCl_4$, $NbCl_5$ with $^{t}Bu_2Se$ at 550 °C led to the deposition of dark-purple to dark-green films depending on the flow rate conditions. For a $NbCl_5$ to $TiCl_4$ molar-flow ratio greater than 48.1 $mmol.min^{-1}$: 1.8 $mmol.min^{-1}$, the films produced were mostly dark-green, whilst films grown for smaller ratios were dark-purple. The growth profile of the films was concentrated towards the leading edge of the substrate, indicating a mass transport limited reaction. The extent of the film coverage was not found to be dependent of the flow-rate ratios used. The films produced failed the Scotch tape test and were easily scratched with a steel scalpel. They were found to be soluble in common organic solvents and quickly decomposed in nitric acid and bleach.

3.5.1.3 Scanning Electron Microscopy

Scanning electron microscopy of the films grown from $TiCl_4$, $NbCl_5$ with $^{t}Bu_2Se$ showed the presence of two different morphologies in the films (Figure 3.25). The first morphology, which was composed of 1 μm plate like crystallites orientated perpendicularly to the substrate, was predominant for the highest $NbCl_5$ to $TiCl_4$ molar-flow ratio conditions. The second morphology observed in the films, was composed of longer and thicker plates which appeared brighter by SEM. The average length of the platelets was 2 μm, notably the plates had also a degree of texturing with some preferred growth perpendicular to the substrate. As the $NbCl_5$ to $TiCl_4$ molar-flow ratio decreased, the proportion of large and bright plates was observed to increase. This morphological segregation in the films is likely to indicated the co-formation of $TiSe_2$ and $NbSe_2$ rather than the mixed compounds $Ti_{1-x}Nb_xSe_2$. Considering that the smallest plates were predominant for the highest concentrations of $NbCl_5$ entering the reaction

chamber, and the biggest plates for the lowest concentrations of $NbCl_5$ entering the reaction chamber, the smallest plates would likely be composed of $NbSe_2$ and the biggest ones, appearing brighter by SEM, to be $TiSe_2$. These plates have been previously observed while studying the APCVD reactions of $TiCl_4$ with $^tBu_2Se$ and $NbCl_5$ with $^tBu_2Se$. At 600 °C, the APCVD reaction of $NbCl_5$ and $^tBu_2Se$ produced 0.6 μm plates-like crystallites of metallic $NbSe_2$, which are similar in size and shape to the 1 μm platelets produced here. The APCVD reaction of $TiCl_4$ and $^tBu_2Se$ produced similar 2 μm plates at 600 °C as the one observed here. Moreover, the $TiSe_2$ plates are expected to appear brighter by SEM than the $NbSe_2$ plates, as $TiSe_2$ is semimetallic and $NbSe_2$ is metallic. This was later confirmed by point WDX analysis.

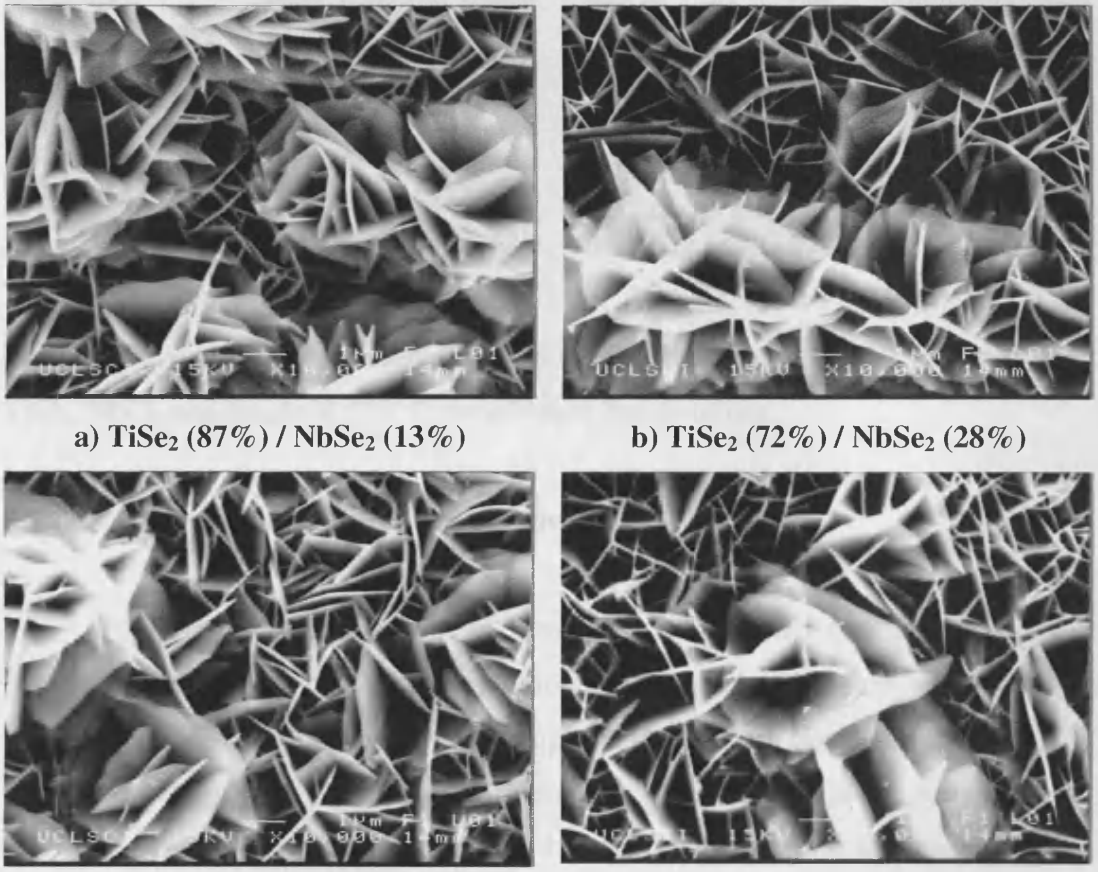

a) $TiSe_2$ (87%) / $NbSe_2$ (13%) **b) $TiSe_2$ (72%) / $NbSe_2$ (28%)**

c) $TiSe_2$ (61%) / $NbSe_2$ (39%) **d) $TiSe_2$ (50%) / $NbSe_2$ (50%)**

Figure 3.25 Scanning electron micrographs of the films produced from the APCVD of $TiCl_4$, $NbCl_5$ and $^tBu_2Se$ at 550 °C for different compositions.

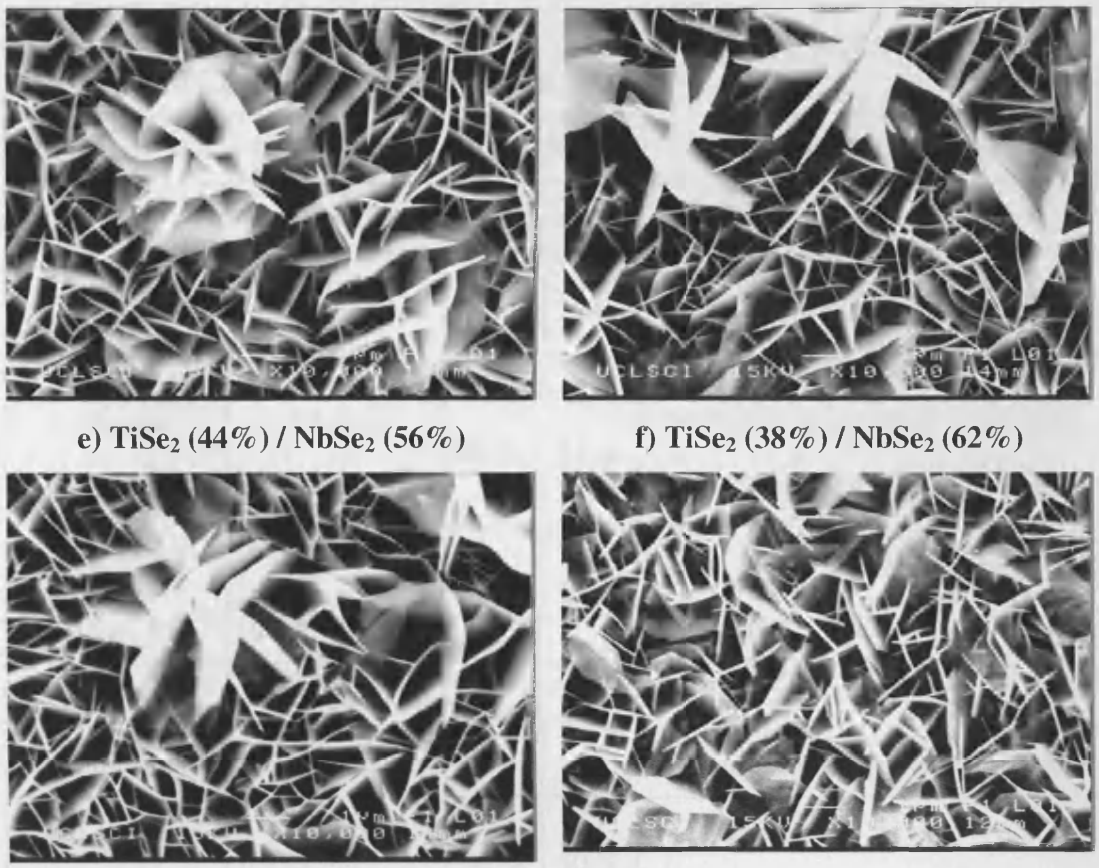

e) $TiSe_2$ (44%) / $NbSe_2$ (56%) **f) $TiSe_2$ (38%) / $NbSe_2$ (62%)**

g) $TiSe_2$ (33%) / $NbSe_2$ (67%) **h) $TiSe_2$ (10%) / $NbSe_2$ (90%)**

Figure 3.25 Scanning electron micrographs of the films produced from the APCVD of $TiCl_4$, $NbCl_5$ and $^tBu_2Se$ at 550 °C for different compositions.

3.5.1.4 Wavelength dispersive X-ray analysis

Wavelength dispersive X-ray analysis of the films showed that they all contained titanium, niobium and selenium with a ratio that depended on the flow rates conditions used (Table 3.6). Spot analysis of the biggest and brightest plates observed by SEM confirmed that they were composed of $TiSe_2$, while the smallest plates were composed of $NbSe_2$. The overall stoichiometry of the film could then be written as $(TiSe_2)_{1-x}(NbSe_2)_x$ rather than $Ti_{1-x}Nb_xSe_2$. Change of flow rates conditions during the deposition allowed mixtures of $TiSe_2$ and $NbSe_2$ in different concentrations. The $NbCl_5$ to $TiCl_4$ molar-flow ratio of 48.1 mmol.min^{-1} : 0.9 mmol.min^{-1} led to the formation of films with the following composition $(TiSe_2)_{0.1}(NbSe_2)_{0.9}$, while a $NbCl_5$ to $TiCl_4$ molar-flow ratio of 36.1 mmol.min^{-1} : 7.4 mmol.min^{-1} produced $(TiSe_2)_{0.87}(NbSe_2)_{0.13}$.

Table 3.6 WDX and X-ray diffraction data for the films produced by APCVD reaction of $NbCl_5$ and $TiCl_4$ with $^tBu_2Se$ at 600 °C.

Gas Phase Ratio $TiCl_4$: $NbCl_5$		**EDAX**		**XRD; lattice constant in Å**
$TiCl_4$	$NbCl_5$	$TiSe_2$	$NbSe_2$	
2 L.min^{-1} 18.3 mmol.min^{-1}	0 L.min^{-1} 0 mmol.min^{-1}	100 %	0 %	1T-$TiSe_2$; a = 3.51 Å, c = 6.00 Å -
0.8 L.min^{-1} 7.4 mmol.min^{-1}	1.5 L.min^{-1} 36.1 mmol.min^{-1}	87 %	13 %	1T-$TiSe_2$; a = 3.52 Å, c = 5.98 Å 2H-$NbSe_2$; a = 3.41 Å, c = 12.58 Å
0.7 L.min^{-1} 6.4 mmol.min^{-1}	1.5 L.min^{-1} 36.1 mmol.min^{-1}	72 %	28 %	1T-$TiSe_2$; a = 3.50 Å, c = 5.99 Å 2H-$NbSe_2$; a = 3.41 Å, c = 12.60 Å
0.6 L.min^{-1} 5.5 mmol.min^{-1}	1.5 L.min^{-1} 36.1 mmol.min^{-1}	61 %	39 %	1T-$TiSe_2$; a = 3.51 Å, c = 6.00 Å 2H-$NbSe_2$; a = 3.41 Å, c = 12.60 Å
0.5 L.min^{-1} 4.6 mmol.min^{-1}	1.5 L.min^{-1} 36.1 mmol.min^{-1}	50 %	50 %	1T-$TiSe_2$; a = 3.51 Å, c = 6.00 Å 2H-$NbSe_2$; a = 3.44 Å, c = 12.61 Å
0.4 L.min^{-1} 3.7 mmol.min^{-1}	1.5 L.min^{-1} 36.1 mmol.min^{-1}	44 %	56 %	1T-$TiSe_2$; a = 3.51 Å, c = 5.98 Å 2H-$NbSe_2$; a = 3.42 Å, c = 12.58 Å
0.3 L.min^{-1} 2.8 mmol.min^{-1}	1.5 L.min^{-1} 36.1 mmol.min^{-1}	38 %	62 %	1T-$TiSe_2$; a = 3.50 Å, c = 5.99 Å 2H-$NbSe_2$; a = 3.44 Å, c = 12.59 Å
0.3 L.min^{-1} 2.8 mmol.min^{-1}	2 L.min^{-1} 48.1 mmol.min^{-1}	33 %	67 %	1T-$TiSe_2$; a = 3.49 Å, c = 5.99 Å 2H-$NbSe_2$; a = 3.44 Å, c = 12.60 Å
0.2 L.min^{-1} 1.8 mmol.min^{-1}	2 L.min^{-1} 48.1 mmol.min^{-1}	20 %	80 %	1T-$TiSe_2$; a = 3.52 Å, c = 6.00 Å 2H-$NbSe_2$; a = 3.41 Å, c = 12.58 Å
0.1 L.min^{-1} 0.9 mmol.min^{-1}	2 L.min^{-1} 48.1 mmol.min^{-1}	10 %	90 %	1T-$TiSe_2$; a = 3.50 Å, c = 5.99 Å 2H-$NbSe_2$; a = 3.44 Å, c = 12.58 Å
0 L.min^{-1} 0 mmol.min^{-1}	2 L.min^{-1} 48.1 mmol.min^{-1}	0 %	100 %	- 2H-$NbSe_2$; a = 3.43 Å, c = 12.58 Å

3.5.1.5 X-ray Diffraction

XRD analysis of the films produced from the APCVD reaction of $TiCl_4$, $NbCl_5$ and $^tBu_2Se$ showed the presence of two phases. The reflections observed matched the reference spectrum for 1T-$TiSe_2$ (JCPDS File No. 30-1383) and 2H-$NbSe_2$ (JCPDS File No. 18-0923). 1T-$TiSe_2$ being the major phase observed for the richer films in titanium, and 2H-$NbSe_2$ when the films were niobium rich (Figure 3.26). The lattice parameters (Table 3.6) of the $TiSe_2$ and $NbSe_2$ phases observed in all the films produced compared well with the corresponding literature lattice parameters of 1T-$TiSe_2$ (a = 3.54 Å; c = 6.00 Å) and 2H-$NbSe_2$ (a = 3.44 Å; c = 12.55 Å) indicating that it is very unlikely that Nb or Ti are incorporated within each others lattice. No preferential orientation was noticed in the 1T-$TiSe_2$ phase of the $(TiSe_2)_{1-x}(NbSe_2)_x$ films, this compares well with the XRD pattern observed during the APCVD reaction of $TiCl_4$ and $^tBu_2Se$. However the preferred orientation of the 2H-$NbSe_2$ phase in $(TiSe_2)_{1-x}(NbSe_2)_x$ was quite different to the one observed in pure $NbSe_2$ thin films. While the APCVD reaction of $NbCl_5$ and $^tBu_2Se$ produced $NbSe_2$ thin films strongly orientated along the (002) direction, the $NbSe_2$ crystals showed preferred orientation along the (002), (101), (102) and (106) directions.

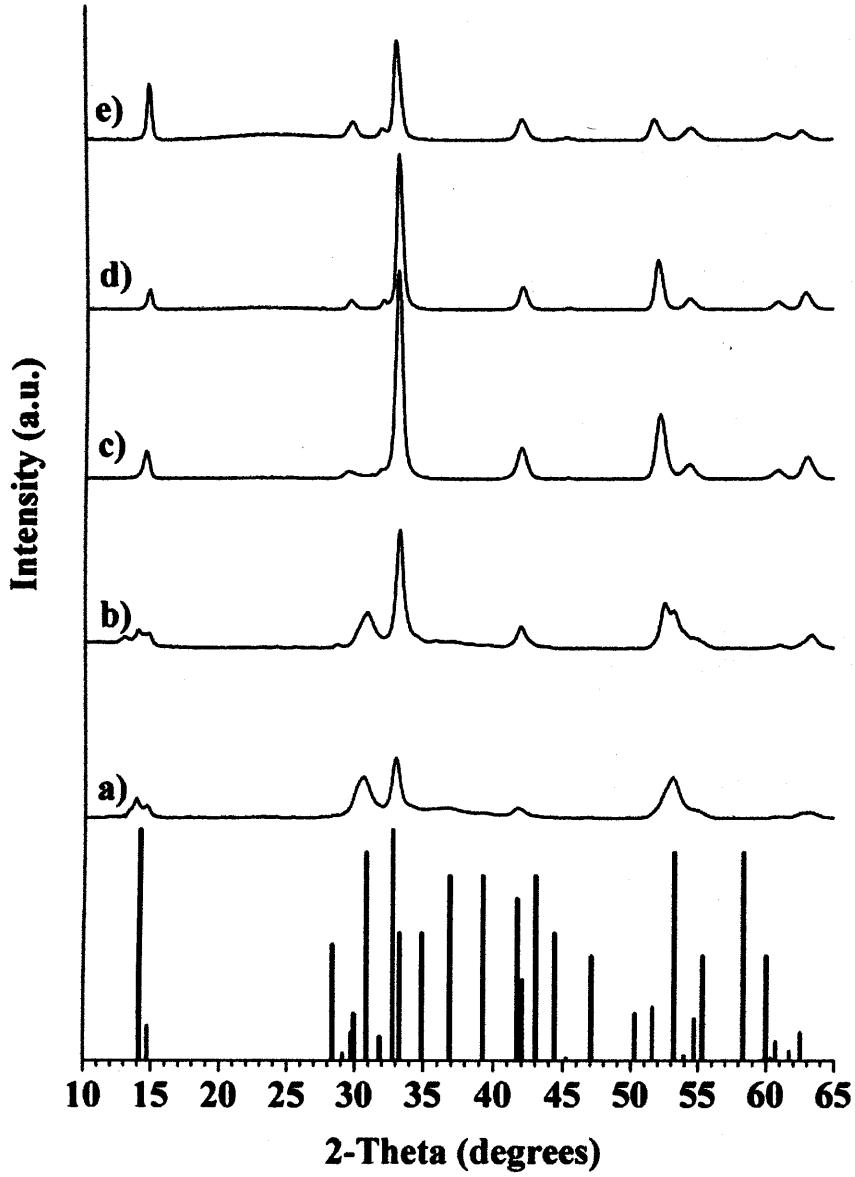

Figure 3.26 XRD patterns obtained for the films formed on glass from the APCVD of $TiCl_4$, $NbCl_5$ and $^tBu_2Se$ at 550 °C for different compositions: $(TiSe_2)_{0.1}(NbSe_2)_{0.9}$ (a), $(TiSe_2)_{0.2}(NbSe_2)_{0.8}$ (b), $(TiSe_2)_{0.61}(NbSe_2)_{0.39}$ (c), $(TiSe_2)_{0.72}(NbSe_2)_{0.28}$ (d) and $(TiSe_2)_{0.87}(NbSe_2)_{0.13}$ (e). Literature stick patterns for $NbSe_2$ (black) and $TiSe_2$ (grey) powders (JCPDS Files No. 018-0923 and 030-1383) are shown.

3.5.1.6 Raman Microscopy

Raman analyses of the films produced from $TiCl_4$, $NbCl_5$ and $^tBu_2Se$ at 550 °C showed different patterns for the different flow rates conditions used.

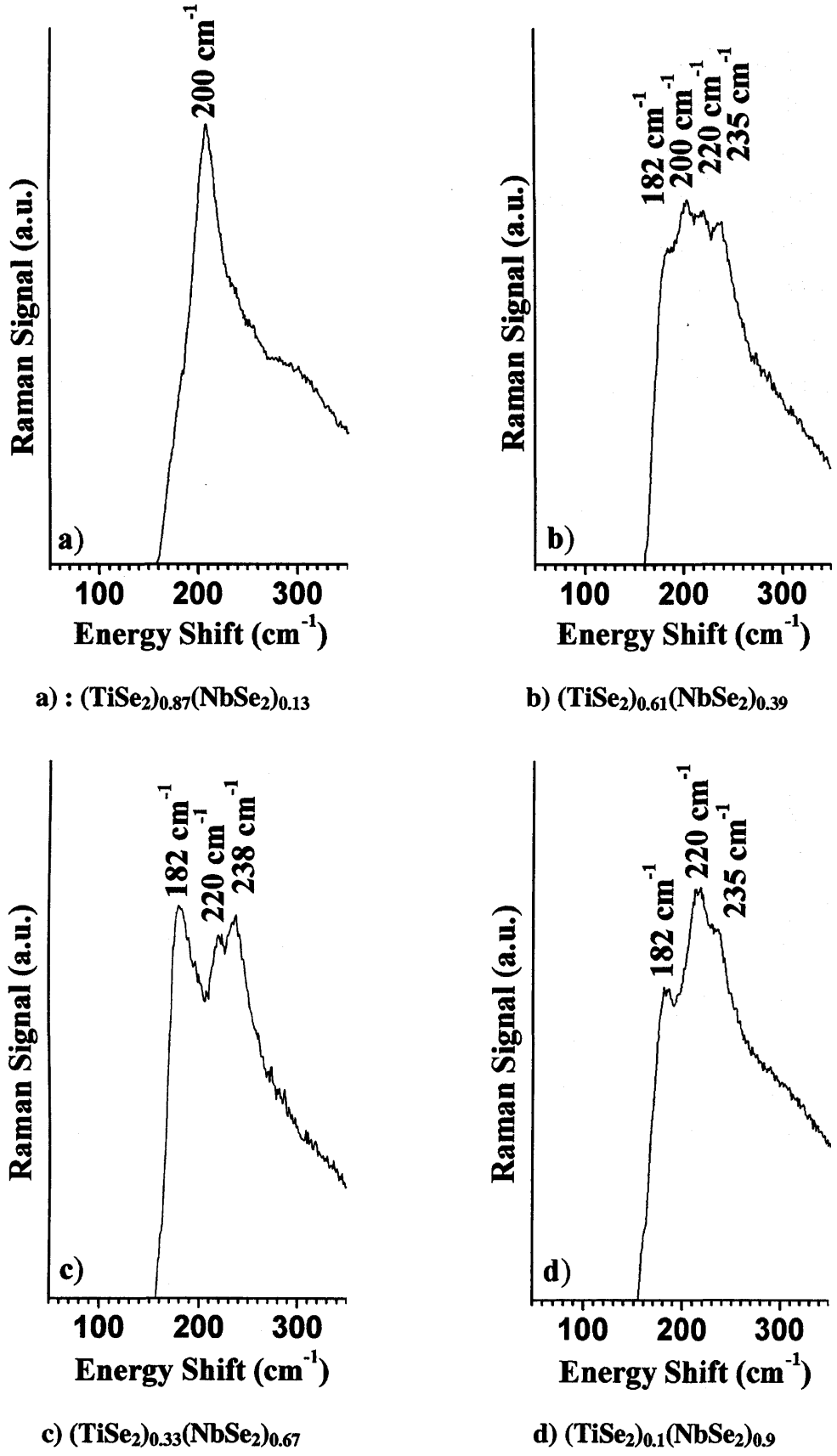

a) : $(TiSe_2)_{0.87}(NbSe_2)_{0.13}$ b) $(TiSe_2)_{0.61}(NbSe_2)_{0.39}$

c) $(TiSe_2)_{0.33}(NbSe_2)_{0.67}$ d) $(TiSe_2)_{0.1}(NbSe_2)_{0.9}$

Figure 3.27 Raman pattern obtained for the films produced from the APCVD reaction of $TiCl_4$, $NbCl_5$ and $^tBu_2Se$ at 550 °C for different compositions.

The Raman patterns observed for the films produced from $TiCl_4$, $NbCl_5$ and $^tBu_2Se$ at 550 °C were found to be strongly related to the flow rates conditions used. The peak observed at 200 cm^{-1} for $(TiSe_2)_{0.87}(NbSe_2)_{0.13}$ was assigned to 1T-$TiSe_2$ (Figure 3.27a). This peak became weaker as the percentage of $TiSe_2$ in the films decreased and could not be observed for the films mostly composed of $NbSe_2$ (Figure 3.27b-d). The peaks around 182 cm^{-1}, 220 cm^{-1} and 235-238 cm^{-1} were identified as the distinctive 2H-$NbSe_2$ Raman pattern. These peaks were observed to be more intense as the percentage of $NbSe_2$ detected by WDX increased. No evidence was seen in the films for an additional phase - such as the superstoichiometric $NbSe_{2+x}$ (x = 0.4 – 0.6) observed during the APCVD of $NbCl_5$ and $^tBu_2Se$ below 550 °C.

3.5.2 Discussion

SEM, spot-WDX, XRD and Raman analyses indicated that the APCVD reaction of $TiCl_4$ and $NbCl_5$ with $^tBu_2Se$ at 550 °C formed multiphase films. The $TiSe_2$ and $NbSe_2$ crystals grew separately during the CVD process rather than forming a mixed niobium-titanium selenide ($Ti_{1-x}Nb_xSe_2$). This segregation of the two phases was clearly observed by SEM. Other CVD reactions involving $TiCl_4$ have been reported to form multiphase films. The CVD reaction of $TiCl_4$ with SiH_2Cl_2, C_4H_{10} and H_2 led to Si-Ti-C multiphase materials (SiC and $TiSi_2$, Ti_3SiC_2 or TiC).[45,46] While studies have shown the possibility to produce multiphase composites films such as AlN + BN + TiN, BN + TiN, BN + TiB_2, BN + TiB_2 + TiN, and TiB_2 + TiN, from the CVD reaction of $TiCl_4$, BCl_3, $AlCl_3$, NH_3 and H_2.[47] $Ti_{1-x}Nb_xO_2$ thin films have been reported by metal-organic chemical vapour deposition using titanium tetraisopropoxide [$Ti(OCH(CH_3)_2)_4$] and pentaethoxy niobium [$Nb(OC_3H_5)_5$].[48]

3.6 Conclusion

APCVD provides a convenient route to $TiSe_2$, VSe_2 and $NbSe_2$ thin films. The APCVD reaction of $TiCl_4$ and Et_2Se_2 or $^tBu_2Se$ led to the formation of films composed of plate-like crystallites orientated parallel to the substrate. $^tBu_2Se$ was identified as a better precursor as it gave films with a better stoichiometry and quality. Moreover,

unlike previous single-source routes to this material, the $TiSe_2$ films produced were stable in air for prolonged periods.

The APCVD of VSe_2 thin films is highly sensitive to the vanadium source used and vanadium tetrachloride and vanadium oxychloride were found to be unsuitable precursors. APCVD reaction of $[V(NMe_2)_4]$ and $^tBu_2Se$ provides a convenient route to vanadium diselenide films on glass. Between 300 and 500 °C, the films were crystalline with a preferential growth either along (101) or the (110) direction. SEM showed that the films were composed of plate-like crystallites that were orientated parallel to the substrate and EDAX analysis showed a vanadium to selenium ratio close to 1 : 2. Raman analysis was also consistent with the formation of VSe_2.

Niobium selenide films were deposited on glass from the APCVD reaction of $NbCl_5$ and $^tBu_2Se$. Between 300 and 500 °C, the films were crystalline and selenium rich with a niobium to selenium ratio of 1 : 2.5. The films produced at a deposition temperature of 600 °C showed exactly the Nb : Se ratio expected for $NbSe_2$. No chlorine, carbon or other contamination was found by the EDAX in these films. The films produced at 600 °C were highly crystalline with a preferential growth either along (101) or the (002) direction. The $NbSe_2$ films were stable in air, insoluble in the common organic solvents, and were only slowly decomposed in nitric acid. The APCVD reaction of $TiCl_4$ and $NbCl_5$ with $^tBu_2Se$ formed mixed $NbSe_2$-$TiSe_2$ composites rather than a solid solution $Ti_{1-x}Nb_xSe_2$.

3.7 References

[1] C. J. Carmalt, I. P. Parkin, E. S. Peters, *Polyhedron*, **2003**, *22*, 1263.

[2] S. A. O'Neill, R. J. Clark, I. P. Parkin, N. Elliott, A. Mills, *Chem. Mater.*, **2003**, *15*, 46.

[3] E. S. Peters, Ph.D Thesis, **2004**, University of London.

[4] C. Webb, P. M. Williams, *Phys. Rev. B*, **1975**, *11*, 2082.

[5] S. O. Saied, J. L. Sullivan, T. Choudhury, *Vacuum*, **1988**, *38*, 917.

[6] P. Bernusset, *Rev. Chim. Min.*, **1966**, *3*, 135.

[7] J. Chen, Z. L. Tao, S. L. Li, x. B. Fan, S. L. Chou, *Adv. Mater.*, **2003**, *15*, 1379.

[8] G. A. Freund, R. D. Kirby, *Phys. Rev. B*, **1984**, *30*, 7122.

[9] J. Zhu, J. Zhang, F. Chen, M. Anpo, *Mater. Lett.*, 2005, 59, 3378.

[10] A. Turkovic, D. Sokcevic, *Appl. Surf. Sci.*, **1993**, *68*, 477.

[11] S. Gunst, A. Klein, W. Jaegermann, Y. Tomm, H. J. Crawack, H. Jungblut, *Ionics*, **2000**, *6*, 180.

[12] E. Roest, L. Gjertsen, *Z. Anorg. Allg. Chem.*, **1964**, *328*, 299.

[13] D. Barreca, L. E. Depero, E. Franzato, G. A. Rizzi, L. Sangaletti, E. Tondello, U. Vettori, *J. Electrochem. Soc.*, **1999**, *146*, 551.

[14] T. D. Manning, I. P. Parkin, R. J. H. Clark, D. Sheel, M. E. Pemble, D. Vernadou, *J. Mat. Chem.*, **2002**, *12*, 2936.

[15] B. Horvath J. Strutz, J. Geyer-Lippmann, E. G. Horvath, *Z. Anorg. Allg. Chem.*, **1981**, *483*, 181.

[16] M. Shenasa, S. Sainkar, D. Lichtman, *J. Electron. Spectrosc. Relat. Phenom.*, **1986**, *40*, 329.

[17] A. H. Reshak, S. Auluck, *Phys. B*, **2004**, *349*, 310.

[18] G. V. Kamarchuk, A. V. Khotkevich, V. M. Bagatsky, V. G. Ivanov, P. Molinie, A. Leblanc, E. Faulques, *Phys. Rev. B*, **2001**, *63*, 073107.

[19] N. Nagaosa, E. Hanamura, *Phys. Rev. B*, **1984**, *29*, 2060.

[20] F. J. DiSalvo, J. V. Waszczak, *Phys. Rev. B*, **1981**, *23*, 457.

[21] A. H. Thompson, B. G. Silbernagel, *J. Appl. Phys.*, **1978**, *49*, 1477.

[22] A. H. Thompson, B. G. Silbernagel, *Phys. Rev. B*, **1979**, *19*, 3420.

[23] L. F. Schneemeyer, A. Stacy, M. J. Sienko, *Inorg. Chem.*, **1980**, *19*, 2659.

[24] C. S. Blackman, C. J. Carmalt, S. A. O'Neill, I. P. Parkin, K. C. Molloy, L. Apostolico, *J. Mat. Chem.*, **2003**, *13*, 1930.

[25] C. S. Blackman, C. J. Carmalt, S. A. O'Neill, I. P. Parkin, K. C. Molloy, L. Apostolico, *Chem. Vapor Dep.*, **2004**, *10*, 253.

[26] M.N. Field, I.P. Parkin, *J. Mat. Chem.*, **2000**, *10*, 1863.

[27] T.D. Manning, I.P. Parkin, *Polyhedron*, **2004**, *23*, 3087.

[28] M. Seman, J. Marino, W. Yang, C.A. Wolden, *J. Non-Cryst. Solids*, **2005**, *351*, 1987.

[29] G.S. Elwin, I.P. Parkin, *Chem. Vapor Dep.*, **2000**, *6*, 59.

[30] A. Leonhardt, K. Bartsch, M. Schoenherr, E. Wolf, M. Seidler, Ger. (East), 3 pp. CODEN:GEXXA8; DD288629, **1991**.

[31] A. Leonhardt, M. Seidler, E. Wolf, M. Schoenherr, A. Zetzsche, H. Mai, Ger. (East), 3 pp. CODEN:GEXXA8; DD288628, **1991**.

[32] H. Mikami, C.J. Zhou, S. Takahashi, T. Sato, K. Shimakage, *Shigen to Sozai*, **1992**, *108*, 808.

[33] H. Mikami, C.J. Zhou, S. Takahashi, T. Sato, K. Shimakage, *Shigen to Sozai*, **1994**, *110*, 313.

[34] S. O'Neill, I. P. Parkin, R. J. H. Clark, A. Mills, N. Elliott, *J. Mater. Chem.*, **2003**, *13*, 2952.

[35] C. J. Carmalt, E. S. Peters, I. P. Parkin, T. D. Manning, A. L. Hector, *Eur. J. Inorg. Chem.*, **2004**, *22*, 4470.

[36] S. Motojima, K. Sugiyama, Y. Takahashi, *J. Cryst. Growth*, **1975**, 30, 233.

[37] T. Takahashi, H. Itoh, T. Yamaguchi, *J. Cryst. Growth*, **1979**, 46, 69.

[38] Y. Tanaka, T. Asano, K. Tachikawa, *Proc. Int. Conf. Vac. Metall.*, **1982**, *1*, 46.

[39] M. K. Bahl, *J. Phys. Chem. Solids*, **1975**, *36*, 485.

[40] D. Briggs and M. P. Seah (eds) *Practical Surface Analysis-Auger and X-ray photoelectron spectroscopy*, **1999**, Wiley, Chicester.

[41] J. C. Tsang, J. E. Smith, M. W. Shafer, *Phys. Rev. Lett.*, **1976**, *37*, 1407.

[42] C. M. Pereira, W. Y. Liang, *J. Phys. C: Solid State Phys.*, **1982**, *15*, L991.

[43] C. M. Pereira, W. Y. Liang, *J. Phys C: Solid State Phys.*, **1985**, *18*, 6075.

[44] C. J. Carmalt, E. S. Peters, I. P. Parkin, T. D. Manning, A. L. Hector, *Eur. J. Inorg. Chem.* **2004**, *22*, 4470.

[45] M. Touanen, F. Teyssandier, M. Ducarroir, J. L. Derep, *Mater. Sci. Eng.*, **1991**, *A147*, 239.

[46] M. Maline, M. Ducarroir, F. Teyssandier, R. Hillel, R. Berjoan, F. J. J. Van Loo, W. Wakelkamp, *Surf. Sci.*, **1993**, *286*, 82.

[47] T. S. Moss, J. A. Hanigofsky, W. J. Lackey, *J. Mater. Res.*, **1992**, *7*, 754.

[48] Y. Gao, *Thin Solid Films*, **1999**, *346*, 73.

Chapter 4
APCVD of Group VI Selenides

4.1 Introduction

This chapter describes the APCVD of group VI metal selenides. Molybdenum diselenide thin films were produced from the APCVD reaction of molybdenum pentachloride with ditertiarybutylselenide or diethylselenide. Tungsten diselenide thin films were produced from tungsten hexachloride and diethylselenide.

4.2 Molybdenum Diselenide Films

Two series of films were prepared using molybdenum pentachloride with two different selenium sources; ditertiarybutylselenide and diethylselenide. Other possible molybdenum precursor include $[Mo(CO)_5]$,[1] $[Mo(CO)_6]$,[2] MoF_6,[3] and MoO_2Cl_2.[4] However $MoCl_5$ was chosen following its successful use in the past to grow molybdenum metal,[5] molybdenum carbides,[6] molybdenum nitrides,[7] molybdenum disilicide,[3] molybdenum phosphide[8] and molybdenum disulfide.[9]

4.2.1.1 Films from $MoCl_5$ and $^tBu_2Se$: Reaction Conditions

The APCVD reaction of molybdenum pentachloride ($MoCl_5$) with ditertiarybutylselenide ($^tBu_2Se$) was investigated from the onset deposition temperature, 450 °C, up to 650 °C. The $^tBu_2Se$ and $MoCl_5$ bubblers were heated to 90 °C and 255 °C respectively. Flow rates of nitrogen through the $^tBu_2Se$ bubbler and the $MoCl_5$ bubbler were kept constant at 2 $L.min^{-1}$ for all depositions. For each experiment the flow rate through the mixing chamber was 6 $L.min^{-1}$ and the deposition time was one minute. These conditions corresponded to a $MoCl_5$ flow of 40.2 $mmol.min^{-1}$ and a $^tBu_2Se$ flow of 29.3 $mmol.min^{-1}$.

4.2.1.2 Appearance, Substrate Coverage and Adherence of the Films

Films produced from the APCVD of $MoCl_5$ and $^tBu_2Se$ were brown in appearance and visually reflective. The films were adherent and passed the Scotch tape test, however they were easily scratched with a steel scalpel. They were air and water stable, insoluble in common organic solvents, but were decomposed in nitric acid and bleach. At a deposition temperature of 450 °C, the films only covered the last 6 cm of the substrate. With higher deposition temperatures, the growth profile expanded closer to the leading edge of the substrate such that at substrate temperatures of 550 °C and above, films of 100 nm thickness were grown across the entire substrate.

4.2.1.3 Scanning Electron Microscopy

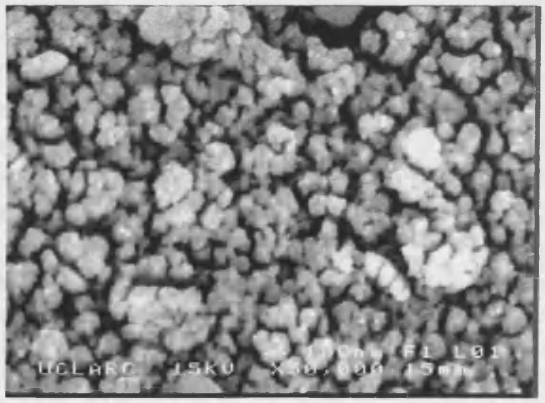

450 °C

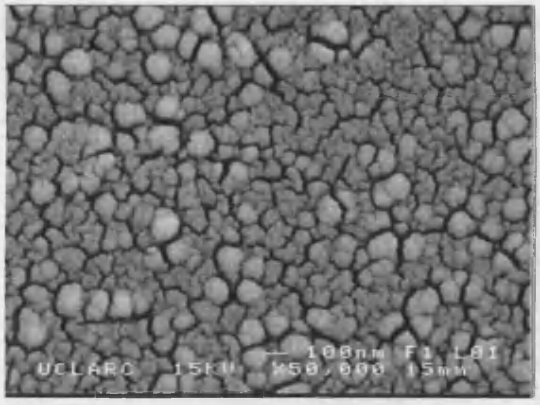

550 °C

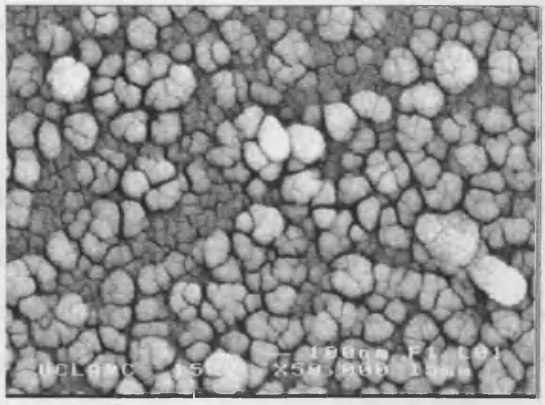

600 °C

Figure 4.1 Scanning electron micrographs of the films produced from the APCVD of $MoCl_5$ and $^tBu_2Se$ at 450 – 650 °C.

The SEM images show that the films grown from $MoCl_5$ and $^tBu_2Se$ have a 'crazy-paving' type morphology (Figure 4.1) indicative of an island growth type mechanism. This is a consequence of stronger interactions between atoms of the film, rather than interactions between the film and the substrate. The size of the clusters increased with temperature; from 100 nm at 450 °C to 200 nm at 600 °C.

4.2.1.4 Energy Dispersive X-ray Analysis

Table 4.1 EDAX, Raman, and XRD data for the films produced by APCVD reaction of $MoCl_5$ with $^tBu_2Se$. Position across the substrate: (a) 4 cm from the inlet; (b) 12 cm from the inlet.

Deposition Temperature	EDAX	XRD; lattice constant in Å	Raman
550 °C (a)	$MoSe_{1.8}Cl_{0.2}$	2H- & 3R-$MoSe_2$; a = 3.29 Å, c = 6.51 Å	$MoSe_2$
600 °C (a)	$MoSe_{2.0}$	2H- & 3R-$MoSe_2$; a = 3.29 Å, c = 6.41 Å	$MoSe_2$
650 °C (a)	$MoSe_{1.8}$	2H- & 3R-$MoSe_2$; a = 3.29 Å, c = 6.46 Å	$MoSe_2$
450 °C (b)	$MoSe_{1.7}Cl_{0.3}$	2H- & 3R-$MoSe_2$; a = 3.30 Å, c = 6.52 Å	$MoSe_2$
500 °C (b)	$MoSe_{1.9}Cl_{0.2}$	2H- & 3R-$MoSe_2$; a = 3.29 Å, c = 6.52 Å	$MoSe_2$
550 °C (b)	$MoSe_{1.8}Cl_{0.2}$	2H- & 3R-$MoSe_2$; a = 3.30 Å, c = 6.49 Å	$MoSe_2$
600 °C (b)	$MoSe_{1.3}$	2H- & 3R-$MoSe_2$; a = 3.28 Å, c = 6.48 Å	$MoSe_2$
650 °C (b)	$MoSe_{1.4}$	2H- & 3R-$MoSe_2$; a = 3.28 Å, c = 6.50 Å	$MoSe_2$

EDAX analysis shows that the stoichiometry of the films produced from $MoCl_5$ and $^tBu_2Se$ is closely related to the deposition temperature and the position of the films along the substrate. It was observed that a temperature of 600 °C or more is required to avoid chlorine incorporation. Below this temperature, the films contained from 5 to 10 atomic percent of chlorine and was slightly substoichiometric with a molybdenum to selenium ratio varying from $MoSe_{1.7}$ to $MoSe_{1.9}$ (Table 4.1). Above 600 °C, films with the expected stoichiometry for $MoSe_2$ were deposited on the leading edge of the substrate. However the last few centimetres of these films were found to be substoichiometric (ca. $MoSe_{1.3}$ and $MoSe_{1.4}$). These changes in the selenium

concentration along the substrate (Figure 4.2), are due to the fast depletion of the selenium precursor over time within the reactor.

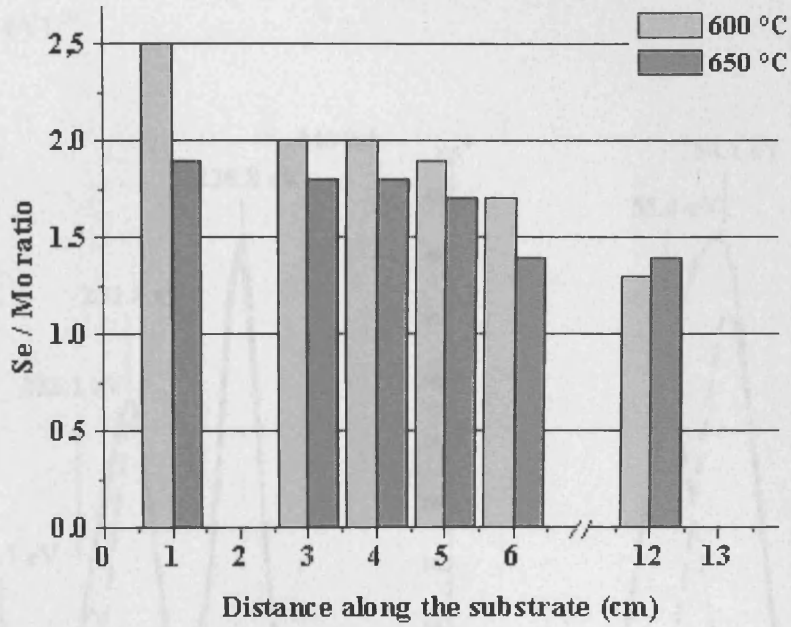

Figure 4.2 Histogram of the selenium to molybdenum ratio relative to deposition position on the substrate (distance indicates the distance along the substrate as measured from the inlet of the reactor). Films were produced from the APCVD of $MoCl_5$ and $^tBu_2Se$ at substrate temperatures of 600 °C and 650 °C.

4.2.1.5 X-ray Photoelectron Spectroscopy

The XPS of a film deposited from $MoCl_5$ and $^tBu_2Se$ at 600 °C revealed the presence of two molybdenum environments in the film (Figure 4.3). The stronger peaks observed at 228.8 and 231.8 eV correspond to the Mo $3d_{3/2}$ = 231.7 eV and Mo $3d_{5/2}$ = 228.5 eV of molybdenum diselenide.[10] The second molybdenum environment in the films is due to oxide contamination. The identified peaks at 233.1 and 235.7 eV for the molybdenum oxide matched the literature values reported for molybdenum in MoO_3 (Mo $3d_{3/2}$ = 235.7 eV and Mo $3d_{5/2}$ = 232.5 eV).[11] The oxygen content within the samples was found to decrease markedly (to less than 5 %) with longer sputtering times. This, together with the fact that the smoother, less porous films showed less oxygen content, indicates that the oxidation seen in some films is due to transport of the

samples and is not inherent in the CVD process. The selenium peak for the same film shows that there is only one selenium environment present in the films (Figure 4.3). The fitted curves show the presence of the two peaks at 54.1 eV and 55.0 eV which are due to Se $3d_{5/2}$ and Se $3d_{3/2}$ peaks of the molybdenum diselenide (Se $3d_{3/2}$ = 54.9 eV and Se $3d_{5/2}$ = 54.0 eV).[10]

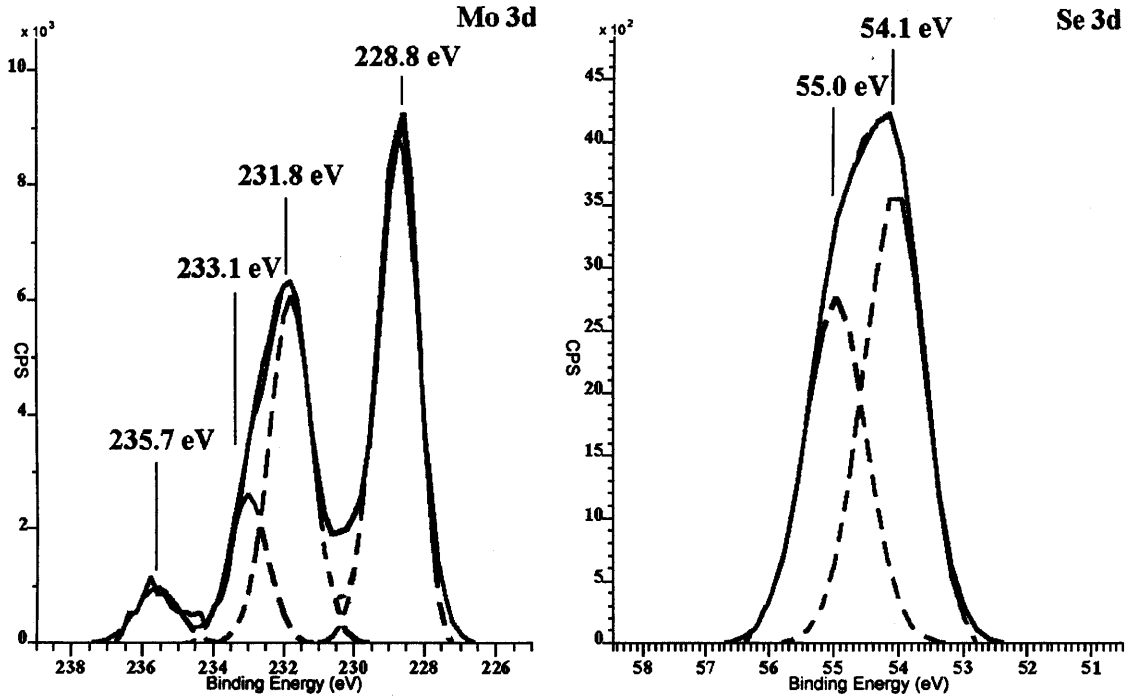

Figure 4.3 XPS spectra of the Mo 3d and Se 3d peaks from the surface of a film deposited from the APCVD reaction of $MoCl_5$ and $^tBu_2Se$ at 650 °C. The uppermost solid curves are the experimental data and the dashed lines a best fit.

4.2.1.6 X-ray Diffraction

XRD of the films produced from $MoCl_5$ and $^tBu_2Se$ show that they were all crystalline with a mixed stacking of $2H_b$- and 3R-type layers (JCPDS File Nos. 015-0029 and 020-0757).[12] This mixture of both polytypes is often known to be found in the same crystal. These polytypes have identical interlayer structures and only differ by their repeat distances between corresponding positions, with the $2H_b$ form having a doubling, and the 3R form a trebling, of the unit cell *c*-axis. The lattice parameters reported in Table 4.1, which do not show any multiplication of the *c*-axis, are in good agreement with the reported values for $MoSe_2$, a = 3.296 Å, c = 6.464 Å (× 2) for $2H_b$

and a = 3.296 Å, c = 6.464 Å (× 3) for 3R. The films deposited from $MoCl_5$ and $^tBu_2Se$ were all found to be preferentially orientated along (002) or (003) (Figure 4.4).

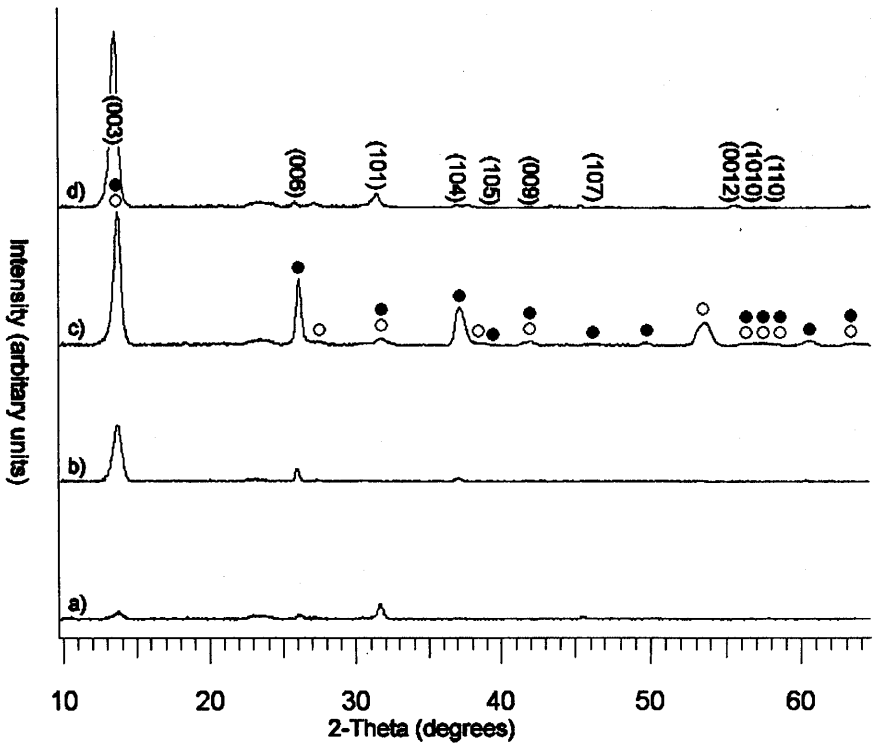

Figure 4.4 The XRD patterns obtained for the films formed from the APCVD of $MoCl_5$ and $^tBu_2Se$ at 450 °C (a), 550 °C (b), 600 °C (c) and 650 °C (d). Clear circles refer to the $2H_b$ polytype (JCPDS File No. 015-0029) and filled circles to the 3R form (JCPDS File No. 020-0757). The figure shows the indexing for the 3R polytype only.

4.2.1.7 Raman Microscopy

The films deposited from $MoCl_5$ and $^tBu_2Se$ gave the characteristic $MoSe_2$ Raman pattern,[13] with bands at 148 cm^{-1} (E_{1g}), 245 cm^{-1} (A_{1g}), 286 cm^{-1} (E_{2g}), 289 cm^{-1} (E_{1u}) and 325 cm^{-1} (A_{2u}) (Figure 4.5).

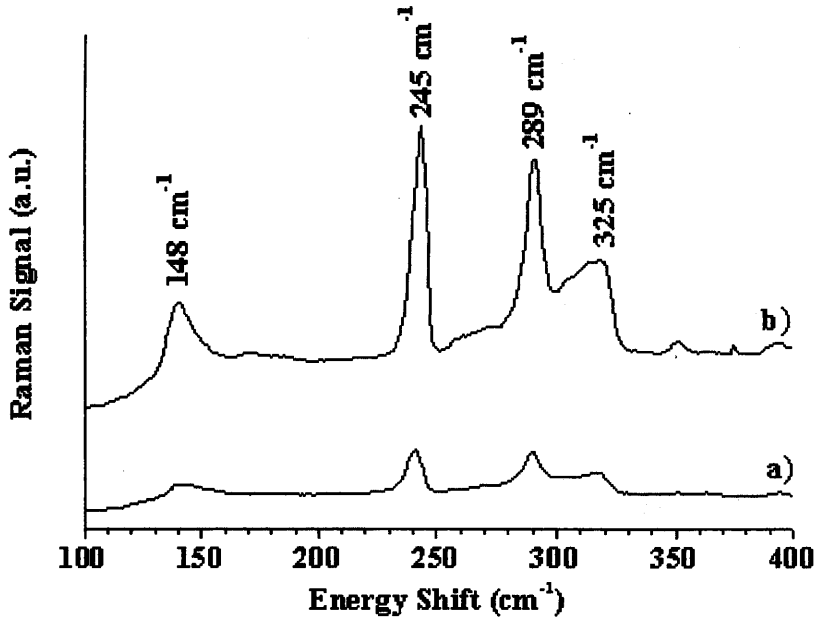

Figure 4.5 Raman patterns obtained for the film formed from the APCVD of $MoCl_5$ and $^tBu_2Se$ at 500 °C (a), and 650 °C (b).

4.2.1.8 Optical Properties

The transmittance of the 100 nm thick films produced from $MoCl_5$ and $^tBu_2Se$ was fairly low; between 400 - 500 nm (approximately 20 %), but quickly increased to approximately 50 % at the longest visible wavelength and near-infrared region. It is clear that increasing the thickness of the films results in a lower transmittance. For a thickness of 500 nm, the films showed almost no transmission at all in the visible region, but increased to approximately 20 % in the IR region (Figure 4.6).

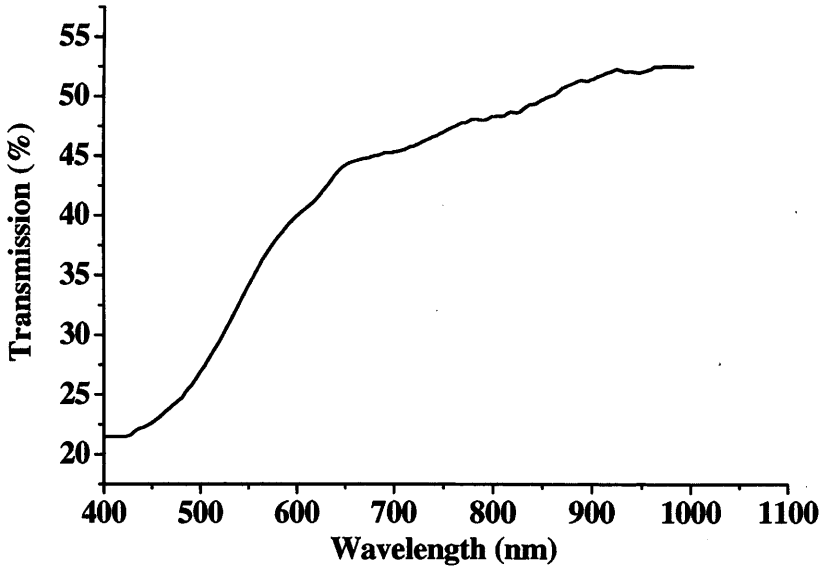

Figure 4.6 Transmittance spectra of a 100 nm film produced at 600 °C from the APCVD of $MoCl_5$ and $^tBu_2Se$ with a deposition time of 1 minute.

4.2.2.1 Films from $MoCl_5$ and Et_2Se: Reaction Conditions

The APCVD reaction of molybdenum pentachloride ($MoCl_5$) with diethylselenide (Et_2Se) was studied for the range 500 – 650 °C. The Et_2Se and $MoCl_5$ bubblers were heated to 70 °C and 255 °C, respectively. Flow rates of nitrogen through the Et_2Se bubbler, $MoCl_5$ bubbler and mixing chamber were kept constant at 0.2 $L.min^{-1}$, 1 $L.min^{-1}$ and 2.2 $L.min^{-1}$, respectively, and the deposition was for either 2 or 5 minutes. These conditions corresponded to a flow of $MoCl_5$ of 20.0 $mmol.min^{-1}$ and of Et_2Se of 2.9 $mmol.min^{-1}$. Longer deposition times were required, as the APCVD reaction of $MoCl_5$ and Et_2Se failed to produce thick and uniform films after a one minute deposition.

4.2.2.2 Appearance, Substrate Coverage and Adherence of the Films

Films produced from the APCVD of $MoCl_5$ and Et_2Se were brown in appearance and visually reflective. The films were adherent and passed the Scotch tape test, however they were easily scratched with a steel scalpel. They were air and water stable, insoluble in common organic solvents, but were decomposed in nitric acid and bleach.

4.2.2.3 Scanning Electron Microscopy

The SEM images of the films produced above 600 °C from the APCVD of Et_2Se and $MoCl_5$ show a needlelike morphology (Figure 4.7). The needles, from 4 μm at 600 °C to 10 μm at 650 °C, are orientated perpendicular to the substrate and are made up of a series of clusters. The clusters are all intergrown and their size increases with temperature, from 100 nm at 600 °C to 200 nm at 650 °C. At lower deposition temperatures (ca. 550 °C) the number of rod-shaped particles increases and the rods themselves get shorter and thinner (ca. 500 nm).

550 °C

600 °C

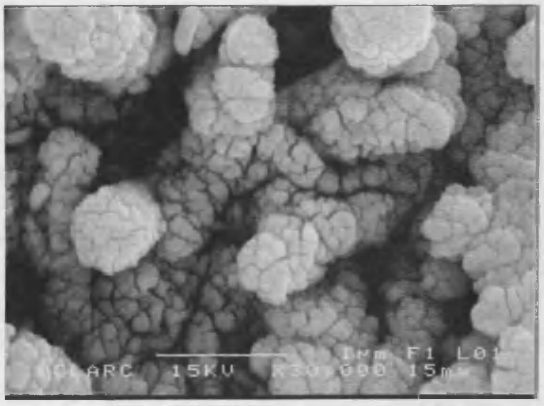

650 °C

Figure 4.7 Scanning electron micrographs of the films produced from the APCVD of $MoCl_5$ and Et_2Se at 550 – 650 °C.

The thickness of the films produced from $MoCl_5$ and Et_2Se, measured at 5 centimetres from the inlet of reactor, had values in the region of 200 nm to 600 nm, with

a two to five minute deposition time. The film thickness did not change measurably with substrate temperature provided the substrate was above the onset deposition temperature (ca. 500 °C). The films were grown with uniform thickness on the first six centimetres of the substrate. On the rest of the substrate films were thinner, tailing off to a thickness of ca. 10 – 20 nm at the back end of the substrate (ca. 15 cm from inlet). This, together with the relative insensitivity of the film thickness to deposition temperature, indicates a mass transport-limited reaction.

4.2.2.4 Energy Dispersive X-ray Analysis

Table 4.2 EDAX, Raman, and XRD data for the films produced by APCVD reaction of $MoCl_5$ with Et_2Se. Position across the substrate: (a) 4 cm from the inlet; (b) 12 cm from the inlet.

Deposition Temperature	EDAX	XRD; lattice constant in Å	Raman
500 °C (a)	$MoSe_{1.7}Cl_{0.3}$	2H- & 3R-$MoSe_2$; a = 3.30 Å, c = 6.47 Å	$MoSe_2$
550 °C (a)	$MoSe_{1.7}Cl_{0.3}$	2H- & 3R-$MoSe_2$; a = 3.29 Å, c = 6.51 Å	$MoSe_2$
600 °C (a)	$MoSe_{2.0}Cl_{0.2}$	2H- & 3R-$MoSe_2$; a = 3.29 Å, c = 6.37 Å	$MoSe_2$
650 °C (a)	$MoSe_{2.0}$	2H- & 3R-$MoSe_2$; a = 3.28 Å, c = 6.45 Å	$MoSe_2$
500 °C (b)	$MoSe_{1.7}Cl_{0.3}$	2H- & 3R-$MoSe_2$; a = 3.24 Å, c = 6.48 Å	$MoSe_2$
550 °C (b)	$MoSe_{1.8}Cl_{0.3}$	2H- & 3R-$MoSe_2$; a = 3.27 Å, c = 6.47 Å	$MoSe_2$
600 °C (b)	$MoSe_{2.1}Cl_{0.1}$	2H- & 3R-$MoSe_2$; a = 3.27 Å, c = 6.42 Å	$MoSe_2$
650 °C (b)	$MoSe_{2.1}$	2H- & 3R-$MoSe_2$; a = 3.30 Å, c = 6.45 Å	$MoSe_2$

EDAX analysis of the films produced from the APCVD reaction of $MoCl_5$ and Et_2Se above 600 °C, shows that they contained molybdenum and selenium with a Mo : Se ratio close to the one expected for $MoSe_2$ (Table 4.2). At lower deposition temperatures, the films were found to be substoichiometric (ca. $MoSe_{1.7}$). Except for the first few centimetres of the substrate, which were substoichiometric, all of the films showed a good uniformity in composition along the length of the substrate and across their width (Figure 4.8). It was found that a deposition temperature of 650 °C was

required to produce chlorine and carbon free films. At deposition temperatures of 600 °C and below, the films contained from 3 to 10 atomic percent of chlorine.

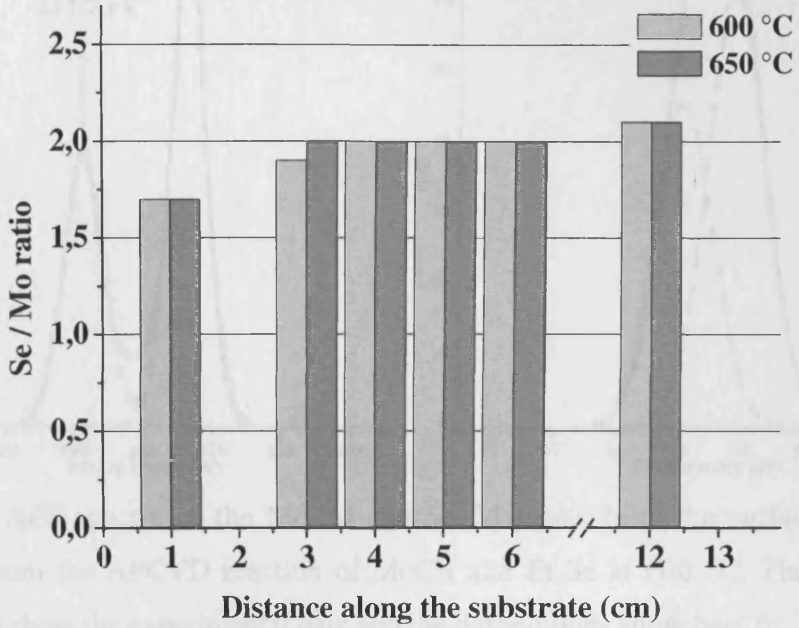

Figure 4.8 Histogram of the selenium to molybdenum ratio relative to deposition position on the substrate (distance indicates the distance along the substrate as measured from the inlet to the reactor). Films were produced from the APCVD of $MoCl_5$ and diethylselenide at substrate temperatures of 600 °C and 650 °C.

4.2.2.5 X-ray Photoelectron Spectroscopy

The X-ray photoelectron spectroscopy of a film deposited from the APCVD reaction of $MoCl_5$ and Et_2Se at 600 °C shows that there is only one molybdenum environment and one selenium environment in the film. The peaks of Mo $3d_{3/2}$ = 231.7 eV, Mo $3d_{5/2}$ = 228.7 eV, and Se $3d_{3/2}$ = 54.9 eV, Se $3d_{5/2}$ = 54.0 eV (Figure 4.9) all correspond to that reported for molybdenum diselenide (Mo $3d_{3/2}$ = 231.7 eV, Mo $3d_{5/2}$ = 228.5 eV and Se $3d_{3/2}$ = 54.9 eV, Se $3d_{5/2}$ = 54.0 eV).[14] No chlorine contamination was found in the film by XPS within the detection limit of the instrument.

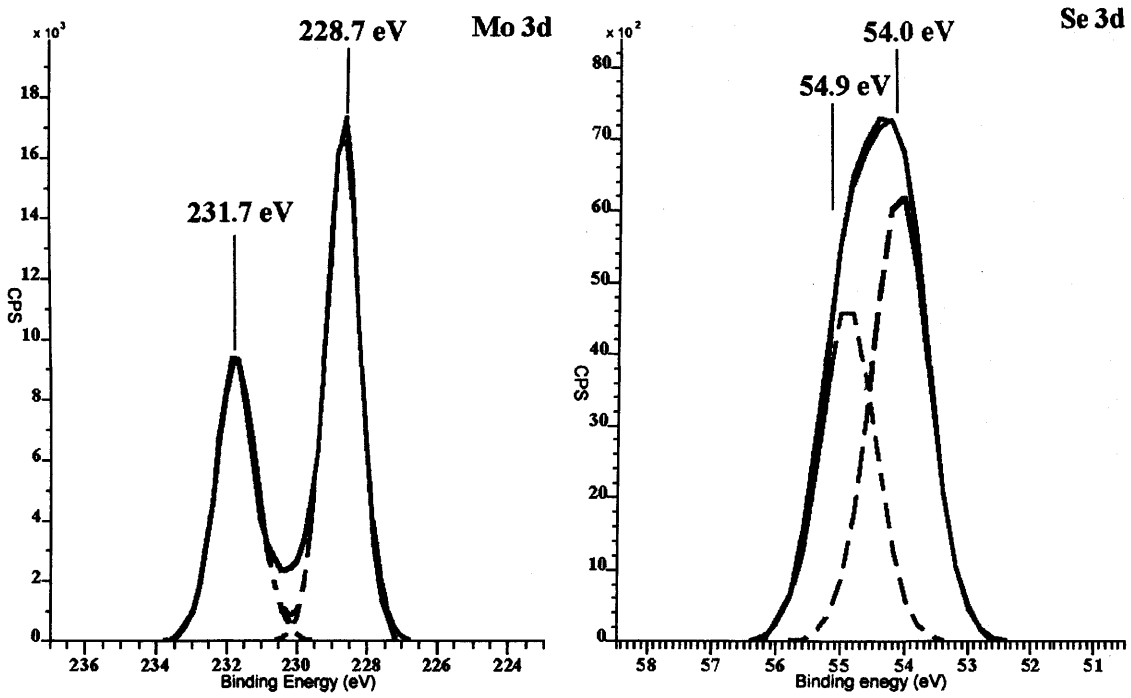

Figure 4.9 XPS spectra of the Mo 3d and Se 3d peaks from the surface of a film deposited from the APCVD reaction of $MoCl_5$ and Et_2Se at 600 °C. The uppermost solid curves show the experimental data and the dashed lines show best fit.

XPS of a film deposited at 600 °C shows the presence of chlorine, which correlated with the EDAX results. The Cl 2p peak is spread between 199 – 202 eV and is rather broad and ill defined (Figure 4.10). The Mo 3d and Se 3d peaks for the same sample shows the presence of only one molybdenum environment and one selenium environment in the film, suggesting that the chlorine is not directly bound to molybdenum. It is possible that the chlorine present in the film is intercalated within the $MoSe_2$ structure as the material is known to be a good intercalation host. No carbon was detected in any of the films indicating that the carbon from the precursor did not contaminate the films.

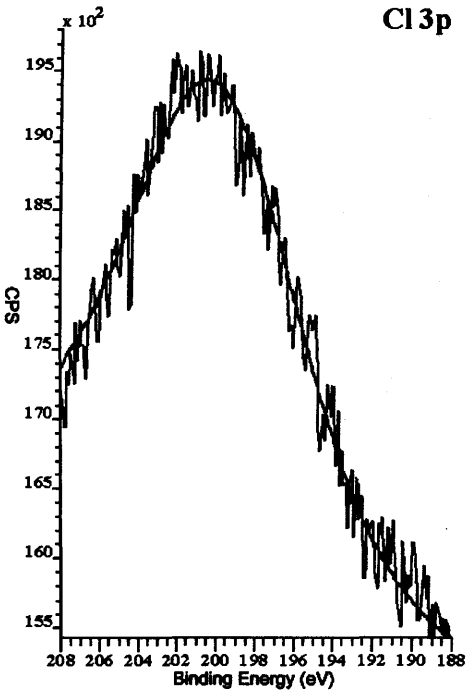

Figure 4.10 XPS spectra of the Cl 3p peaks from the surface of a film deposited from the APCVD reaction of $MoCl_5$ and Et_2Se at 600 °C.

4.2.2.6 X-ray Diffraction

The XRD data of the films produced from $MoCl_5$ and Et_2Se show that all the films were crystalline with a mixed stacking of 2Hb- and 3R-type layers (JCPDS File Nos. 015-0029 and 020-0757). By comparison with previous findings, the ratio of 2Hb : 3R was estimated to be about 85 : 15 in virtually all runs.[12] The lattice parameters shown in Table 4.2, are in good agreement with the reported values for $MoSe_2$, a = 3.296 Å, c = 6.464 Å.[15] The films grown at and below 600 °C showed no preferred growth orientation, whereas the films produced at 650 °C were strongly orientated along the (002) axis for the 2Hb polytype or (003) axis for 3R polytype (Figure 4.11).

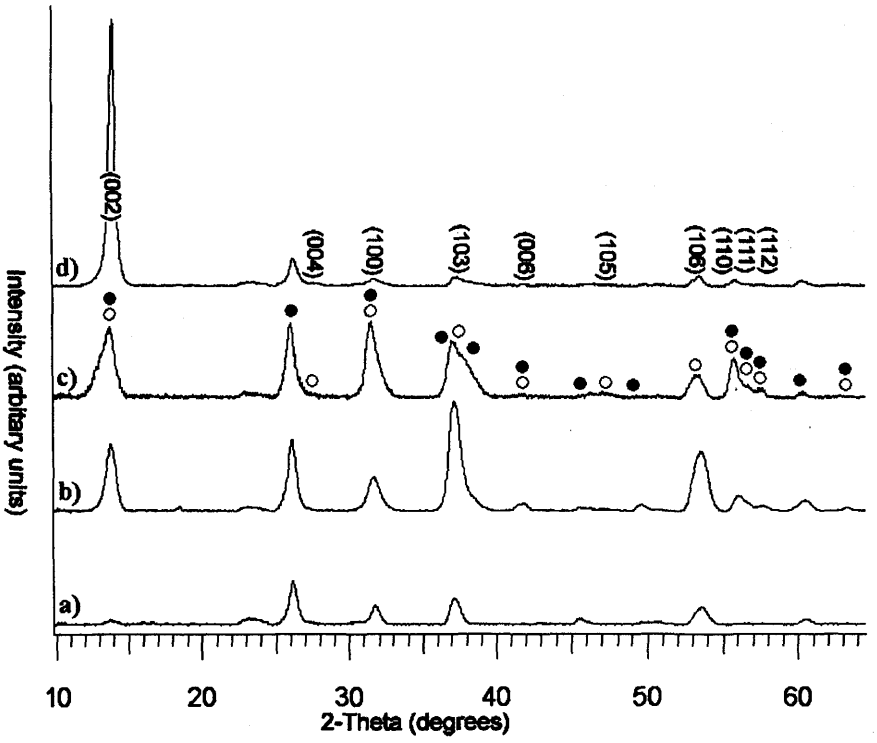

Figure 4.11 The XRD patterns obtained for the films formed from the APCVD of $MoCl_5$ and Et_2Se at 500 °C (a), 550 °C (b), 600 °C (c) and 650 °C (d). Clear circles refer to the 2Hb polytype (JCPDS File No. 015-0029) and filled circles to the 3R form (JCPDS File No. 020-0757). The figure shows the indexing for the 2H polytype only.

4.2.2.7 Raman Microscopy

The Raman pattern obtained for the films deposited from $MoCl_5$ and $^tBu_2Se$ gave the characteristic $MoSe_2$ Raman pattern (Figure 4.12).[13] The bands at 150, 241, 286, 289 and 320 cm^{-1} were respectively assigned to the E_{1g}, A_{1g}, E_{2g}, E_{1u} and A_{2u} modes.

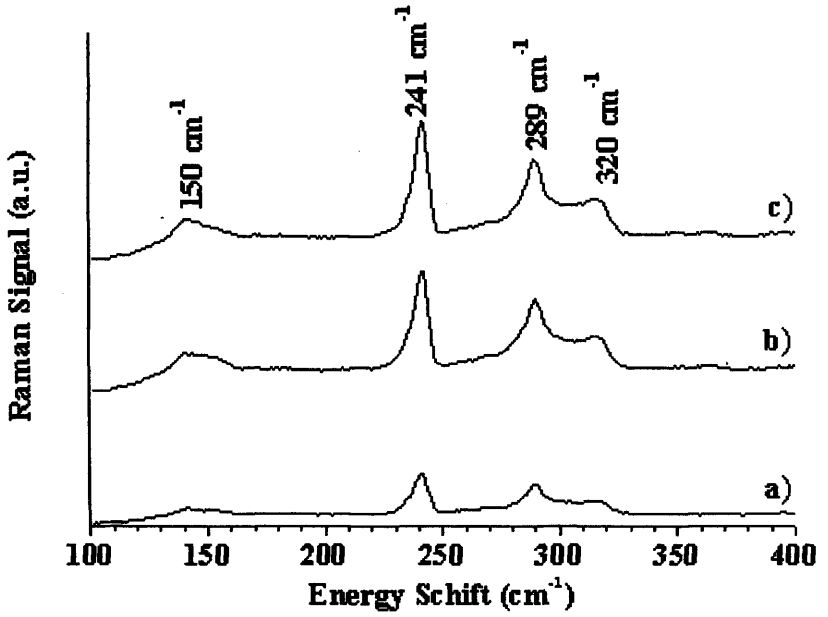

Figure 4.12 Raman patterns obtained for the films formed from the APCVD of $MoCl_5$ and Et_2Se at 550 °C (a), 600 °C (b) and 650 °C (c).

4.2.2.8 Optical Properties

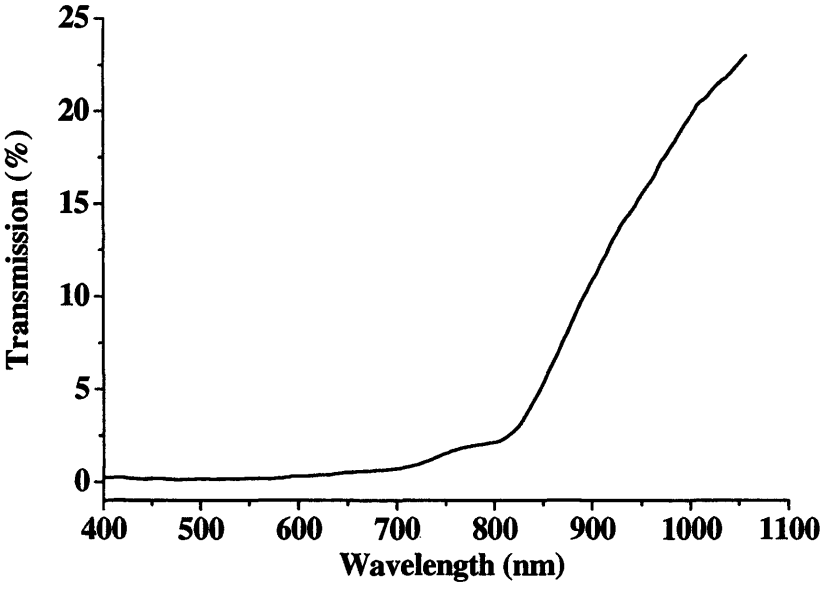

Figure 4.13 Transmittance spectra of a 600 nm film produced at 650 °C from the APCVD of $MoCl_5$ and Et_2Se with a deposition time of 5 minutes.

The $MoSe_2$ films produced from $MoCl_5$ and Et_2Se had a very low transmission in the visible, which increased significantly in the near-IR region. For a thickness of 600 nm, the films showed no transmission at all in the visible region, but increased to approximately 20 % in the infrared region (Figure 4.13).

4.2.3 Comparison and Discussion

The results show that the selenide precursor used has a significant effect on the quality of the $MoSe_2$ films formed. When ditertiarybutylselenide was used as a precursor, the stoichiometry of the films formed was found to dramatically vary along the substrate. While at 600 °C and above, films with a stoichiometry close to that of $MoSe_2$ were deposited on the leading edge of the substrate. The last few centimetres of the same films were found to be substoichiometric (ca. $MoSe_{1.3}$ and $MoSe_{1.4}$). These changes in the selenium concentration along the substrate, can be assigned to the fast depletion of the ditertiarybutylselenide over time within the reactor. Furthermore XPS of the films showed evidence of the formation of an oxide of molybdenum (MoO_3).

The diethylselenide proved to be a more effective precursor for making molybdenum diselenide films. Films grown in this system gave a more uniform and complete coverage of the substrate. Above 600 °C, films with the expected stoichiometry for $MoSe_2$ were grown along the entire substrate. XPS shows there is only one molybdenum environment and one selenium environment present in the films, also there was no evidence of surface oxidation.

The flow rate conditions used for the two selenium precursors were quite different. This is due to the fact that these conditions were found to give the best coverage of the substrate after trial experiments. In the case of diethylselenide, the Et_2Se to $MoCl_5$ relative molar gas flow ratio was 1.3 $mmol.L^{-1}.min^{-1}$: 9.1 $mmol.L^{-1}.min^{-1}$ (ca. 1 : 6.9), while the $^tBu_2Se$ to $MoCl_5$ relative molar gas flow ratio was 4.9 $mmol.L^{-1}.min^{-1}$: 6.7 $mmol.L^{-1}.min^{-1}$ (ca. 1 : 1.3) in the ditertiarybutylselenide case. Thus, much less selenium precursor was used in the diethylselenide reactions, as the relative molar gas flow of selenium precursor used was around a fifth of that in the ditertiarybutylselenide reactions. However, the films produced from ditertiarybutylselenide were found to be selenium deficient despite the larger amount of selenium precursor provided to the

system. This, together with the better quality and stoichiometry of the films produced from diethylselenide, makes the diethylselenide a superior precursor for the growth of molybdenum diselenide thin films.

4.3 Tungsten Diselenide Films

A number of different tungsten precursors, such as WF_6,[16] $[W(CO)_6]$,[17] $WOCl_4$[17] and WCl_6, have been investigated in CVD processes, the most extensively used and most suitable being tungsten hexachloride. WCl_6 has been succesfully used to grow metallic tungsten,[18] tungsten carbide,[19] tungsten nitride,[20] tungsten oxide,[21] tungsten silicide[22] and tungsten sulfide thin films.[17]

4.3.1.1 Films from WCl_6 and Et_2Se: Reaction Conditions

The APCVD reaction of tungsten hexachloride (WCl_6) with diethylselenide (Et_2Se) was studied over the temperature range 250 – 600 °C for two different flow rate conditions. The WCl_6 and Et_2Se bubblers were heated to 260 °C and 70 °C respectively. Flow rates of nitrogen through the WCl_6 bubbler and the Et_2Se bubbler were kept within 1.5 – 4.0 $L.min^{-1}$ (10.4 – 27.7 $mmol.min^{-1}$) and 0.2 – 0.3 $L.min^{-1}$ (2.9 – 4.4 $mmol.min^{-1}$), the flow rate through the mixing chamber was between 1.9 and 4.6 $L.min^{-1}$ for all depositions. Deposition time for all experiments was one minute.

4.3.1.2 Appearance, Substrate Coverage and Adherence of the Films

Depositions were only noted at temperatures in excess of 450 °C. At substrate temperatures of 500 °C and above, a matt black film was formed that passed the Scotch tape test. The films were however easily scratched with a steel scalpel. The films were insoluble in common organic solvents but were quickly decomposed in dilute nitric acid and bleach, yielding H_2Se. The films were air and water stable. The extent of film coverage was dependent on the deposition temperature. For a deposition temperature of 500 °C, films of uniform thickness were grown across the entire length of the substrate. With higher deposition temperatures, the growth profile was concentrated closer

towards the leading edge of the substrate, such that at a deposition temperature of 650 °C only the first 6 cm of the substrate was coated.

4.3.1.3 Scanning Electron Microscopy

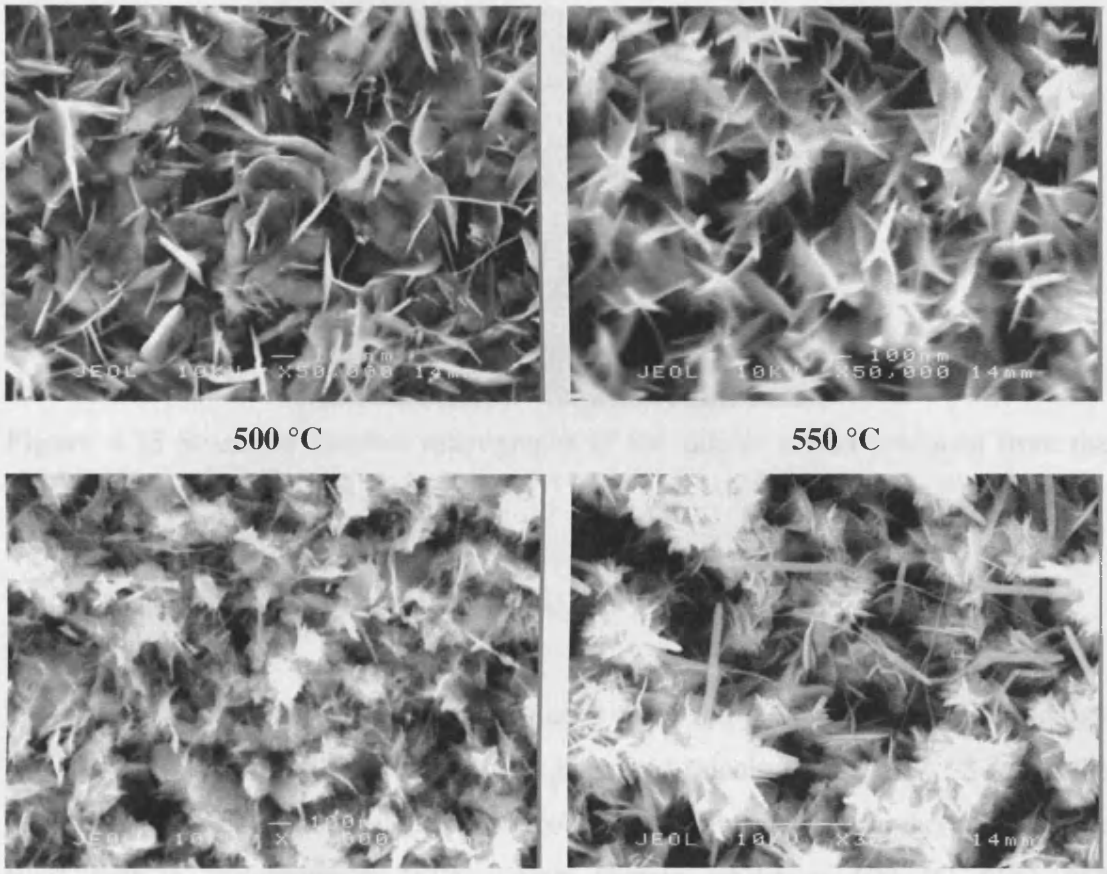

500 °C **550 °C**

600 °C **650 °C**

Figure 4.14 Scanning electron micrographs of the films produced from the APCVD of WCl_6 and Et_2Se at 500 – 650 °C.

Scanning electron microscopy images of the films produced at 650 °C, irrespective of the flow rate conditions, show grains which exhibit several very thin needles with lengths of a few hundred nanometres. Conversely, the SEM images of the films deposited at 550 °C and 600 °C show fewer- thicker needles with lengths of approximately a hundred nanometers. The SEM images of all the films show either plate-like or needle–like crystallites, which seem to be largely orientated perpendicular or radially, away from the substrate (Figure 4.14).

The thickness of the films deposited from the APCVD of WCl_6 and Et_2Se, determined using cross-sectional SEM (Figure 4.15), did not change measurably with substrate temperature. The average thickness of the films for a one minute deposition time was 300 nm.

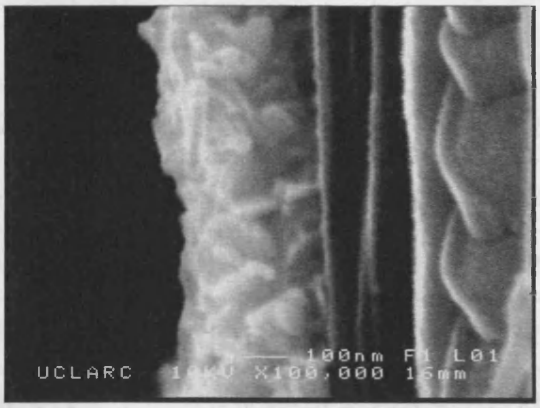

Figure 4.15 Scanning electron micrographs of the side of a film produced from the APCVD of WCl_6 and Et_2Se at 650 °C.

4.3.1.4 Energy Dispersive X-ray Analysis

EDAX analysis of the films produced from the APCVD of WCl_6 and Et_2Se showed that all of the films contained tungsten and selenium with a W : Se ratio that depended on the deposition rate and flow conditions (Table 4.3). At higher temperatures films with a stoichiometry $WSe_{2.5}$ were formed whilst at 500 °C films with stoichiometry $WSe_{1.5}$ were deposited with no chlorine or carbon detected. Furthermore, oxygen levels within the films were virtually undetectable (typically 1 atomic percent). The films showed uniformity in composition along the length of the substrate and across its width for any one film by both wide area (ca. 10 × 10 μm) and point EDAX analysis.

Table 4.3 EDAX, XRD and Raman data of the films produced from APCVD reaction of WCl_6 with Et_2Se. Flow rates through the WCl_6 bubbler, Et_2Se bubbler and the mixing chamber respectively were: (a) 1.5 $L.min^{-1}$, 0.2 $L.min^{-1}$, 1.9 $L.min^{-1}$; (b) 4.0 $L.min^{-1}$, 0.3 $L.min^{-1}$, 4.6 $L.min^{-1}$.

Deposition Temperature	EDAX	XRD; lattice constant in Å	Raman
500°C (a)	$WSe_{1.6}$	2H-WSe_2; a = 3.26 Å, c = 12.84 Å	WSe_2
550°C (a)	$WSe_{1.6}$	2H-WSe_2; a = 3.26 Å, c = 12.84 Å	WSe_2
600°C (a)	$WSe_{1.7}$	2H-WSe_2; a = 3.27 Å, c = 12.84 Å	WSe_2
650°C (a)	$WSe_{1.7}$	2H-WSe_2; a = 3.27 Å, c = 12.82 Å	WSe_2
500°C (b)	$WSe_{1.8}$	2H-WSe_2; a = 3.26 Å, c = 12.84 Å	WSe_2
550°C (b)	$WSe_{1.9}$	2H-WSe_2; a = 3.27 Å, c = 12.82 Å	WSe_2
600°C (b)	$WSe_{2.4}$	2H-WSe_2; a = 3.26 Å, c = 12.84 Å	WSe_2
650°C (b)	$WSe_{2.6}$	2H-WSe_2; a = 3.26 Å, c = 12.86 Å	WSe_2

4.3.1.5 X-ray Photoelectron Spectroscopy

The XPS of a film deposited from WCl_6 and Et_2Se at 650°C shows that there are two tungsten environments present in the film (Figure 4.16). The stronger peaks at 31.9 and 34.0 eV correspond to the W $4f_{7/2}$ = 32.0 eV and W $4f_{5/2}$ = 34.2 eV peaks of tungsten diselenide.[23] The second tungsten environment is due to oxide contaminations, which were both detected only at the surface of the sample (ca. 10 atomic percent). The observed peaks for the tungsten oxide at 35.7 and 37.8 eV matched the reported values for WO_3 (W $4f_{7/2}$ = 35.7 eV and W $4f_{5/2}$ = 37.9 eV).[24] The selenium peak for the same film shows that there is only one selenium environment present in the films. The presence of the two peaks at 54.0 eV and 54.9 eV are due to selenium in WSe_2 (Se $3d_{5/2}$ = 54.1 eV and Se $3d_{3/2}$ = 55.0 eV).[23]

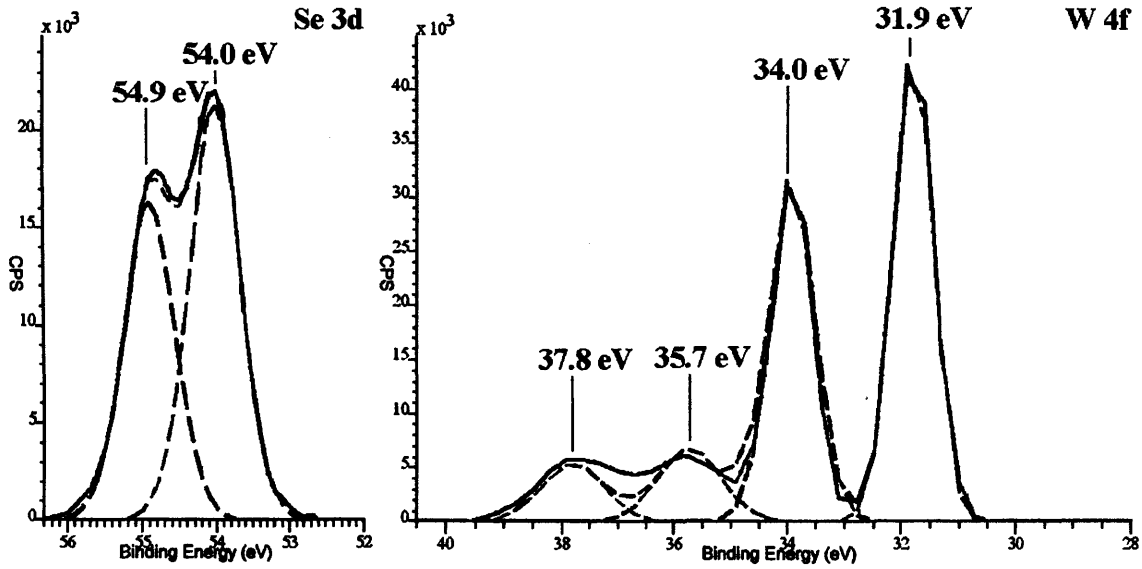

Figure 4.16 XPS spectra of the Se 3d and W 4f peaks from the surface of a film deposited from the APCVD reaction of WCl_6 and Et_2Se at 650 °C. The uppermost solid curves show the experimental data and the dotted lines show a best fit.

4.3.1.6 X-ray Diffraction

The XRD data on the films grown from WCl_6 and Et_2Se between 500 and 650 °C showed that all the films were crystalline and matched with the reported pattern for 2H-WSe_2 (JCPDS File No. 006-0080). The lattice parameters shown in Table 4.3 are in good agreement with the reported values for WSe_2; a = 3.32 Å and c = 12.80 Å.[25] The films produced at temperatures above 550 °C showed no preferred growth orientation. However, the film produced at 500 °C were strongly orientated along the (002) axis (Figure 4.17). A small reflection present in all the XRD patterns of the WSe_2 films at 2θ = 24.9° is attributed to WO_3.[26]

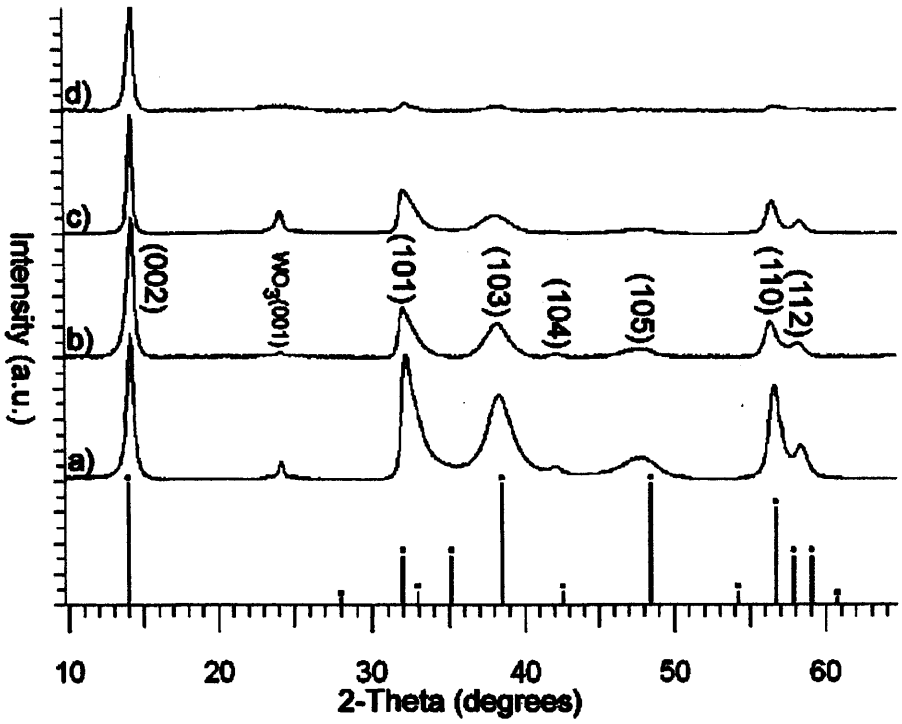

Figure 4.17 The XRD patterns obtained for the films formed from the APCVD of WCl_6 and Et_2Se at 650 °C (a), 600 °C (b), 550 °C (c) and 500 °C (d). Literature stick pattern for WSe_2 powder (JCPDS File No. 006-0080) is shown.

4.3.1.7 Raman Microscopy

Raman analysis of all films formed from the APCVD of WCl_6 and Et_2Se, irrespective of temperature or flow rates, showed the same pattern (Figure 4.18). The principle bands were at 180 cm^{-1} with a double peak around 250 – 256 cm^{-1}; these bands correspond to the frequencies of the Raman active A_{1g}, E_{2g} and E_{1g} modes respectively, of the 2H-WSe_2 polytype.[27]

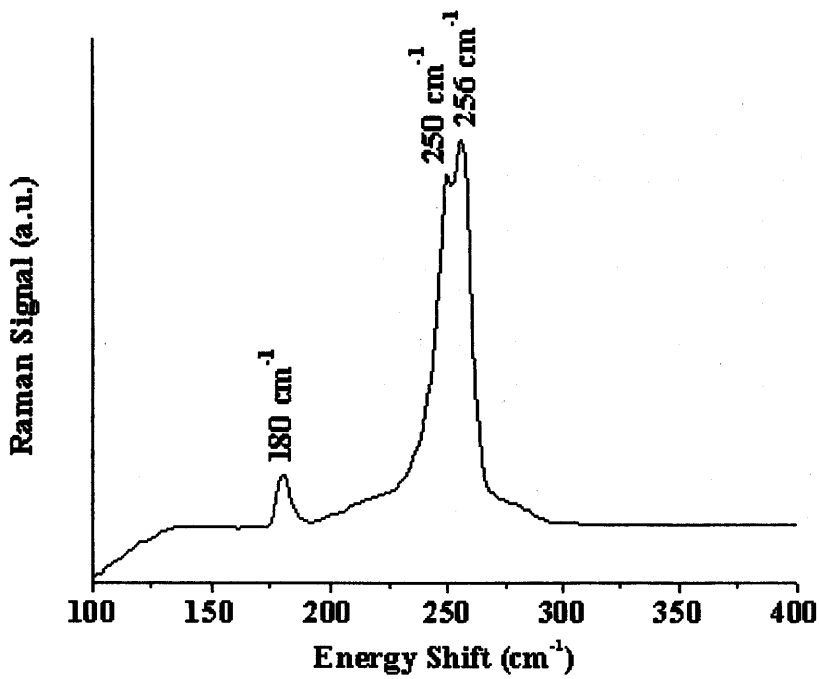

Figure 4.18 Raman pattern obtained for the film formed from the APCVD of WCl_6 and Et_2Se at 650 °C.

4.3.1.8 Contact Angle

The water contact angle measurements for the CVD prepared tungsten selenide films show that the films were highly hydrophobic for all the deposition temperatures with values in the range 135 – 145°. The contact angle was lowest (135°) for the films formed at 500 °C and increased with substrate deposition temperature to 145° for the film deposited at 650 °C. The contact angle measurements were consistent across the whole coated glass, and did not change on weekly inspection over a period in excess of two months.

Tilting experiments show that the water droplets cling to the surface of the film despite the highly hydrophobic character of the films. Indeed small droplets of water (1 mg) remain rounded with a tipping angle of 90° and do not roll or even slide at this acute angle. The surface can even be tipped upside down and the water droplets remain adhered to the surface (Figure 4.19). In fact the droplets evaporate instead of moving across the surface. This is exceptional as very hydrophobic films typically have extremely low tipping angles of a few degrees before the droplet slides off of the

surface. Furthermore large water droplets of 50 mg and above in size remain stationary on the surface at the 90° tilt angle.

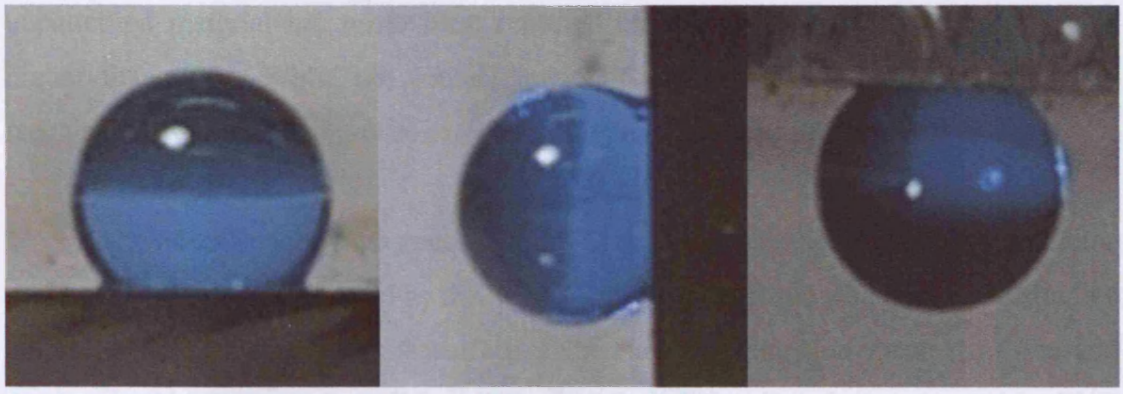

0° **90°** **180°**

Figure 4.19 Water droplets (1 mg) on the tungsten selenide thin films. Left: water droplet on a film at 0° tipping angle; middle: water droplet at a 90° tilt angle; right: water droplet suspended upside down on the film. The water droplets contained a small amount of methylene blue dye to aid visualisation, this was not found to alter the contact angles on the droplet sizes used.

4.3.2 Discussion

The sticky hydrophobicity, as referred to by Quéré,[28] of the tungsten diselenide films prepared by the APCVD reaction of WCl_6 with Et_2Se has been described by Wenzel's theory.[29] In the Wenzel model, the liquid droplet retains contact at all points with the rough surface of a hydrophobic solid. To minimise the surface contact with the hydrophobic film, the droplet will increase its contact-angle, enhancing the hydrophobic property of the film. The droplet being impaled into the porosity, strongly sticking to the surface and gives the material its sticky hydrophobic behaviour.

The Wenzel model is in contrast to the Cassie-Baxter model where the water droplets do not penetrate the surface porosities.[30] In the Cassie-Baxter case, the drops rest partially on air contained in the porosity and the peaks of the film protrusions, which lead to a more hydrophobic state and a slippery surface, typically showing a low tip angle before the droplets slide across the surface. Hence the films produced here are best described by Wenzel theory, which suggests that it is the surface microstructure

that is dominating the materials behaviour – as contact angles greater than 125° have not been reported for a flat surface. It is well known that the roughness or texture of a film can influence the contact angle of a water droplet at its surface. To date, an unpatterned material has never been reported before this work with a contact angle higher than 125°. While the contact angle of a micro-textured material, typically mechanically constructed groves or pillars, can jump to above 150°.

The exceptionally high contact angles of the films prepared here suggest extreme roughness, which is confirmed by the SEM pictures of the films which show needle like points radiating away from the surface. Other layered transition metal disulfide and diselenide thin films, such as TiS_2,[31] WS_2,[17] NbS_2,[32] $TiSe_2$, have been prepared by CVD methods in the past. The water contact angles of these films was typically between 5° and 100°. Usually the films produced have a plate like microstructure - often orientated perpendicular to the substrate as observed in Chapter 3 during the APCVD reaction of $^tBu_2Se$ with $TiCl_4$, $[V(NMe_2)_4]$ or $NbCl_5$ – or exhibit a rod shaped structure as showed previously by the films produced from $MoCl_5$ with Et_2Se or $^tBu_2Se$. None of the CVD prepared films have ever shown a microstructure that resembles the one produced here for WSe_2 and indeed the rough spiky surface produced here is probably the primary reason for the high hydrophobicity. Furthermore this extreme roughness accounts for why the water droplets do not slide down the surface even when exposed to very large tipping angles.

It is also possible that the layer structure exhibited by tungsten diselenide enhances the sticky hydrophobic character of the films (Figure 4.20). The WSe_2 structure consists of two-dimensional strongly bound layers of Se-W-Se, which are weakly bound to each other leading to the following stacking sequence Se-W-Se-□-Se-W-Se. Due to this structural arrangement, the basal planes of WSe_2 have a relatively low surface energy, which enable the layers to shear easily and give WSe_2 its lubricant properties. The basal planes, because of their low surface energy, are expected to be hydrophobic. The edge faces of the WSe_2 layers obtained by rupture of chemical bonds have a higher surface energy and are more likely to be hydrophilic. Moreover, the edge faces could be partly oxide terminated, forming hydrophilic WO_3 as suggested by the XRD and XPS results.[33] It could be considered that the WSe_2 layers are made of two different materials with different properties. The basal planes of the layers being

hydrophobic, giving to the film its hydrophobic behaviour, while the edge faces of the layers are hydrophilic and give to the film its sticky properties.

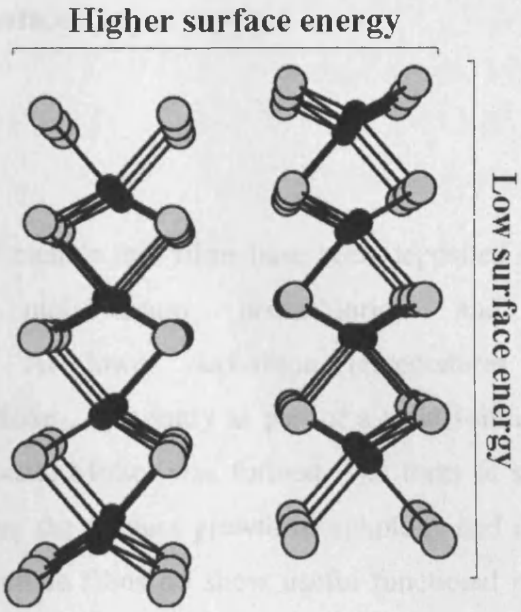

Figure 4.20 Crystal structure of 2H-WSe_2. The basal planes have a relatively low surface energy and the edge faces have a higher surface energy.

Compared to previously reported adhesive hydrophobic films,[34] the films prepared here were made in a single processing step and do not have a low surface energy polymer coating. Furthermore the surfaces are extremely resistant to water sliding and very large water droplets of 50 mg or more remain stationary on the surface even with a tip angle of 90°. For Jiang's work, however, droplets in excess of 8 mg move across the surface at these tilt angles. This very sticky hydrophobic property could readily be used as surfaces for biological micropipetting and assay where recovery of material from the surface is enhanced from a hydrophobic plate. However the use of a metal selenide surface for such a purpose, with a potential associated toxicity issue, may limit application. Classically very hydrophobic surfaces have found a wide range of applications such as self-cleaning glass or in inkjet printing devices. This is not the case for the tungsten selenide films reported here because the water droplets do not move across the surface even at the maximum tilt angles, unless they are very large in size. This kind of surface architecture has been described as an ideal theoretical surface for making highly rough hydrophobic surfaces. By coating the film with a low surface

energy polymer, the water droplets would have minimal contact points with the surface and the film would become super hydrophobic. Nature has produced many such hydrophobic surfaces - for example lotus leaves have numerous small spiky protrusions on the leaf surface which are covered in a wax like substance and are examples of slippery hydrophobic surfaces.

4.4 Conclusion

Molybdenum diselenide thin films have been deposited on glass substrate from the APCVD of molybdenum pentachloride and diethylselenide or ditertiarybutylselenide. At lower deposition temperatures some chlorine was incorporated into the $MoSe_2$, seemingly as part of a solid solution. At higher substrate temperatures stoichiometric $MoSe_2$ was formed. The form of selenium precursor was important in determining the product growth morphology and the rate of film growth. The molybdenum diselenide films do show useful functional properties, being highly absorbing in the region of the visible spectrum, but significantly transparent at longer wavelengths. Such films could find application as optical filters or in solar-cell applications.

Tungsten diselenide films have been deposited on glass substrate from the APCVD reaction of tungsten hexachloride and diethylselenide. The films did not contain any chlorine contamination, were stable in air and insoluble in common organic solvents. Films grown above 550 °C show grains which exhibit many very thin needles that matched the reported pattern for 2H-WSe_2. The films grown at 500 °C show plate crystallites orientated perpendicular to the substrate. This perpendicular orientation is confirmed by the XRD pattern, which shows preferred growth orientated along the (002) axis. All the films produced, irrespective of the deposition temperature, were highly hydrophobic with values in the range 135 – 145°. They were not quite in the class of material that would be described as super-hydrophobic, as this requires a contact angle in excess of 150°, however they are significantly more hydrophobic than a wide range of commercially made polymer coatings. The fact that these can be made by CVD opens up many possibilities for patterned substrates, simply by using a masking technique.

4.5 References

[1] K. A. Gesheva, T. Ivanova, A. Iossifova, D. Gogova, R. Porat, *J. Phys. IV*, **1999**, *9*, 1999.

[2] J. S. Cross, G. L. Schrader, *Chem. Vap. Dep.*, **1993**, *2*, 59.

[3] N. Patibandla, W. B. Hillig, *J. Mater. Synth. Process.*, **1994**, *2*, 93.

[4] E. E. Chain, B. O. Seraphin, *Thin Solid Films*, **1985**, *123*, 197.

[5] N. Yoshikawa, A. Kikuchi, S. Taniguchi, *Chem. Vap. Dep.*, **1998**, *6*, 241.

[6] J. Lu, U. Jansson, *Thin Solid Films*, **2001**, *396*, 53.

[7] S. L. Roberson, D. Finello, R. F. David, *Surf. Coat. Technol.*, **1998**, *102*, 256.

[8] C. S. Blackman, C. J. Carmalt, T. D. Manning, S. A. O'Neill, I. P. Parkin, *Chem. Vap. Dep.*, **2003**, *9*, 10.

[9] I. Endler, A. Leonhardt, U. Konig, H. van den Berg, W. Pitschke, V. Sottke, *Surf. Coat. Technol.*, **1999**, *120*, 482.

[10] J. C. Bernede, J. Pouzet, Z. K. Alaoui, *Appl. Phys.*, **1990**, *51*, 155.

[11] O. M. Hussain, K. S. Rao, *Mater. Chem. Phys.* **2003**, *80*, 638.

[12] M. S. Silverman, *Inorg. Chem.* **1967**, *6*, 1063.

[13] T. Sekine, M. Izumi, T. Nakashizu, K. Uchinokura, E. Matsuura, *J. Phys. Soc. Jpn.*, **1980**, *49*, 1069.

[14] D. F. Foster, N. L. Pickett, D. J. Cole-Hamilton, *Polyhedron* **1999**, *18*, 1329.

[15] R. Bichsel, F. Levy, *Thin Solid Films*, **1984**, *116*, 367.

[16] C. M. Melliar-Smith, A. C. Adams, R. H. Kaiser, R. A. Kushner, *J. Electrochem. Soc.*, **1974**, *121*, 298.

[17] C. J. Carmalt, I. P. Parkin, E. S. Peters, *Polyhedron*, **2003**, *22*, 1499.

[18] C. M. Melliar-Smith, A. C. Adams, R. H. Kaiser, R. A. Kushner, *J. Electrochem. Soc.*, **1974**, *121*, 298.

[19] M. Fitzsimmons, V. K. Sarin, *Surf. Coat. Technol.*, **1995**, *76*, 250.

[20] M. Nagai, N. Hirano, S. Omi, *Jpn. J. Appl. Phys.*, **2000**, *39*, 4558.

[21] C. S. Blackman, I. P. Parkin, *Chem. Mater.*, **2005**, *17*, 1583.

[22] F. Trincat, J. L. Regolini, J. Mercier, D. Bensahel, *Appl. Phys Lett.*, **1991**, *59*, 3291.

[23] R. Tenne, E. Galun, A. Ennaoui, S. Fiechter, K. Ellmer, M. Kunst, Ch. Koelzow, Ch. Pettenkofer, S. Tiefenbacher, R. Scheer, H. Jungblut, W. Jaegermann, *Thin Solid Films*, **1996**, 272, 38.

[24] D. Briggs and M. P. Seah (eds) *Practical Surface Analysis-Auger and X-ray photoelectron spectroscopy*, **1999**, Wiley, Chicester.

[25] S. Benhida, J. C. Bernede, J. Pouzet, A. Barreau, *Thin Solid Films*, **1993**, 224, 39.

[26] ICDD powder diffraction file 20-1324.

[27] D. G. Mead, J. C. Irwin, *Can. J. Phys.*, **1977**, *55*, 379.

[28] D. Quéré, A. Lafuma, J. Bico, *Nanotechnol.*, **2003**, 14, 1109.

[29] R. N. Wenzel, *Ind. Eng. Chem.*, **1936**, *28*, 988.

[30] A. B. D. Cassie and S. Baxter, *Trans. Faraday Soc.*, **1944**, *40*, 546.

[31] C. J. Carmalt, I. P. Parkin, E. S Peters, *Polyhedron*, **2003**, *22*, 1263.

[32] C. J. Carmalt, T. D. Manning, I. P. Parkin, E. S Peters, A. L. Hector, *J. Mater. Chem.*, **2004**, *14*, 290.

[33] R. Azimirad, N. Naseri, O. Akhavan, A. Z. Moshfegh, *J. Phys. D: Appl. Phys.*, **2007**, *40*, 1134

[34] M. Jin, X. Feng, L. Feng, T. Sun, J. Zhai, T. Li, L. Jiang, *Adv. Mater.*, **2005**, *17*, 1977.

Chapter 5
APCVD of Tin Selenides

5.1 Introduction

In this chapter, the APCVD of tin monoselenide and tin diselenide is described. Films were obtained by the APCVD reaction of tin tetrachloride with diethylselenide. Deposition was observed on both the top substrate and the bottom substrate, which is quite common in CVD, but normally only the heated bottom substrate is analysed in detail. However in this set of experiments both plates were analysed as this gave some important insights into the reaction chemistry and also enabled a variety of different growth microstructures to be investigated. The top substrate was not directly heated in these experiments and was between 75 - 100 °C colder than the bottom substrate. All temperature values given in this chapter are for actual measured temperatures on either the bottom substrate or top substrate. At a bottom substrate temperature below 550 °C, no films were formed on the bottom substrate, whereas, a film was deposited onto the top substrate for a temperature as low as 350 °C. Moreover, the films deposited on the bottom substrate and the films deposited on the top substrate were found to be very different in their composition, morphology and appearance.

5.2 Tin Selenides Films

Atmospheric pressure CVD reactions of tin tetrachloride with diethylselenide were studied on glass substrates at 350 – 650 °C. Tin tetrachloride was chosen following its successful use in CVD processes. Tin phosphide,[1] tin oxide[2] and tin sulfide thin films[3,4] with negligible chlorine incorporation have previously been prepared using $SnCl_4$.

5.2.1.1 Films formed on the Top Substrate from $SnCl_4$ and Et_2Se : Reaction Conditions

Tin tetrachloride ($SnCl_4$) and diethylselenide (Et_2Se) were placed into two different stainless steel bubblers, which were heated to 70 °C by an external jacket. They were both introduced into the gas streams by passing hot N_2 through the bubblers. Flow rates of nitrogen through the $SnCl_4$ bubbler and the diethyl selenide bubbler were kept within 0.2 - 4.0 $L.min^{-1}$ (2.6 - 58.6 $mmol.min^{-1}$) and the flow rate through the mixing chamber was kept constant to 6 $L.min^{-1}$ for all depositions. Deposition time for all experiments was one minute.

5.2.1.2 Appearance, Substrate Coverage and Adherence of the Films

At 350 °C and above a reflective silver-black film composed of large plate-like crystals formed on the top substrate. All the films passed the Scotch tape test, however the films could be scratched with a steel scalpel. The films were insoluble in common organic solvents and were only slowly decomposed in dilute nitric acid and bleach. The films were air and water stable. The extent of the film coverage was dependent on the deposition temperature. Only the last five centimeters of the top substrate were coated at a deposition temperature of 400 °C, whilst the whole top substrate, apart from the first two centimeters, was coated with uniform thickness at 550 °C.

5.2.1.3 Scanning Electron Microscopy

The pronounced layer character of $SnSe_2$ was observed by scanning electron microscopy of the films deposited on the top substrate at 400 – 500 °C (Figure 5.1). Images of the films showed plate-like crystallites, which became surprisingly smaller with increasing deposition temperature, while the lengths varied from ca 80 μm at 500 °C to 10 μm at 550 °C (Figure 5.2). Notably, for all the deposition temperatures, the plates have a degree of texturing with some preferred growth perpendicular to the substrate. Using cross-sectional SEM, the thickness of the films was determined to be close to 10 μm.

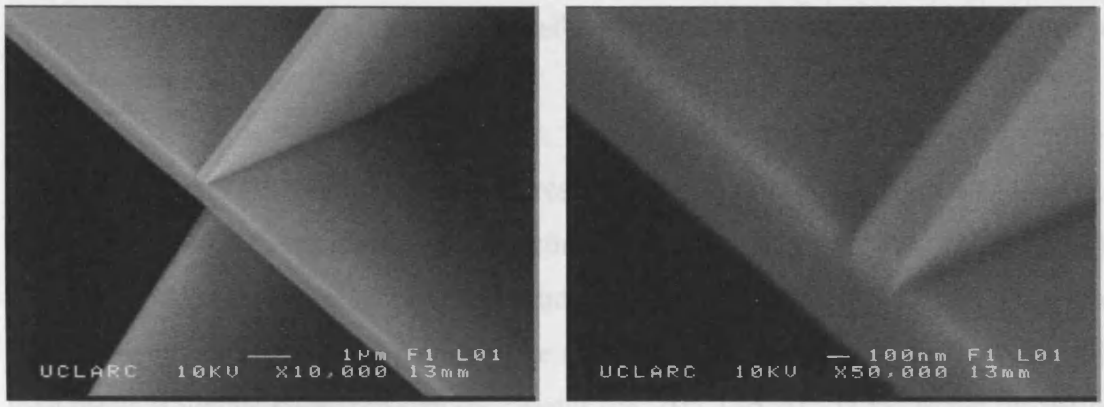

a) 500 °C (1 : 1) **b) 500 °C (1 : 1)**

Figure 5.1 SEM images of the films produced on the top substrate from the APCVD of $SnCl_4$ and Et_2Se at 500 °C.

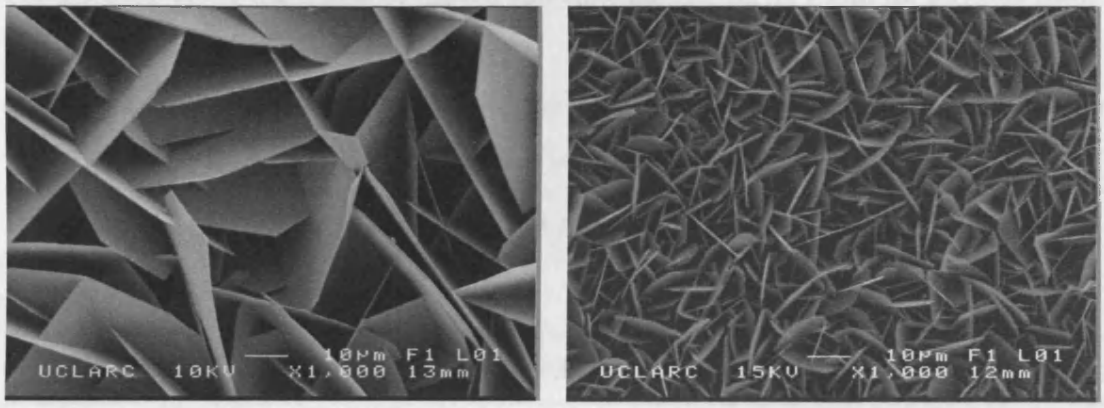

a) 500 °C (1 : 1) **b) 550 °C (1 : 1)**

Figure 5.2 SEM images of the films produced on the top substrate from the APCVD of $SnCl_4$ and Et_2Se at 500 °C and 550 °C.

5.2.1.4 Wavelength Dispersive X-ray Analysis

Wavelength dispersive X-ray analysis showed that all of the films contained selenium and tin with a Sn : Se ratio that depended on the deposition rate and flow conditions (Table 5.1). Under identical flow rate conditions (1 : 1; Et_2Se : $SnCl_4$), the Sn : Se ratio in the film decreased with decreasing deposition temperature. At the highest temperatures (525 - 550 °C), films with the expected stoichiometry for $SnSe_2$ were formed whilst at 400 °C films with an overall stoichiometry $SnSe_{1.5}$ were deposited. Nevertheless, the large size of the crystals observed by SEM allowed us to perform spot analysis on the crystals and showed they had the expected stoichiometry of $SnSe_2$

(Figure 5.1). This result indicates the possible formation of a secondary phase such as tin monoselenide (SnSe).

For identical deposition temperatures, the Sn : Se ratio of the films was found to be directly related to the diethylselenide concentration in the gas phase (Table 5.1). At 550 °C and at identical flow rate conditions (1 : 1), films with the expected stoichiometry for $SnSe_2$ were formed. The use of a higher amount of tin (IV) chloride than diethylselenide going through the reactor (ca. 10 : 1 to 20 : 1) led to the formation of films with an overall stoichiometry that layed between $SnSe_{1.76}$ and $SnSe_{1.58}$. No chlorine was detected within the films, while the presence of trace amounts of carbon (ca. 1 atomic percent) was revealed by WDX. The films showed uniformity in composition along the length of the top substrate and across its width for any one film.

Table 5.1 Reaction conditions, WDX and XRD data of the films formed on the top substrate from the APCVD reaction of $SnCl_4$ with Et_2Se.

Deposition temperature	**Gas Phase Ratio $SnCl_4$: Et_2Se**		**WDX**	**XRD; lattice constant in Å**
400 °C	1:1	4.8 mmol.L^{-1} : 4.8 mmol.L^{-1}	$SnSe_{1.47}$	$SnSe_2$; a = 3.77 Å, c = 6.06 Å
425 °C	1:1	4.8 mmol.L^{-1} : 4.8 mmol.L^{-1}	$SnSe_{1.70}$	$SnSe_2$; a = 3.77 Å, c = 6.07 Å
450 °C	1:1	4.8 mmol.L^{-1} : 4.8 mmol.L^{-1}	$SnSe_{1.72}$	$SnSe_2$; a = 3.77 Å, c = 6.07 Å
500 °C	1:1	4.8 mmol.L^{-1} : 4.8 mmol.L^{-1}	$SnSe_{1.77}$	$SnSe_2$; a = 3.77 Å, c = 6.06 Å
525 °C	1:1	4.8 mmol.L^{-1} : 4.8 mmol.L^{-1}	$SnSe_{2.07}$	$SnSe_2$; a = 3.78 Å, c = 6.07 Å
525 °C	2:1	4.0 mmol.L^{-1} : 8.0 mmol.L^{-1}	$SnSe_{1.86}$	$SnSe_2$; a = 3.77 Å, c = 6.06 Å
550 °C	1:1	4.8 mmol.L^{-1} : 4.8 mmol.L^{-1}	$SnSe_{2.02}$	$SnSe_2$; a = 3.78 Å, c = 6.06 Å
550 °C	5:1	1.6 mmol.L^{-1} : 8.0 mmol.L^{-1}	$SnSe_{2.07}$	$SnSe_2$; a = 3.77 Å, c = 6.06 Å
550 °C	10:1	0.8 mmol.L^{-1} : 8.0 mmol.L^{-1}	$SnSe_{1.76}$	$SnSe_2$; a = 3.76 Å, c = 6.07 Å
550 °C	20:1	0.4 mmol.L^{-1} : 8.0 mmol.L^{-1}	$SnSe_{1.58}$	$SnSe_2$; a = 3.77 Å, c = 6.07 Å

5.2.1.5 X-ray Photoelectron Spectroscopy

X-ray photoelectron spectroscopy of the film formed at 550 °C at a 1 : 1 $SnCl_4$ to Et_2Se ratio showed a single environment for the Sn and Se atoms in the films with Sn $3d_{5/2}$ = 486.6 eV, Sn $3d_{3/2}$ = 495.0 eV and Se $3d_{5/2}$ = 54.3 eV, Se $3d_{3/2}$ = 55.1 eV (Figure 5.3). These values correspond to those reported for $SnSe_2$ (Sn $3d_{5/2}$ = 486.2 eV, Sn $3d_{3/2}$ = 494.9 eV and Se $3d_{5/2}$ = 54.1 eV, Se $3d_{3/2}$ = 55.0 eV).[5] No obvious peaks for tin oxides, tin monoselenide, elemental tin or elemental selenium were observed indicating good purity of the as-synthesized product and confirming the stoichiometry measured by WDX (ca. $SnSe_{2.02}$).

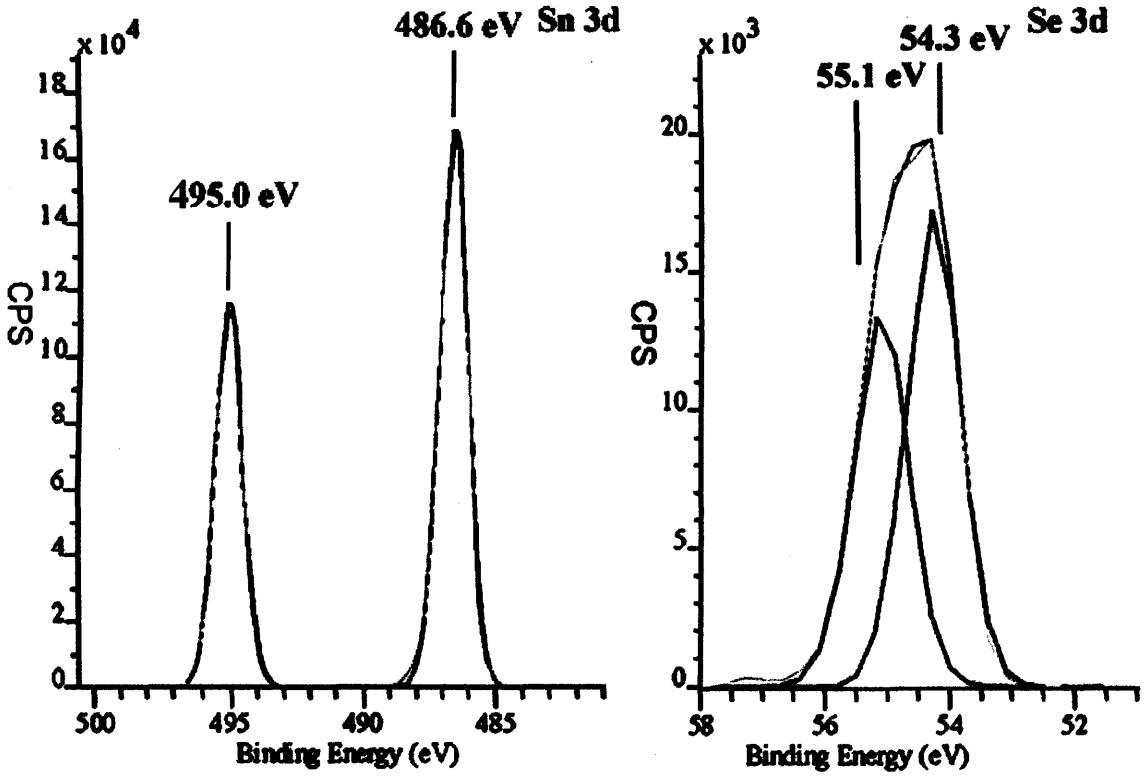

Figure 5.3 XPS spectra of the Sn 3d and Se 3d peaks from the surface of a film deposited on the glass top substrate from the reaction of $SnCl_4$ and Et_2Se at 550 °C for a $SnCl_4$: Et_2Se ratio of 1 : 1. The grey lines show the experimental data and the darker lines show a best fit.

5.2.1.6 X-ray Diffraction

The XRD data show that all of the films were crystalline and showed a good match with the reported pattern for $SnSe_2$ (JCPDS File No. 023-0602). The lattice parameters are calculated as a = 3.77 Å and c = 6.07 Å (Table 5.1), which are in reasonable agreement with the reported values for $SnSe_2$ (a = 3.81 Å and c = 6.14 Å).[6] All the films produced were strongly orientated along the (001) axis parallel to the substrate plane (Figure 5.4). The films deposited at the lower temperatures (450 °C) were shown to be more crystalline than the ones deposited at higher temperatures (550 °C). This compares well with the SEM micrographs (Figure 5.2), which shows larger plates at 450 – 500 °C, than at 550 °C. Notably no secondary phase such as tin monoselenide was detected by powder diffraction.

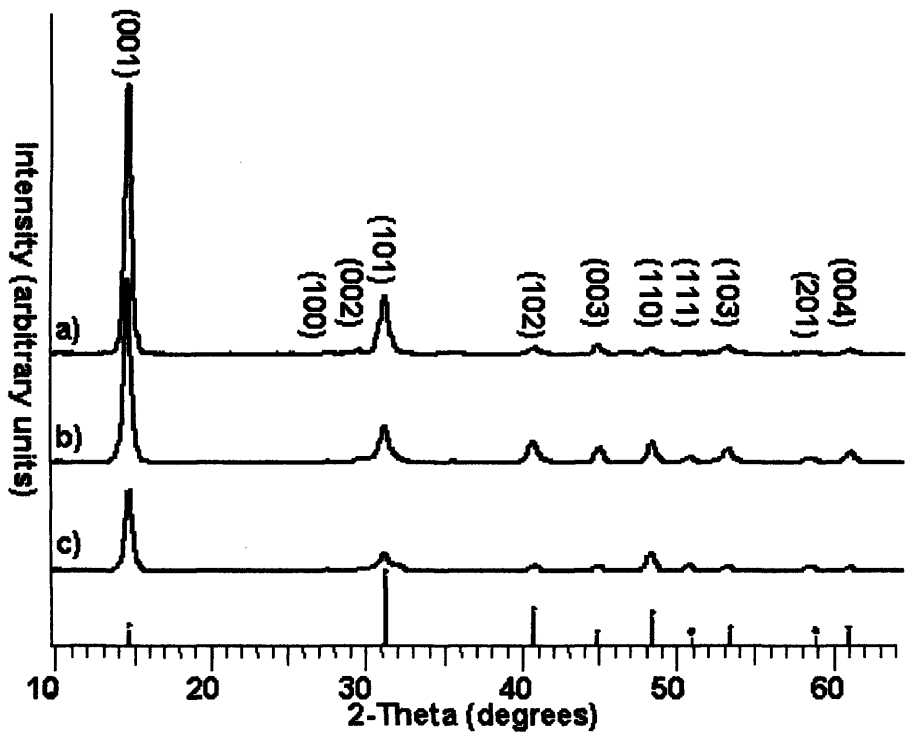

Figure 5.4 The XRD patterns obtained for the films formed on the top substrate from the APCVD of $SnCl_4$ and Et_2Se at 450 °C (a), 500 °C (b) and 550 °C (c). Literature stick pattern for $SnSe_2$ powder (JCPDS File No. 023-0602) is showed.

5.2.1.7 Raman Microscopy

Raman analysis of all films deposited on the glass top substrate, irrespective of temperature or flow rates, showed the same pattern (Figure 5.5). The sharp intense peak observed at 185 cm^{-1} was identified as the frequency of the Raman active A_{1g} mode of $SnSe_2$.[7,8] Raman microscopy did not reveal the presence of any secondary phase in the films produced on the top substrate.

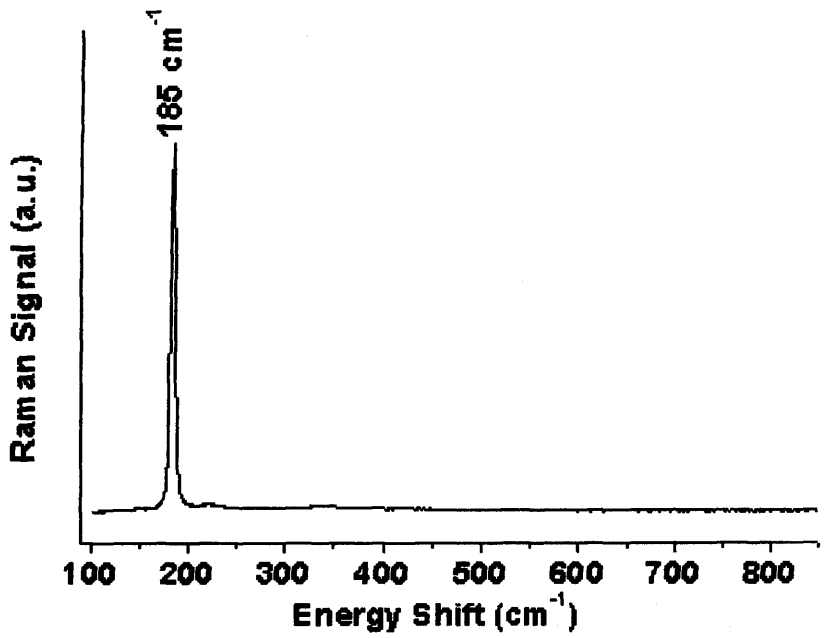

Figure 5.5 Raman pattern obtained for the film formed on the top substrate from the APCVD of $SnCl_4$ and Et_2Se at 500 °C.

5.2.2.1 Films formed on the Bottom Substrate from $SnCl_4$ and Et_2Se : Reaction Conditions

The APCVD reaction of tin tetrachloride ($SnCl_4$) and diethylselenide (Et_2Se) on the bottom substrate was investigated from the onset temperature, 550 °C, up to 650 °C. The $SnCl_4$ and Et_2Se bubblers were heated to 70 °C. Flow rates of nitrogen through the $SnCl_4$ bubbler and the diethyl selenide bubbler were kept within 0.2 - 4.0 $L.min^{-1}$ (2.6 - 58.6 $mmol.min^{-1}$) and the flow rate through the mixing chamber was kept constant to 6 $L.min^{-1}$ for all depositions. Deposition time for all experiments was one minute.

5.2.2.2 Appearance, Substrate Coverage and Adherence of the Films

Films produced from the APCVD of diethylselenide and $SnCl_4$ at 550 – 600 °C on the bottom substrate had a silver-black appearance. The films passed the Scotch tape test but were easily scratched with a steel scalpel. Like the films produced on the top substrate, the films were insoluble in common organic solvents but were slowly decomposed in nitric acid and bleach. At a substrate temperature of 650 °C, the films only covered the last 12 cm of the substrate and at 550 °C, only the last 8 cm. This indicates that the deposition is surface-reaction rate limited.

5.2.2.3 Scanning Electron Microscopy

The SEM images for the films deposited on the bottom substrate at 550 - 600 °C (Figure 5.6) showed a morphology similar to the films deposited on the top substrate (Figure 5.2), with plate-like crystallites orientated perpendicularly from the substrate. In contrast the SEM micrographs for the films deposited at 650 °C show a series of hexagonal platelets orientated parallel to the substrate (Figure 5.7).

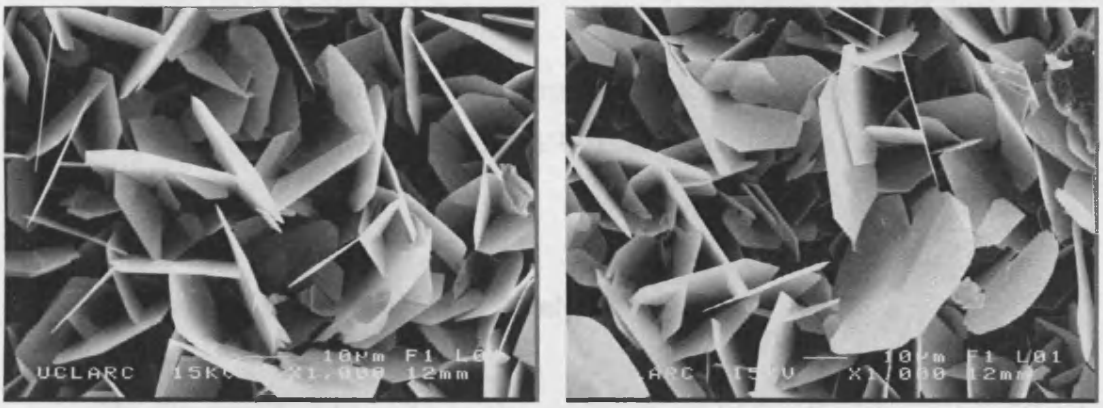

a) 550 °C (1 : 1) **b) 600 °C (1 : 1)**

Figure 5.6 SEM images of the films produced on the bottom substrate from the APCVD of $SnCl_4$ and Et_2Se at 550 °C and 600 °C for a $SnCl_4$: Et_2Se ratios of 1 : 1.

The hexagonal plates formed at 650 °C were observed to become longer and thicker with increasing $SnCl_4$ to Et_2Se gas phase ratio (Figure 5.7). The average length

of the platelets was found to be comprised between 10 μm and 40 μm depending on the flow rates. The stacked layered structure of SnSe can be clearly seen in Figure 5.7.d.

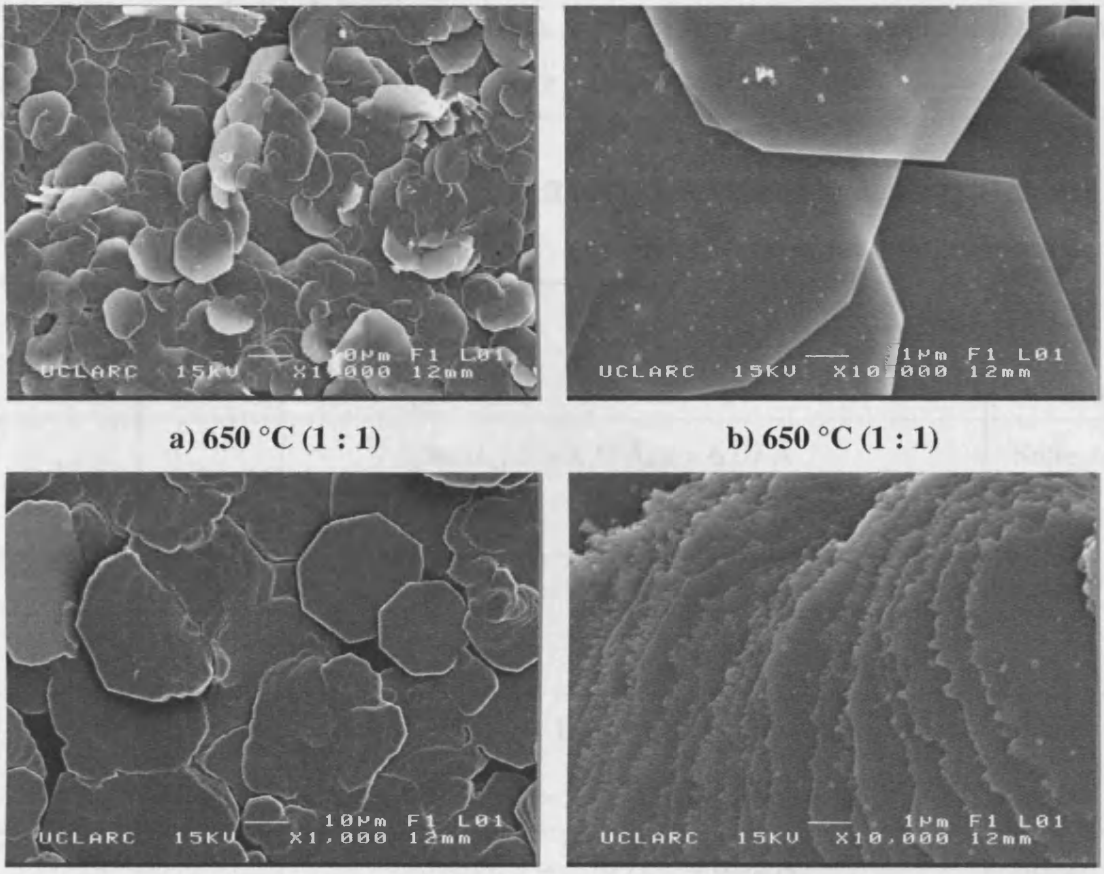

a) 650 °C (1 : 1) **b) 650 °C (1 : 1)**

c) 650 °C (10 : 1) **d) 650 °C (10 : 1)**

Figure 5.7 SEM images of the films produced on the bottom substrate from the APCVD of $SnCl_4$ and diethyl selenide at 650 °C for two different $SnCl_4$: Et_2Se ratios: 1 : 1 and 10 : 1.

5.2.2.4 Wavelength Dispersive X-ray Analysis

The films produced at a deposition temperature of 650 °C with a ratio of $SnCl_4$: diethyl selenide of 5 : 1 (1.6 mmol.L^{-1} : 8.0 mmol.L^{-1}) or higher 20 : 1 (0.4 mmol.L^{-1} : 8.0 mmol.L^{-1}) showed the Sn : Se ratio expected for SnSe by WDX (Table 5.2). The films grown at lower temperature or with a lower $SnCl_4$ / Et_2Se ratio were selenium rich with a tin to selenium ratio between 1.2 and 1.7. This intermediate stoichiometry could indicate the co-formation of SnSe and $SnSe_2$. Carbon (ca. 1 atomic percent) was

detected within the films, whilst no chlorine or other contamination was found by WDX.

Table 5.2 WDX, Raman and XRD data for the films produced onto the bottom substrate by APCVD reaction of $SnCl_4$ with Et_2Se.

Deposition Temperature	**Ratio $SnCl_4$: Et_2Se**	**WDX**	**XRD; lattice constant in Å**	**Raman**
550 °C	1 : 1	-	- -	- -
600 °C	1 : 1	$SnSe_{1.72}$	$SnSe_2$; a = 3.77 Å, c = 6.07 Å -	$SnSe_2$ -
625 °C	1 : 1	$SnSe_{1.48}$	$SnSe_2$; a = 3.78 Å, c = 6.06 Å -	$SnSe_2$ -
625 °C	2 : 1	$SnSe_{1.21}$	SnSe; a = 11.53 Å, b = 4.07 Å, c = 4.28 Å $SnSe_2$; a = 3.78 Å, c = 6.06 Å	SnSe $SnSe_2$
650 °C	1 : 1	$SnSe_{1.34}$	$SnSe_2$; a = 3.78 Å, c = 6.05 Å -	$SnSe_2$ SnSe
650 °C	5 : 1	$SnSe_{1.05}$	SnSe; a = 11.48 Å, b = 4.09 Å, c = 4.25 Å $SnSe_2$; a = 3.75 Å, c = 6.07 Å	SnSe $SnSe_2$
650 °C	10 : 1	$SnSe_{1.02}$	SnSe; a = 11.52 Å, b = 4.06 Å, c = 4.28 Å (001) $SnSe_2$	SnSe -
650 °C	20 : 1	$SnSe_{0.99}$	SnSe; a = 11.50 Å, b = 4.07 Å, c = 4.26 Å (001) $SnSe_2$	SnSe -

5.2.2.5 X-ray Photoelectron Spectroscopy

The XPS of the film deposited on the bottom substrate from $SnCl_4$ and Et_2Se at 650 °C (10 : 1) shows that only one tin environment and one selenium environment

(Figure 5.8) were present in the film. The two doublets at 485.8 and 494.3 eV, and at 53.5 eV and 54.4 eV were attributed respectively to Sn and Se in SnSe (Sn $3d_{5/2}$ = 485.7 eV, Sn $3d_{3/2}$ = 494.2 eV and Se $3d_{5/2}$ = 53.7 eV, Se $3d_{3/2}$ = 54.5 eV).[9,10] No obvious peaks for tin oxides, tin diselenide, elemental tin or elemental selenium were observed indicating high purity of the as-synthesized product.

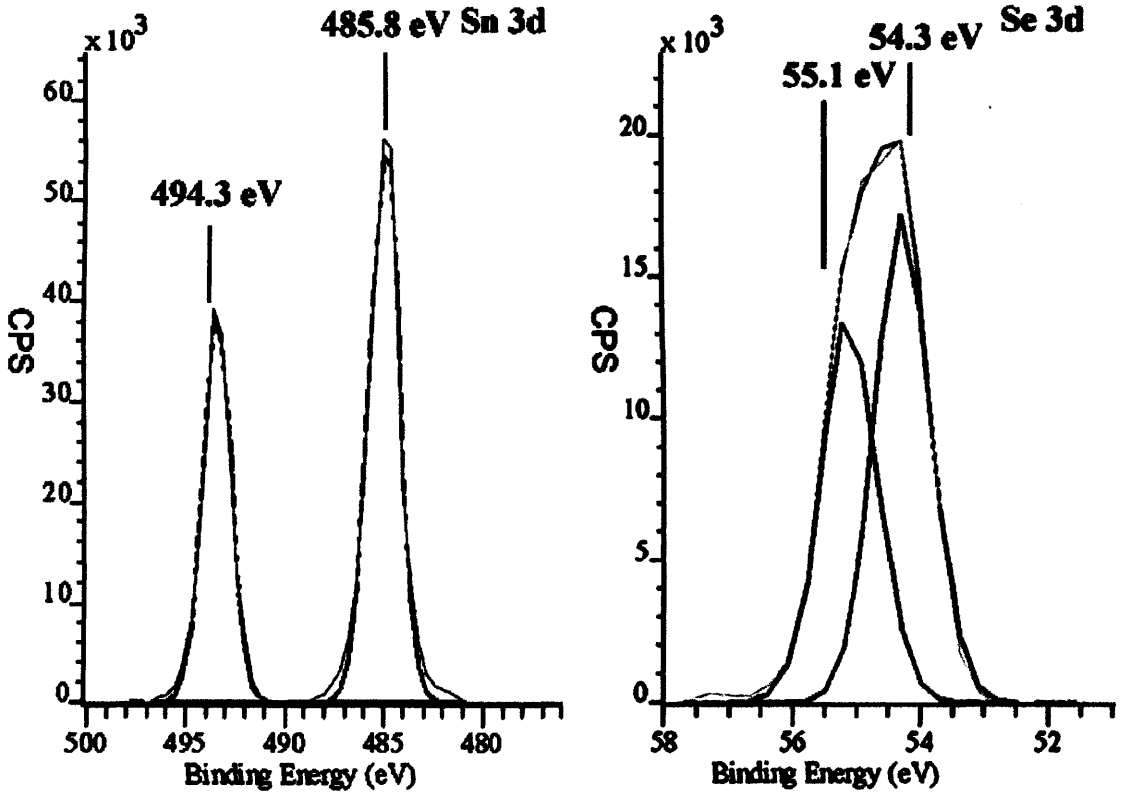

Figure 5.8 XPS spectra of the Sn 3d and Se 3d peaks from the surface of a film deposited on the bottom glass substrate from the reaction of $SnCl_4$ and Et_2Se at 650 °C for a $SnCl_4$: Et_2Se ratio of 10 : 1. The lighter lines are the experimental data and the darker lines a best fit.

5.2.2.6 X-ray Diffraction

The XRD data show that all the films deposited on the bottom substrate were crystalline. For a $SnCl_4$: Et_2Se ratio of 1 : 1, all the films show a good match with the reported pattern for $SnSe_2$ (JCPDS File No. 023-0602). The indexed cell constants given in Table 5.2 and calculated as a = 3.77 Å and c = 6.06 Å are in good agreement with the reported values for $SnSe_2$.[11] The films were strongly orientated along the (001) axis (Figure 5.9).

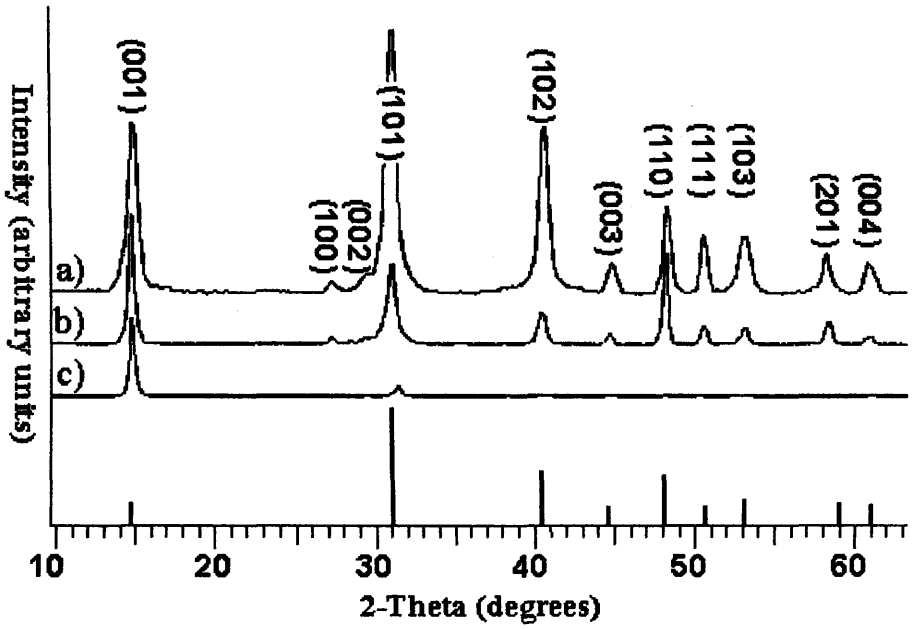

Figure 5.9 The XRD patterns obtained for the films formed on the bottom substrate from the APCVD of $SnCl_4$ and Et_2Se at 600 °C (a), 625 °C (b) and 650 °C (c). Literature stick pattern for $SnSe_2$ powder (JCPDS File No. 023-0602) is showed.

The XRD patterns of the films produced at 650 °C with a higher amount of tin (IV) chloride than diethyl selenide going through the reactor (ca. 5 : 1 to 20 : 1) shown in Figure 5.10, match the reported pattern for SnSe (JCPDS File No. 032-1382). The calculated lattice parameters (Table 5.2), a = 11.50 Å, b = 4.07 Å, c = 4.26 Å, are in good agreement with the reported values for SnSe.[12] The SnSe films showed pronounced preferential orientation parallel to the substrate plane along the (400) direction for the highest $SnCl_4$: Et_2Se ratios. This preferential growth is observed in the SEM pictures where layers seem to stack upon each other along the c-axis. The small reflection present in all the XRD patterns of the SnSe films at $2\theta = 14.8°$ is attributed to the (001) reflection of $SnSe_2$. The presence of this $SnSe_2$ peak within the orthorhombic SnSe patterns has been previously observed.[6] The intensity of this peak suggests that SnSe is the major phase present in these samples, indeed this is confirmed by WDX which shows Sn : Se ratios close to unity.

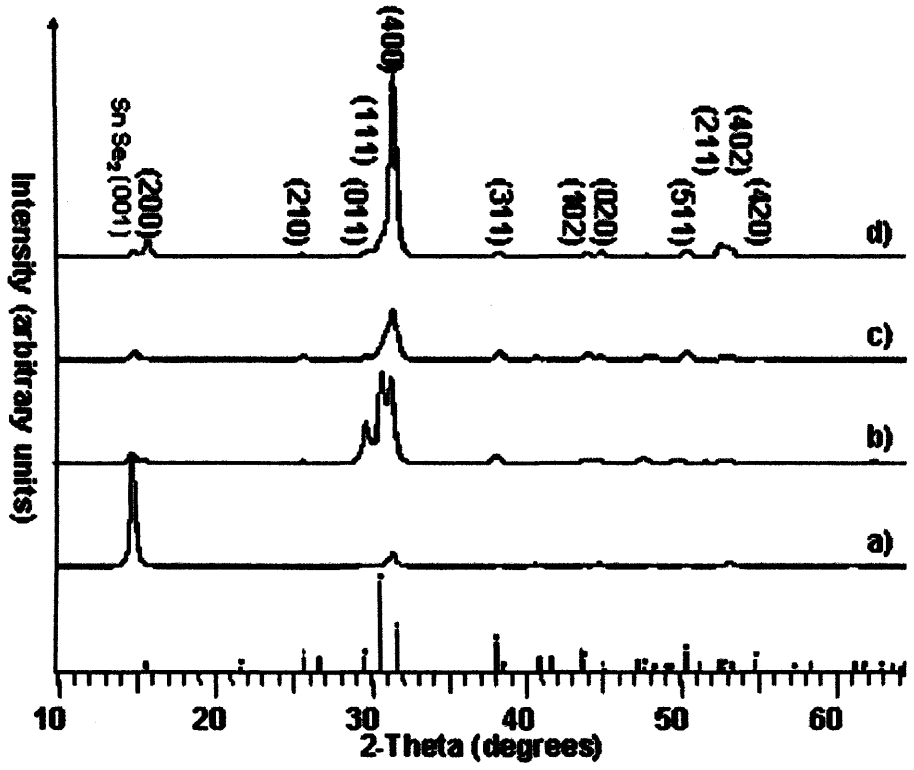

Figure 5.10 The XRD patterns obtained for the film formed on the bottom glass substrate from the APCVD of $SnCl_4$ and diethyl selenide at 650 °C for the following $SnCl_4$: Et_2Se ratios: 1 : 1 (a), 5 : 1 (b), 10 : 1 (c), 20 : 1 (d). Literature stick pattern for SnSe powder (JCPDS File No. 032-1382) is showed.

5.2.2.7 Raman Microscopy

Raman analysis of the films deposited on the bottom substrate show strong variations depending on the flow rate conditions and deposition temperature. For deposition temperature below 650 °C, the Raman spectrum irrespective of flow rates, showed the $SnSe_2$ pattern with the sharp intense peak of the A_{1g} mode at 185 cm^{-1} (Figure 5.5). At 650 °C, in addition to the $SnSe_2$ peak at 185 cm^{-1}, two peaks were observed at 131 cm^{-1} and 149 cm^{-1} (Figure 5.11). These two peaks, which correspond to the A_g Raman active mode of SnSe, were found to increase with the gas phase $SnCl_4$: Et_2Se reactant ratio.[13] Whereas the band associated with the $SnSe_2$ phase was seen to have almost disappeared.

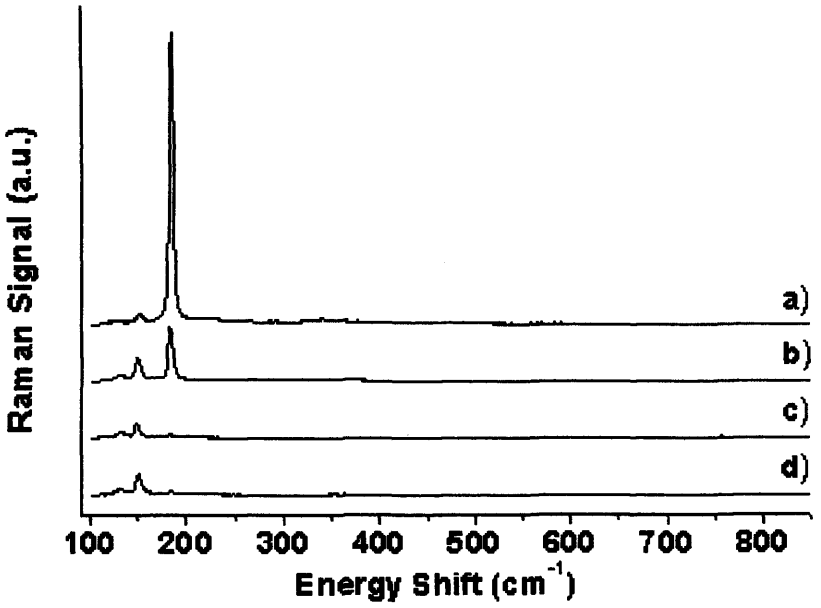

Figure 5.11 Raman pattern obtained for the film formed on the bottom substrate from the APCVD of $SnCl_4$ and Et_2Se at 650 °C for different $SnCl_4$: Et_2Se ratios: 1 : 1 (a), 5 : 1 (b), 10 : 1 (c), 20 : 1 (d).

5.2.2.8 Optical Properties

Optical measurements on all the films produced (SnSe, $SnSe_2$ and SnSe - $SnSe_2$), either on the top substrate or bottom substrate, show that they were exceptionally absorbing in the visible and near IR regions. The transmittance and reflectance of films, even as thin as 100 nm, was near 0 % from 400 - 1100 nm (Figure 5.12). This property of exceptionally high absorbtivity explains the interest of this material for solar cell applications.

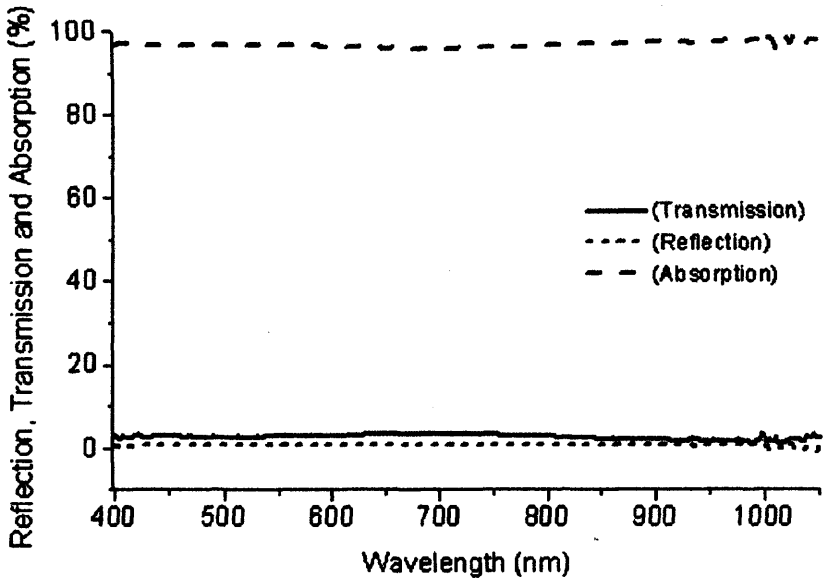

Figure 5.12 Optical reflection, transmission and absorption spectra for a 100 nm film formed on the bottom substrate from the APCVD of $SnCl_4$ and Et_2Se at 650 °C for a $SnCl_4$: Et_2Se ratio of 10 : 1.

5.2.3 Discussion

The results show that the morphology and stoichiometry of films formed from the APCVD reaction of $SnCl_4$ with Et_2Se are strongly dependent on the substrate's position. For films formed on the top substrate, the measured temperatures were some 100 °C lower than the corresponding film grown on the bottom substrate. Films formed with an onset of deposition at 350 °C on the top substrate, significantly lower than those for the bottom substrate which had an onset for deposition of 600 °C. One explanation for this is that gas-phase nucleation is important in the early part of the reaction and that the particles formed are repelled from the heated bottom substrate to the unheated cooler top substrate - in effect they bounce off the boundary layer formed at the bottom substrate- a thermophoretic effect. The position of the deposited film at the back end of the top substrate, ties in well with this observation. Perhaps small amounts of nucleated gas phase particles offer an attractive nucleation point for further film growth. However the morphology seen by SEM of the films formed on the top substrate does not show any formation of gas phase particles, where rounded edges and islands often predominate.[14] The very large size of the $SnSe_2$ crystals formed on the top substrate

could mask or actually absorb these nucleated islands. Notably the $SnSe_2$ phase showed a much larger size and crystallinity at lower deposition temperatures, this is unusual as fast crystal growths are usually seen at elevated temperatures. The marked change in size from ca 70 to 20 micron sized from 500 to 550 °C is probably a consequence of the number of nucleation sites that were generated on the surface. At lower deposition temperatures presumably fewer nucleation sites are present and the crystallites can acquire more precursor and grow larger. However at higher deposition temperature, many more nucleation sites are present and the crystallites have more competition for precursor, and although they have a higher density in terms of number of crystallites per unit area of the film they themselves are significantly smaller.

The amount of selenium found in the films on the top substrate was directly related to temperature and flow rate conditions (Table 5.1). Hence at lower temperature it seems that insufficient Et_2Se is available, perhaps because at this temperature insufficient C-Se bonds are broken. If given enough precursor the favored product on both the top substrate and bottom substrate seems to be $SnSe_2$, indeed this product shows up prominently in both the XRD and Raman results. The orientation of the films on either the top substrate or bottom substrate was related to the phase formed - $SnSe_2$ always formed crystallites perpendicular to the substrate and the SnSe films always parallel to the substrate.

5.3 Conclusion

Tin monoselenide and tin diselenide films were deposited on glass from the APCVD reaction of diethyl selenide and $SnCl_4$. All the films produced were crystalline and adherent. EDAX, Raman, XRD and XPS analysis performed on these films show the ability of CVD to produce pure SnSe, mixed SnSe-$SnSe_2$ phases or pure $SnSe_2$ thin films by modification of the deposition conditions. SnSe films were obtained at 650 °C on the bottom substrate with a $SnCl_4$ to Et_2Se ratio superior to 10. XRD show preferred growth orientated along the (400) axis parallel to the substrate. This preferential growth orientation could be observed on the SEM pictures where layers seem to be stack upon each other along the *c*-axis. $SnSe_2$ films were obtained at 625 - 650 °C on the top substrate; they were black-silver in appearance and composed of big adherent plane

crystals. SEM pictures showed plate-like crystallites orientated perpendicular to the substrate and XRD showed that the films were strongly orientated along the (001) axis parallel to the substrate plane. All the films produced were stable in air and were insoluble in common organic solvents. The CVD route developed here to $SnSe_2$ and SnSe is compatible with photovoltaic device manufacture, as such the high absorbtivity of these films could prove useful as a solar absorbtion element in a photovoltaic stack.

5.4 References

[1] R. Binions. C. J. Carmalt, I. P. Parkin, *Proc. – Electrochem. Soc.*, **2003**, *2*, 1426.

[2] N. Ghoshtagore, *J. Electrochem. Soc.*, **1978**, *125*, 110.

[3] A. Ortiz, J. C. Alonso, M. Garcia, J. Toriz, *Semicond. Sci. Techn.*, **1996**, *11*, 243.

[4] L. S. Price, I. P. Parkin, A. M. Hardy, R. J. H. Clark, G. Thomas, K. C. Molloy, *Chem. Mater.*, **1999**, *11*, 1792.

[5] F. Mirabella, B. A. Parkinson, J. Ghijsen, *Phys. Stat. Sol.*, **2004**, *1*, 372.

[6] K. Bindu, P. K. Nair, *Semicond. Sci. Technol.*, **2004**, *19*, 1348.

[7] D. Walsh, S. Jandl, J. Y. Harbec, *J. Phys. C: Solid St. Phys.*, **1980**, *13*, L125.

[8] A. J. Smith, P. E. Meek, W. Y. Liang, *J. Phys. C: Solid St. Phys.*, **1997**, *10*, 1321.

[9] R. B. Shalvoy, G. B. Fisher, P. J. Stiles, *Phys. Rev. B*, **1977**, 15, 1680.

[10] C. D. Wagner, J. F. Moulder, L.E. Davis, W. M. Riggs, *Handbook of X-Ray Photoelectron Spectroscopy*, Perking-Elmer Corporation; Physical Electronics Division; Eden Prairie, Minnesota, **1979**.

[11] N. Ganesan, V. Sivaramakrishnan, *Semicond. Sci. Technol.*, **1987**, *2*, 519.

[12] Y. Xie, H. Su, B. Li, Y. Qian, *Mater. Res. Bull.*, **2000**, *35*, 459.

[13] H. R. Chandrasekhar, R. G. Humphreys, U. Zwick, M. Cardona, *Phys. Rev. B*, **1976**, *15*, 2177.

[14] K. L. Choy, *Prog. Mater. Science*, **2003**, *48*, 57.

Chapter 6
APCVD and Chemical Vapour Synthesis of Chromium Oxyselenides

6.1 Introduction

This chapter describes the APCVD and chemical vapor synthesis of the new ternary compound chromium oxyselenide. The existence of chromium oxysulfide,[1,2,3] chromium sulfoselenide,[4,5] chromium sulfotelluride[6,7,8,9,10] and chromium selenotelluride[11,12] has been known for a long time and a large number of studies have focused on their magnetic and crystallographic properties. However, the formation of a chromium oxyselenide has not been reported. Several other oxyselenides of transition-metals have been observed in the past,[13,14,15,16] however little is known about their properties. A large number of rare-earth-transition metal oxyselenide have been synthesised. It is possible to form chromium-lanthanum or chromium-cerium oxyselenide by mixing $(LaO)_2Se$ or $(CeO)_2Se$ with Cr_2Se_3 at 1000 °C in ampoules sealed under vacuum.[17,18] In this chapter the synthesis and characterisation of a new solid solution in the system Cr_2O_3 - Cr_2Se_3 is reported.

6.2 APCVD and Chemical Vapour Synthesis of Chromium Oxyselenides Powders and Films

The APCVD and gas-phase reaction of chromyl chloride (CrO_2Cl_2) with diethyl selenide (Et_2Se) was investigated over the range of temperature 400 – 600 °C. CrO_2Cl_2 has been already widely used in CVD to produce Cr_2O_3 and CrO_2 thin films,[19,20] and mixed-metals oxide films such as $Cr_{2-x}Ti_xO_3$[21] and $V_{1-x}Cr_xO_2$.[22] The APCVD reaction of (CrO_2Cl_2) with a sulfide precursor has been investigated in the past, however the reaction of (CrO_2Cl_2) and H_2S produced amorphous and non-uniform films with a stoichiometry varying from $CrS_{0.70}Cl_{0.65}O_{0.07}$ to $CrS_{0.64}Cl_{0.34}O_{2.21}$.[23] Other chromium precursors used in CVD included CrO_3,[24] $[Cr(CO)_6]$,[25] $[Cr[(C_6H_5)C_3H_7)_2]$,[26]

$[Cr(C_5H_7O_2)_3]$,[27] Cr(III)(hexafluoroacetylacetonate) and tris(2,2,6,6-tetra-methyl-3,5-heptanedionato) chromium(III).[28]

6.2.1.1 Films and Powders formed from CrO_2Cl_2 and Et_2Se : Reaction Conditions

Chromyl chloride (CrO_2Cl_2) and diethylselenide (Et_2Se) were placed into two different stainless steel bubblers, which were heated by an external jacket to 75°C and 70°C respectively. Both precursors were introduced into gas streams by passing hot N_2 through the bubblers. Flow rates of nitrogen through the CrO_2Cl_2 bubbler and Et_2Se were kept within 0.1 – 4.0 L min^{-1} (1 – 60 $mmol.min^{-1}$) and the flow rate through the mixing chamber was between 2.0 and 5.0 L min^{-1} for all depositions. The reaction was studied over the temperature range of 400 – 600 °C. All deposition times were one minute.

6.2.1.2 Appearance, Substrate Coverage and Adherence of the Films and Powders Produced.

At reaction temperatures below 550 °C and irrespective of the flow rates, thin films of chromia were grown from CrO_2Cl_2 and Et_2Se across the entire length of the substrate. The films were hard, strongly adherent to the glass and had the characteristic green colour of Cr_2O_3. This is not surprising, as chromyl-chloride is known to be a common precursor for chromia deposition.[29,30,31,32] At 600 °C, the APCVD reaction of CrO_2Cl_2 with Et_2Se was found to be strongly dependant on the molar gas flows. For low Et_2Se : CrO_2Cl_2 ratios (under 14.7 $mmol.min^{-1}$: 10.9 $mmol.min^{-1}$), the films produced were similar to the ones produced at lower temperature. With an increase of the Et_2Se relative gas flow, the films formed were greyish with a weak hardness. They passed the Scotch tape test, however they were easily scratched and removed from the substrate with a steel scalpel. The films were insoluble in common organic solvents but were slowly decomposed in dilute nitric acid and bleach. The films were air stable and water stable. Above a Et_2Se : CrO_2Cl_2 ratio of 1.35 : 1 (14.7 $mmol.min^{-1}$: 10.9 $mmol.min^{-1}$), no films were formed while the formation of a fine black powder was observed at the surface of the glass substrate. The particles formed were air and water stable, insoluble in common organic solvents but were quickly decomposed in dilute nitric acid and bleach. The amount of particles collected on the substrate after each one minute run

varied from 5 to 20 mg. More powder was anticipated to be produced during the APCVD reaction, however due to the non-adherence of the fine particles formed; part of it was probably flushed away by the required high flow rate through the reactor.

6.2.1.3 Scanning Electron Microscopy

Scanning electron microscopy (SEM) images of the films formed at 600 °C with a Et_2Se to CrO_2Cl_2 gas phase ratio inferior to 1.3 : 1 showed a series of crystals which become longer and larger with a decrease in the concentration of selenium precursor in the gas phase (Figure 6.1). The size of the crystals observed varied from 1-2 μm when using CrO_2Cl_2 only, to 100-500 nm when deposited from an equi-molar flow of CrO_2Cl_2 and Et_2Se. No secondary phase was observed by SEM.

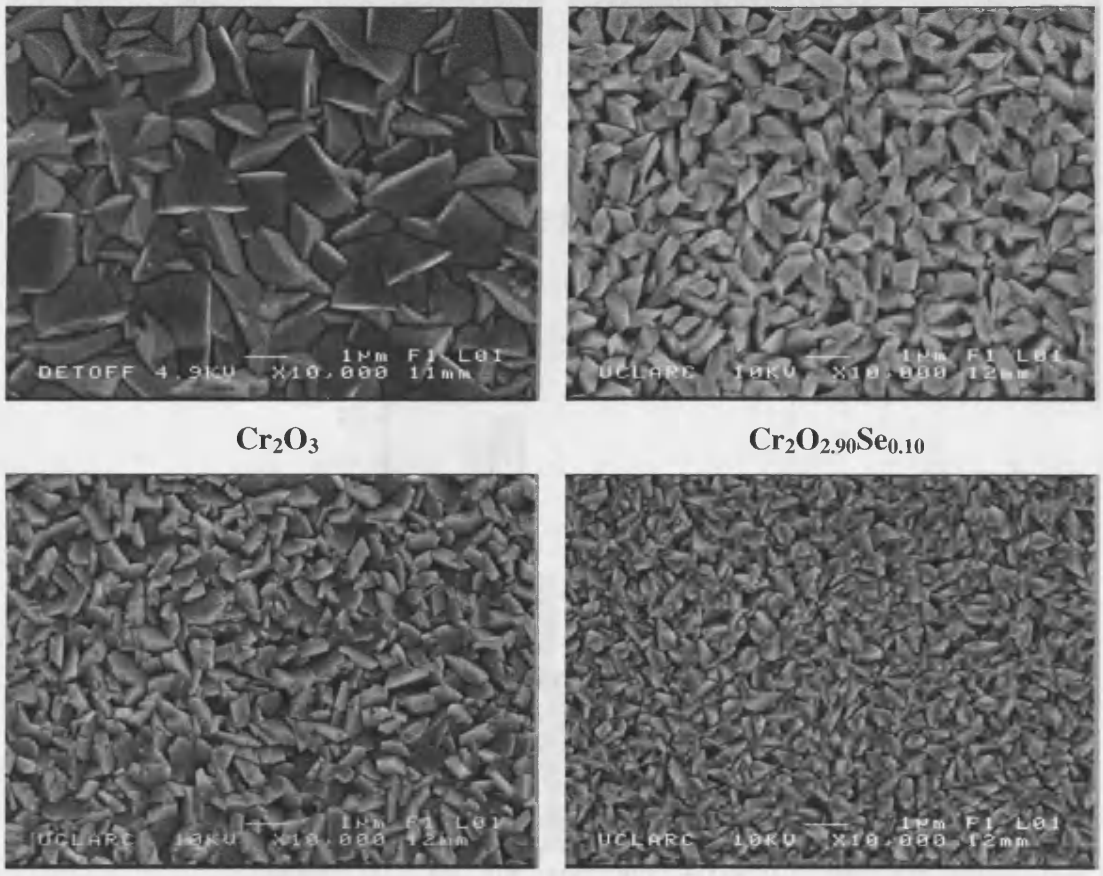

Cr_2O_3 $Cr_2O_{2.90}Se_{0.10}$

$Cr_2O_{2.85}Se_{0.15}$ $Cr_2O_{2.80}Se_{0.20}$

Figure 6.1 SEM images of the films produced from the APCVD of CrO_2Cl_2 and Et_2Se at 600 °C.

SEM images of the powders formed at 600°C with a Et_2Se : CrO_2Cl_2 ratio superior to 1.35 : 1 showed a large number of spherical nanoparticles (Figure 6.2). This spherical and agglomerated morphology is consistent with gas phase formation. The gas phase precipitation is used to produce extremely fine powders as observed here. Increase of the Et_2Se relative gas flow didn't show any change in the size or shape of the nanoparticles. The mean size of these gas phase synthesised nanoparticles was 100 nm, while the size distribution varied from 25 to 300 nm (Figure 6.3). Once again, no secondary phase was observed by SEM.

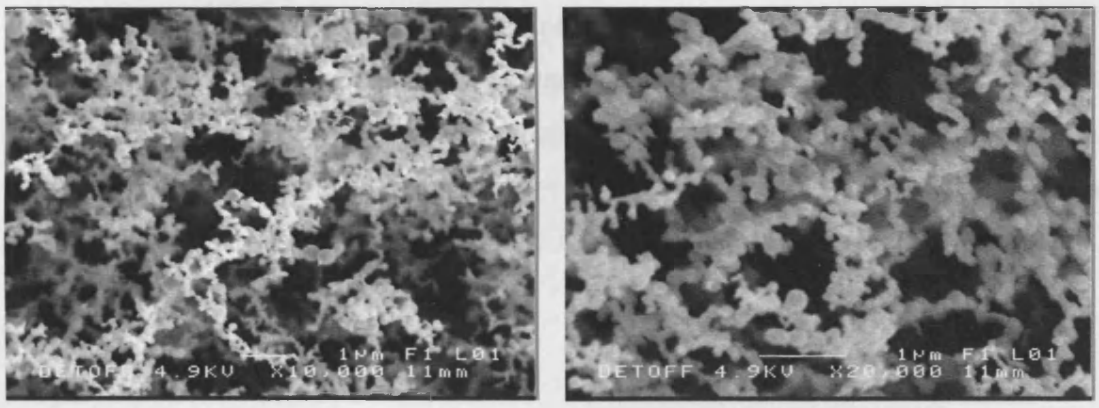

Figure 6.2 SEM images of the nanoparticles produced from the chemical vapour reaction of CrO_2Cl_2 and Et_2Se at 600 °C.

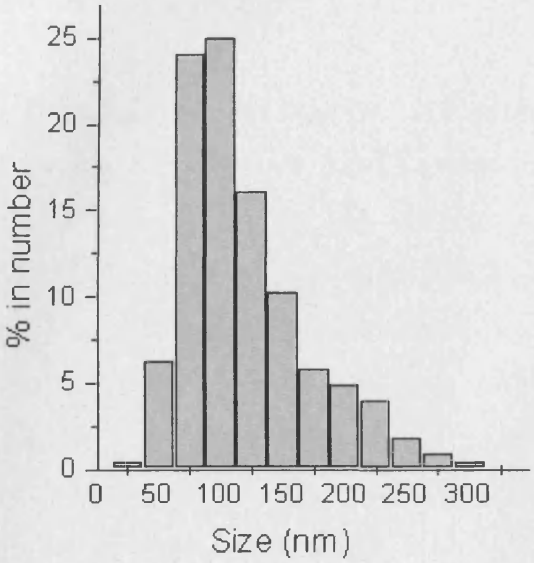

Figure 6.3 Statistical distribution in the nanoparticles size for the particles formed from CrO_2Cl_2 and Et_2Se at 600 °C.

6.2.1.4 Wavelength Dispersive X-ray Analysis

Energy and wavelength-dispersive X-ray analysis (EDX / WDX) showed that the films and the powders produced at 600 °C and above contain chromium, oxygen and selenium in a ratio that strongly depend on the flow rate conditions used. The stoichiometry of the adherent films formed from Et_2Se and CrO_2Cl_2 was determined to vary from Cr_2O_3 to $Cr_2O_{2.8}Se_{0.2}$, while the stoichiometry of the particles produced from the same precursors varied from $Cr_2Se_{0.3}O_{2.7}$ to $Cr_2Se_{2.2}O_{0.8}$ (Table 6.1). In both cases, the chlorine level was found to be less than an atom%. Point WDX analysis on the powders showed disparity in the stoichiometry of the particles from a unique APCVD run. This heterogeneity in composition was more strongly observed with the oxygen-rich particles; with a particle's stoichiometry varying from $Cr_2Se_{0.3}O_{2.7}$ to $Cr_2Se_{0.7}O_{2.3}$ for an overall stoichiometry of the powder between $Cr_2Se_{0.3}O_{2.7}$ and $Cr_2Se_{0.5}O_{2.3}$. The selenium-rich particles were found to show a better homogeneity in their stoichiometry.

Table 6.1 Reaction conditions, WDX, XRD and Raman data of the films formed from the APCVD reaction of CrO_2Cl_2 with Et_2Se at 600 °C.

$Et_2Se : CrO_2Cl_2$	EDX / WDX	XRD ; lattice constants	*c/a*	**Raman**
Reference [33]	Cr_2O_3	Cr_2O_3 ; a = 4.939 Å, c = 13.627 Å	2.76	Cr_2O_3
0 : 1	$Cr_2O_{3.00}$	Cr_2O_3 ; a = 4.981 Å, c = 13.652 Å	2.74	Cr_2O_3
1 : 1	$Cr_2O_{2.90}Se_{0.10}$	Cr_2O_3 ; a = 4.937 Å, c = 13.675 Å	2.77	Cr_2O_3
1 : 1	$Cr_2O_{2.85}Se_{0.15}$	Cr_2O_3 ; a = 4.928 Å, c = 13.602 Å	2.76	Cr_2O_3
1 : 1	$Cr_2O_{2.80}Se_{0.20}$	Cr_2O_3 ; a = 4.988 Å, c = 13.664 Å	2.74	Cr_2O_3
1.3 : 1	$Cr_2Se_{0.30}O_{2.70}$	Cr_2Se_3 ; a = 6.204 Å, c = 17.096 Å	2.756	225 cm^{-1}
2 : 1	$Cr_2Se_{0.40}O_{2.60}$	Cr_2Se_3 ; a = 6.231 Å, c = 17.315 Å	2.779	225 cm^{-1}
5 : 1	$Cr_2Se_{0.50}O_{2.50}$	Cr_2Se_3 ; a = 6.271 Å, c = 17.354 Å	2.767	225 cm^{-1}
10 : 1	$Cr_2Se_{0.70}O_{2.30}$	Cr_2Se_3 ; a = 6.266 Å, c = 17.452 Å	2.785	225 cm^{-1}
20 : 1	$Cr_2Se_{1.50}O_{1.50}$	Cr_2Se_3 ; a = 6.237 Å, c = 17.595 Å	2.821	225 cm^{-1}
40 : 1	$Cr_2Se_{2.15}O_{0.85}$	Cr_2Se_3 ; a = 6.248 Å, c = 17.649 Å	2.825	225 cm^{-1}
Reference [34]	Cr_2Se_3	Cr_2Se_3 ; a = 6.250 Å, c = 17.280 Å	2.765	Cr_2Se_3

6.2.1.5 X-ray Photoelectron Spectroscopy

XPS spectra of as-prepared powder (Figure 6.4) confirm the presence of three elements - chromium, oxygen and selenium in the same ratio as found from WDX analysis ($Cr_2Se_{0.7}O_{2.3}$). Only one environment was observed for each of the element present in the powder; Cr $2p_{1/2}$ = 585.3 eV, Cr $2p_{3/2}$ = 576.2 eV; O 1s = 531.5 eV; Se $3d_{3/2}$ = 55.1 eV and Se 3d = 54.0 eV. The chromium environment for the $2p_{3/2}$ peak is intermediate between that of Cr_2O_3 at 576.6 eV and Cr_2Se_3 at 574.6 eV and indicative of Cr(III).[35,36] The oxygen 1s environment showed a narrow full width half maximum peak at 1.7 eV – indicative of a single environment and a binding energy shift consistent with an oxide and matching that in chromium oxide 530.8 eV.[37] The selenium $3d_{3/2}$ peak matched that found in Cr_2Se_3 at 54.0 eV.[35]

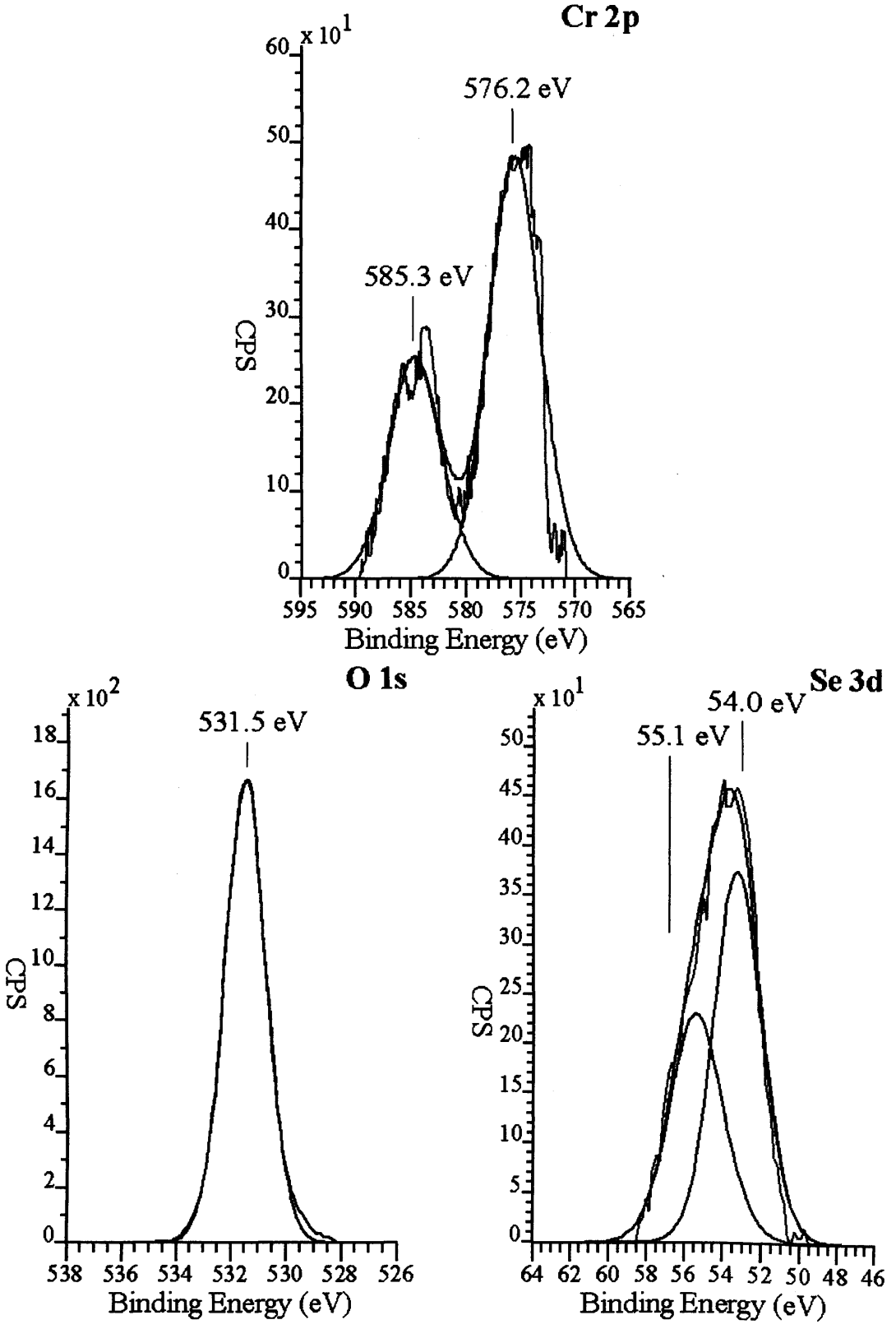

Figure 6.4 Selected area XPS spectra of the chromium oxyselenide ($Cr_2Se_{0.70}O_{2.30}$) powder produced at 600 °C from the gas phase reaction of CrO_2Cl_2 and Et_2Se. Top, Cr 2p region; left, O 1s region; right, Se 3d region. The grey lines show the experimental data and the darker lines show a best fit.

6.2.1.6 X-ray Diffraction

X-ray diffraction showed that all the adherent films produced from CrO_2Cl_2 and Et_2Se were crystalline, and show a good match with the reported patterns for hexagonal Cr_2O_3 (JCPDS File No. 006–0504) and CVD prepared chromia coatings.[38] The evaluated lattice parameters (Table 6.1) are in good agreement with the reported ones for hexagonal Cr_2O_3 a = 4.939 Å, c = 13.627 Å. No evidence of another chromium oxide - such as CrO_2 - or a chromium selenide phase was found by XRD (Figure 6.5).

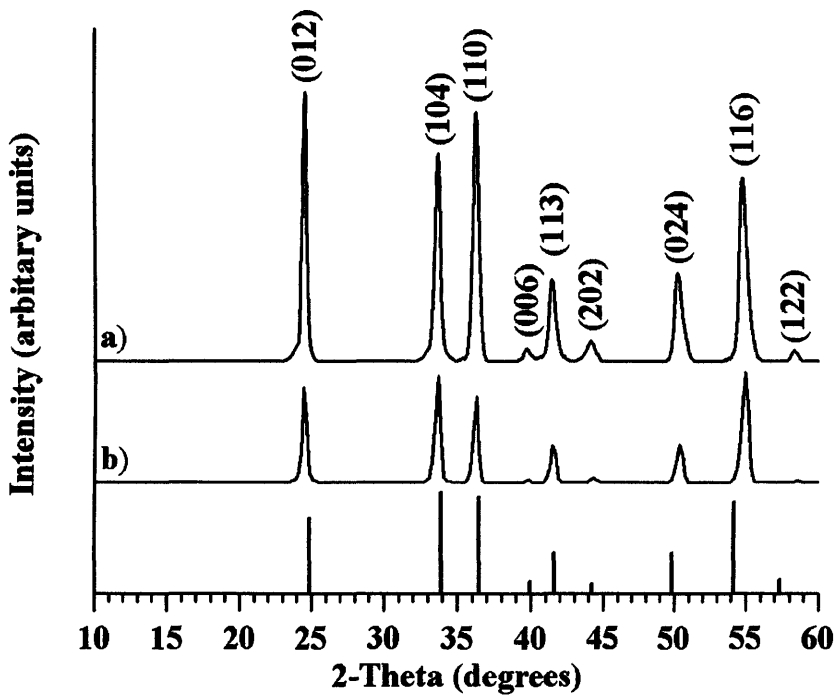

Figure 6.5 XRD pattern obtained for the films formed on glass substrate at 600 °C from the APCVD reaction of chromyl chloride and diethylselenide for the following Et_2Se : CrO_2Cl_2 ratios: 0 : 1 (a) and 1 : 1 (b). Literature stick pattern for Cr_2O_3 powder (JCPDS File No. 006–0504) is shown.

The powders produced from the gas phase reaction of CrO_2Cl_2 and Et_2Se were confirmed to be a single phase by X-ray diffraction (Figure 6.6). XRD data shows that all the powders were crystalline and compared well with the reported pattern for rhombohedral Cr_2Se_3 (JCPDS File No. 040-1403). The diffraction peaks are almost comparable to the stick pattern for rhombohedral Cr_2Se_3 found in the literature. However, the (116) peak was appreciably weaker and broader. The cell constants of the

particles calculated in the hexagonal lattice were found to be slightly different than the one reported for Cr_2Se_3; a = 6.250 Å, c = 17.280 Å (Table 6.1). The lattice parameters were found to increase with selenium to oxygen ratio x in the $Cr_2Se_xO_{3-x}$ particles. For the lowest and highest concentration of selenium in the powders, the cell constants were respectively calculated as a = 6.204 Å, c = 17.096 Å and a = 6.248 Å, c = 17.649 Å. The axial ratio c/a was also found to increase with x, as shown in Table 6.1.

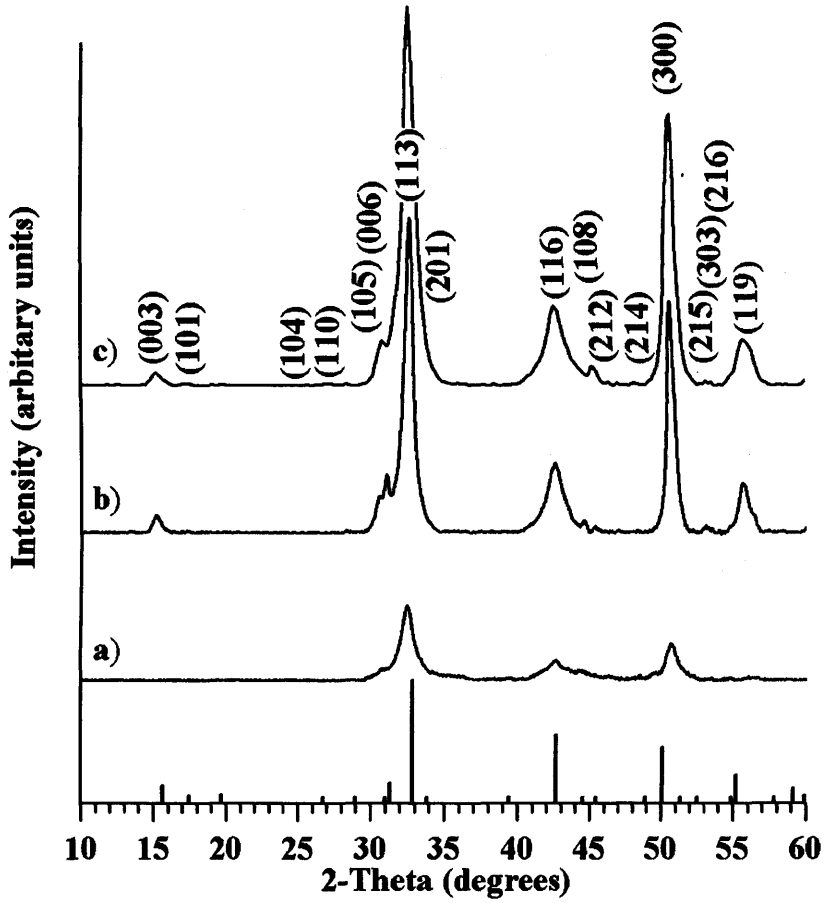

Figure 6.6 XRD pattern obtained for the powders formed at 600 °C from the APCVD reaction of chromyl chloride and diethylselenide for two different Et_2Se : CrO_2Cl_2 ratios: 1.3 : 1 (a), 5 : 1 (b) and 10 : 1 (c). Literature stick pattern for rhombohedral Cr_2Se_3 powder (JCPDS File No. 040–1403) is shown.

6.2.1.7 Raman Microscopy

Raman spectroscopy of all films, irrespective of their green or grey colour showed the same pattern (Figure 6.7). This was readily identified as the distinctive Cr_2O_3 Raman pattern reported in the literature with peaks at 307, 350, 524, 551 and 610

cm^{-1}.[39] The most intense band at 551 cm^{-1} corresponds to the frequency of the Raman active A_{1g} modes, while the other are of the E_g symmetry. No evidence was seen for a secondary phase, such as CrO_2 or Cr_2Se_3.[40,41]

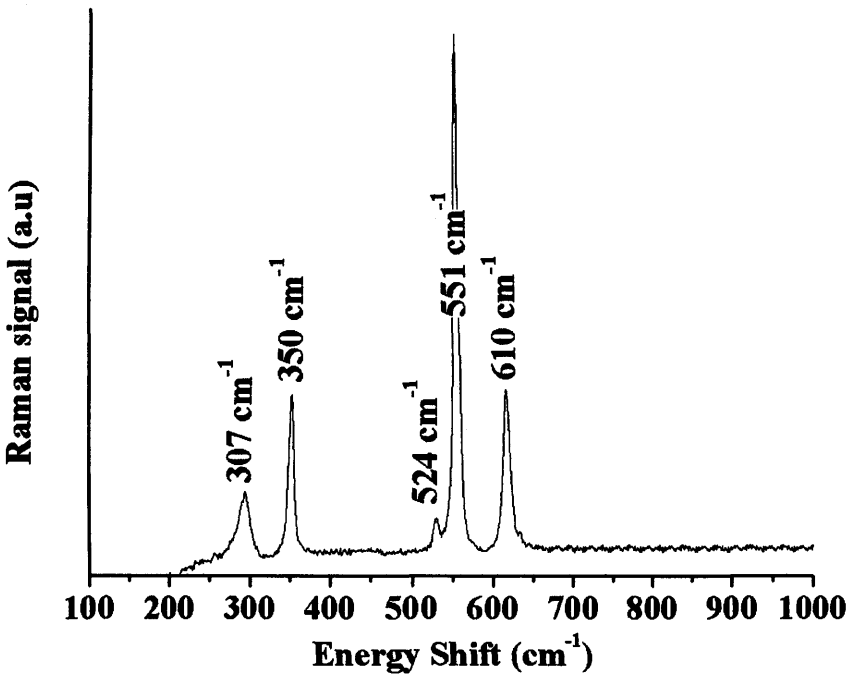

Figure 6.7 Raman pattern obtained for the film formed on glass substrate at 600 °C from the APCVD reaction of CrO_2Cl_2 and Et_2Se.

Raman analysis of the powders formed from the gas phase reaction of CrO_2Cl_2 and Et_2Se revealed a weak and broad peak around 225 cm^{-1} (Figure 6.8). The absence of the bands for Cr_2O_3 and CrO_2, which are excellent Raman scatterers, confirms that no chromium oxide was formed during the APCVD reaction of CrO_2Cl_2 and Et_2Se.

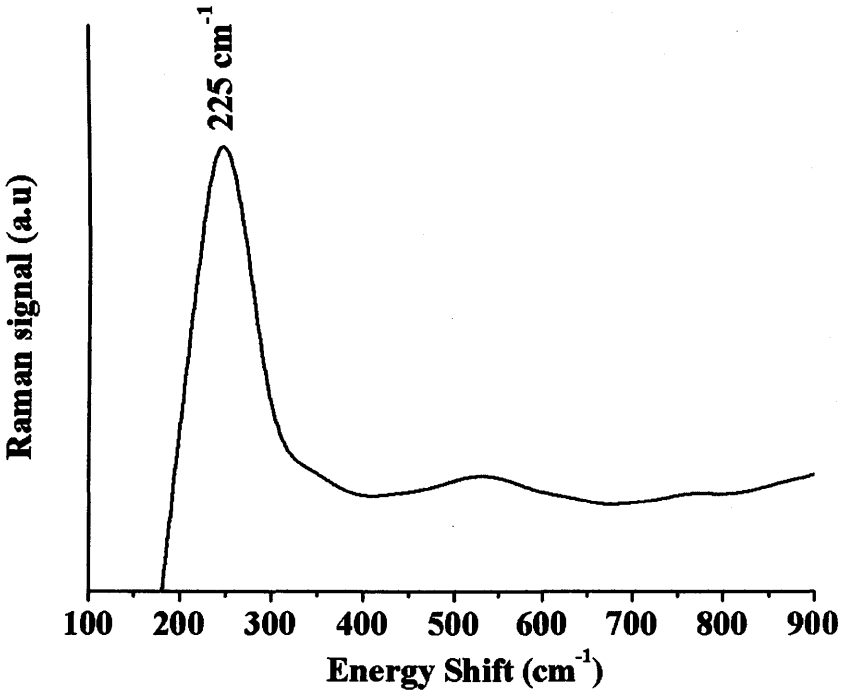

Figure 6.8 Raman pattern obtained for $Cr_2Se_{0.40}O_{2.60}$ nanoparticles.

6.2.1.8 Thermogravimetric Analysis

The thermogravimetric analysis (TGA) of the particles formed from the gas phase reaction of CrO_2Cl_2 and Et_2Se confirmed the results obtained by WDX. The TGA of the $Cr_2Se_{0.7}O_{2.3}$ particles (Figure 6.9) showed a gradual increase of the weight (+24 %) between 60 °C and 420 °C, in which $Cr_2Se_{0.7}O_{2.3}$ oxidized to give $Cr_2(SeO_4)_{0.7}O_{2.3}$. The weight loss (-8 %) observed from 420 °C to 550 °C correspond to the decomposition of $Cr_2(SeO_4)_{0.7}O_{2.3}$ in Cr_2O_3 and SeO_2 by losing O_2. The second weight loss measured as 36 % corresponds to the sublimation of all selenium in the form of SeO_2.[42] The same reaction are observed to occur during the TGA of the $Cr_2Se_{2.15}O_{0.85}$ particles (Figure 6.10). The $Cr_2Se_{2.15}O_{0.85}$ particles gradually oxidized to form $Cr_2(SeO_4)_{2.15}O_{0.85}$, corresponding to a mass gain of 46 %. The particles then decomposed to Cr_2O_3 and SeO_2 at 405 °C. The loss of O_2 resulted in a weight loss of 11 %, and the sublimation of SeO_2 in total mass loss of 82 %.

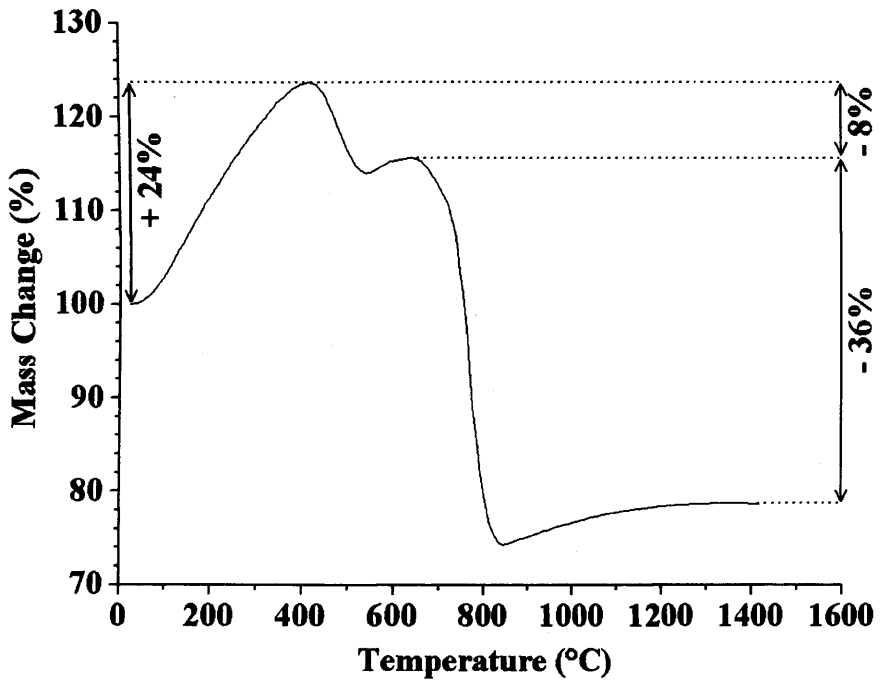

Figure 6.9 Thermogravimetric analysis of the $Cr_2Se_{0.70}O_{2.30}$ particles.

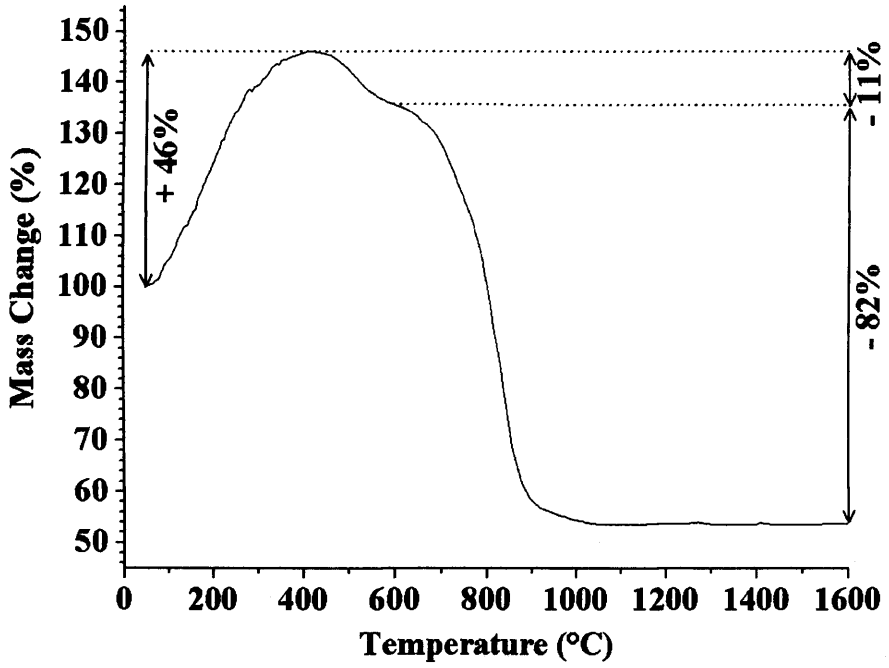

Figure 6.10 Thermogravimetric analysis of the $Cr_2Se_{2.15}O_{0.85}$ particles.

The product of the decomposition of the particles, which had the characteristic colour of Cr_2O_3, was confirm to be Cr_2O_3 by XRD and Raman (Figure 6.11).

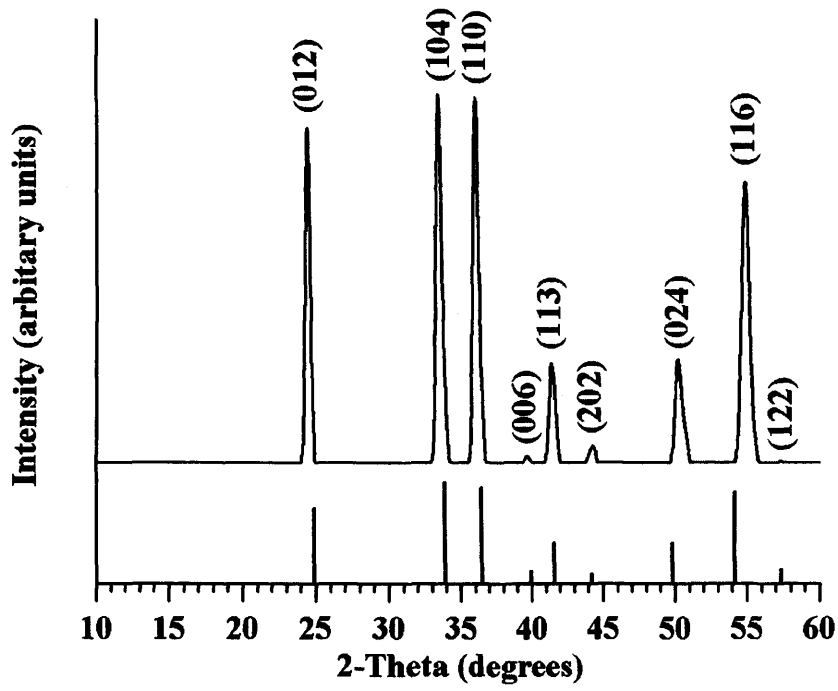

Figure 6.11 XRD pattern of the powder obtained after the TGA of the $Cr_2Se_{0.70}O_{2.30}$ particles in air. Literature stick pattern for Cr_2O_3 powder (JCPDS File No. 006–0504) is shown.

6.2.1.9 SQUID

The dc magnetic susceptibility (χ) as a function of temperature (Figure 6.12) was measured for different x in $Cr_2Se_xO_{3-x}$ particles formed from the gas phase reaction of CrO_2Cl_2 and Et_2Se. All the powders from the range of composition $Cr_2Se_{0.3}O_{2.7}$ to $Cr_2Se_{2.15}O_{0.85}$ showed a peak below 50 K. The large particle size (100 nm) precludes the possibility of this being due to a superparamagnetic blocking transition,[43] and the substitution of oxygen with selenium is unlikely to generate any frustrated magnetic states. We therefore attribute the peak to an antiferromagnetic ordering temperature transition. The shape of the curves was similar to the one obtain for pure Cr_2Se_3.[12] However the Néel temperature measured for all the powders produced was found to be lower than the one reported for Cr_2Se_3 (ca. T_N = 43 K), and much lower than that of Cr_2O_3 (T_N = 307 K). These results suggest that the new materials have somewhat different magnetic properties compared to their parent compounds.

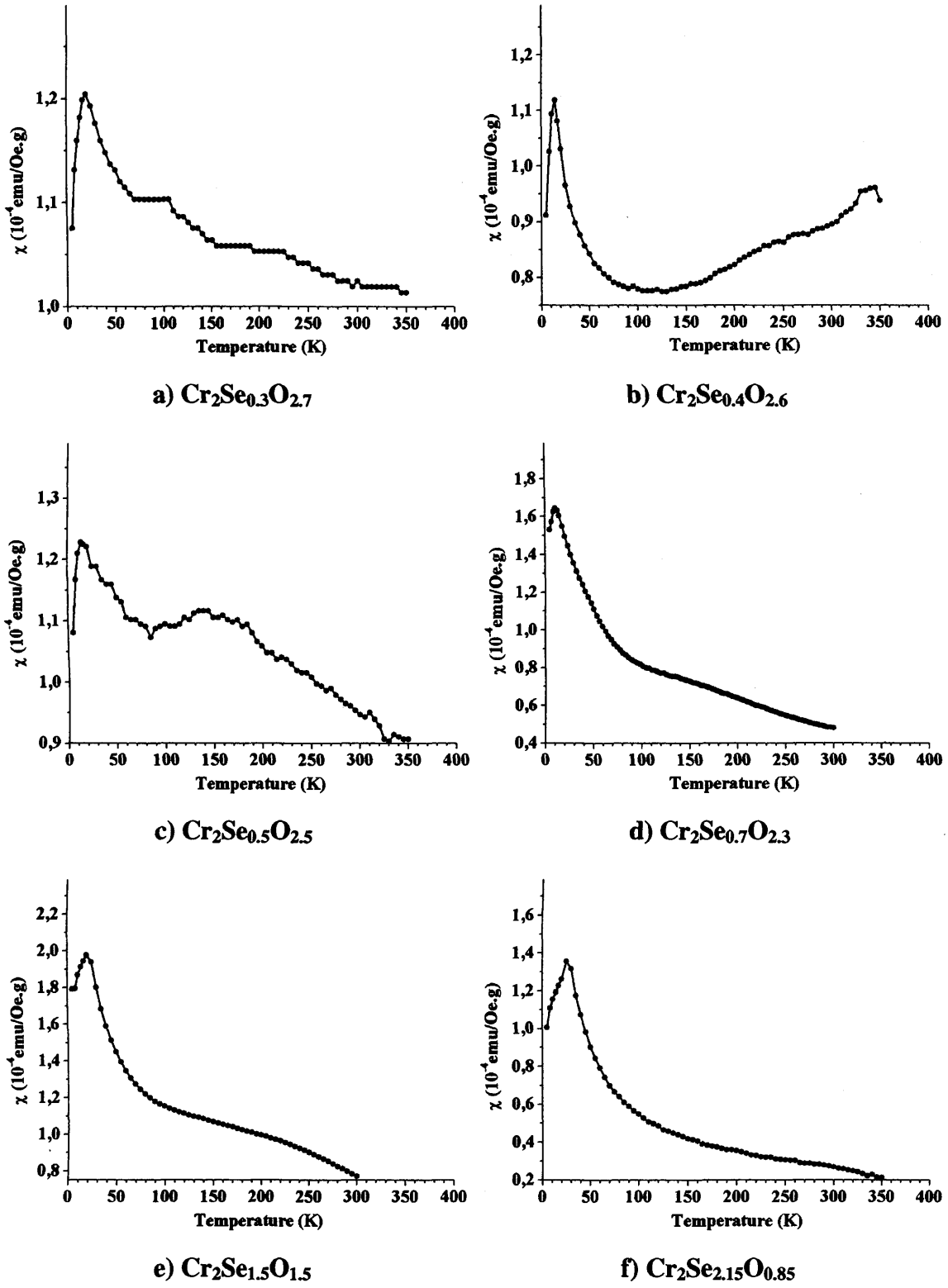

Figure 6.12 DC magnetic susceptibility in a measurement field of 10 Oe as a function of temperature for different x in $Cr_2Se_xO_{3-x}$.

In the chromium oxyselenide powders containing the lowest amount of selenium (ca. 0.3 to 0.5), a series of humps can be observed between 50 K and 350 K. This could

indicate the presence of a small amount of one or several secondary phases such as chromium monoselenide. $Cr_{1-x}Se$ with x between 0 and 0.17 are known to form a series of NiAs-type structured compounds with a Néel temperature varying from 280 K to 83 K.[44] As observed by spot-WDX analysis previously, the chromium oxyselenide powders reported in this thesis containing the lowest amount of selenium showed disparity in the stoichiometry of the particles from a unique APCVD run. This heterogeneity in stoichiometry could confirm the formation of a small amount of one or several secondary phases.

All the $Cr_2Se_xO_{3-x}$ powders produced from the gas phase reaction of CrO_2Cl_2 and Et_2Se showed an antiferromagnetic ordering with a Néel temperature varying with the selenium percentage in the particles (Figure 6.13). The Néel temperature was observed to vary from 20 K for $Cr_2Se_{0.3}O_{2.7}$, through a minimum of 11 K for $Cr_2Se_{0.7}O_{2.3}$, to 25 K for $Cr_2Se_{2.15}O_{0.85}$.

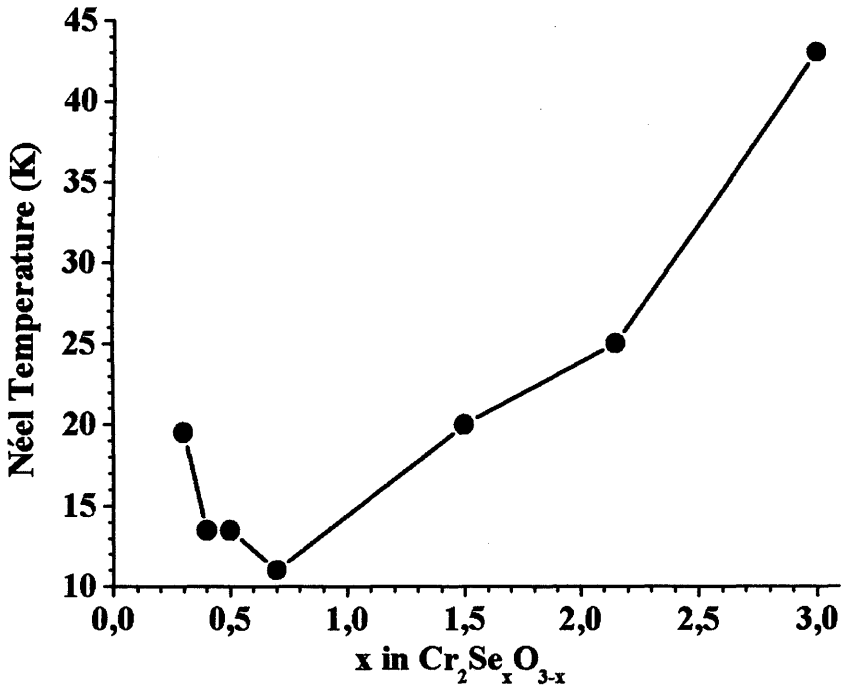

Figure 6.13 Néel temperature for different x in $Cr_2Se_xO_{3-x}$.

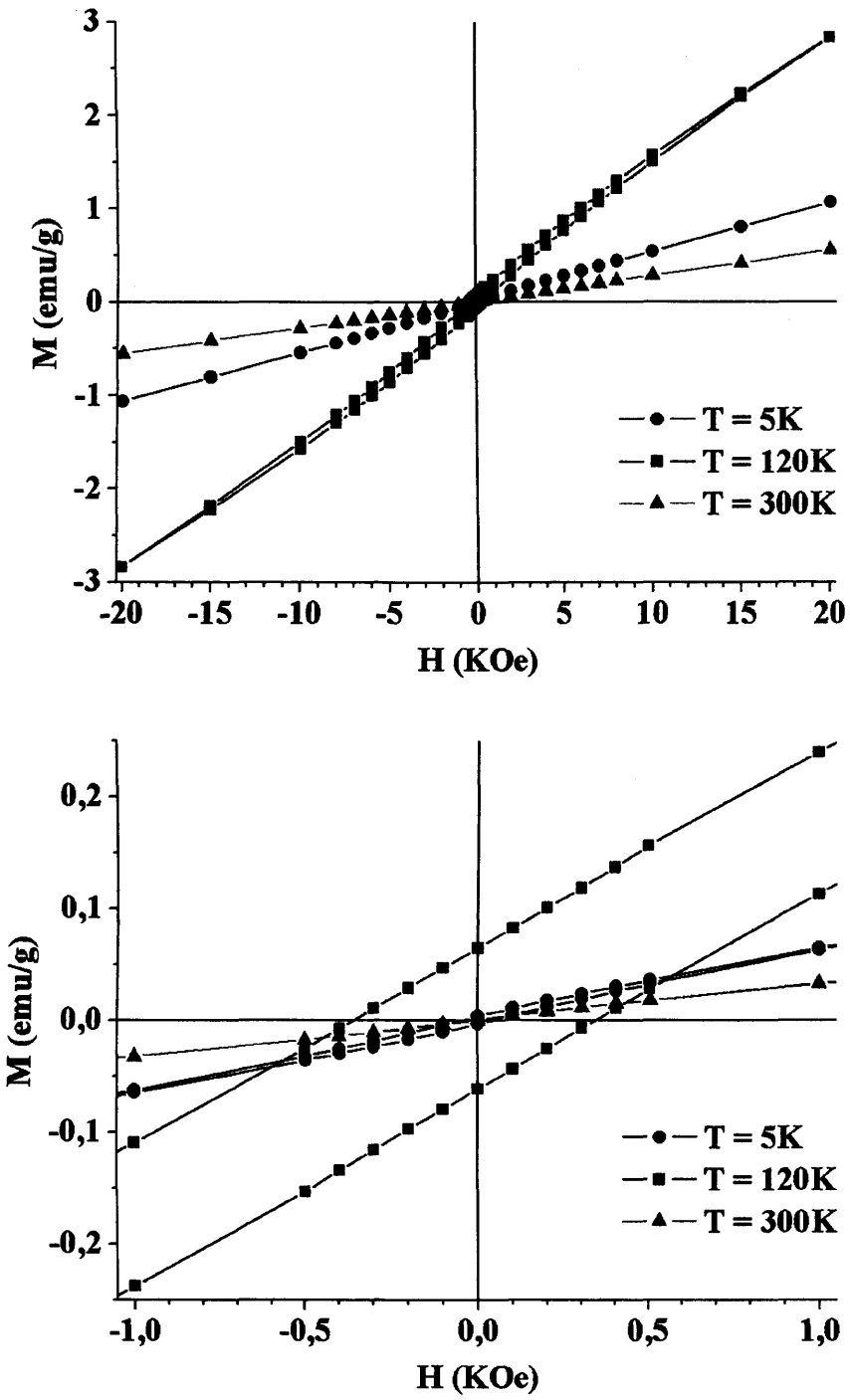

Figure 6.14 Hysteresis loops measured at T = 5, 120 and 300 K for different x in $Cr_2Se_{0.7}O_{2.3}$. A detail of the low field magnetisation is shown below.

The variation of magnetization of the $Cr_2Se_{0.7}O_{2.3}$ nanoparticles with magnetic field H data shows a symmetrical hysteresis loop with a coercive field of 360 Oe and a remanence of 0.064 emu/g at 5 K, whereas the coercivity and remanence at 120 and 300 K are negligible (Figure 3.14). This indicates that the $Cr_2Se_{0.7}O_{2.3}$ nanoparticles exhibit weak ferromagnetism below the Néel temperature. This ferromagnetic behaviour of

antiferromagnetic nanoparticles has been described by Néel and can be explained by the non-compensation of the two magnetic sublattices at the surface of the nanoparticles.[45,46] Perfectly antiferromagnetic nanoparticles do not exist and as the particle size is reduced, a net magnetic moment is observed due to the imbalance of spins 'up' and 'down' at the surface. No superparamagnetism was considered to be present due to the particles size (above 25 nm).

6.2.2 Discussion

The characterization data are all consistent with the formation of a hitherto unknown solid solution of $Cr_2Se_{3-x}O_x$ rather than the formation of two intimately mixed phases of Cr_2O_3 and Cr_2Se_3. The SEM analysis of either the $Cr_2Se_{3-x}O_x$ films or powders produced from the APCVD or gas phase reaction of CrO_2Cl_2 and Et_2Se showed a single type of morphology. Spherical and agglomerated particles were observed rather than two types of crystallite. The WDX and EDX analysis showed that the films had a stoichiometry between Cr_2O_3 and $Cr_2Se_{0.2}O_{2.8}$, while the powders had a stoichiometry varying from $Cr_2Se_{0.3}O_{2.7}$ to $Cr_2Se_{2.15}O_{0.85}$. The films and powders, except the powders with an overall stoichiometry varying from $Cr_2Se_{0.3}O_{2.7}$ to $Cr_2Se_{0.5}O_{2.3}$, were homogeneous to spot analysis with the same elemental formulation across the surface. The X-ray diffraction patterns showed a single-phase material for all the $Cr_2Se_{3-x}O_x$ films or powders produced. All the films produced had the hexagonal Cr_2O_3 structure, while the powders crystallise with the rhombohedral Cr_2Se_3 structure. Cr_2O_3 is known to be crystalline when prepared by CVD at 400 °C and adopt an adhesive film with angular crystallites.[30,47,48] Moreover, reaction of Et_2Se and CrO_2Cl_2 at deposition temperatures from 450 - 600 °C produced a crystalline green chromium oxide films. It was only at 600 °C and above that a chromium oxyselenide phase formed- by gas phase nucleation that "snowed" onto the surface to form a poorly adherent film that could be readily collected. The XPS analysis for the chromium oxyselenide showed only a single chromium environment rather than two well separated peaks for the oxide and selenide, furthermore the quantification of the element abundances matched the WDX analysis. The thermal gravimetric analysis results also correlate well with the elemental formula. The Raman pattern does not show any chromium oxide (corundum) in the powder but is consistent with a layered metal-selenide type structure. Furthermore the magnetic properties of the new material are

unlike either Cr_2Se_3 or Cr_2O_3, which although both are antiferromagnets have Néel temperatures of 43 and 307 K respectively. Hence there is strong evidence for the formation of a new chromium oxyselenide phase.

6.3 Selenisation of Chromium Oxide Films

The selenisation of APCVD prepared chromium oxide (Cr_2O_3) thin films using diethylselenide (Et_2Se) as a selenium source and N_2 as a carrier gas was studied. Et_2Se has been already successfully used in a selenisation process to prepare $CuInSe_2$ and $CuInGaSe_2$ thin films.[49,50] Et_2Se, which is a less-hazardous selenium source than H_2Se, has been reported to have a higher decomposition rate than H_2Se gas or elemental selenium vapour.[51]

6.3.1.1 Films and Powders formed from CrO_2Cl_2 and Et_2Se : Reaction Conditions

The chromia film precursors were prepared by APCVD using chromyl chloride at 500 °C. The Cr_2O_3 APCVD films produced had a shine green appearance and were all found to be crystalline. They showed the distinctive XRD and Raman pattern of Cr_2O_3. Thickness of the film precursors was approximately 1 μm. The films were selenised using pyrolytically decomposed Et_2Se for 10 min in a quartz tube reactor at atmospheric pressure. The selenisation temperature, Et_2Se bubbler and N_2 carrier gas flow rate were 650 °C, 80 °C and 2 $L.min^{-1}$, respectively. These conditions correspond to a Et_2Se flow of 30 $mmol.min^{-1}$.

6.3.1.2 Appearance, Substrate Coverage and Adherence of the Films

The films produced from the selenisation of Cr_2O_3 films became partly grey silver, while some other parts stayed green and unchanged. They passed the Scotch tape test, and were hardly scratched and remove from the substrate with a steel scalpel. The films formed were air stable and water stable, insoluble in common organic solvents but were quickly decomposed in dilute nitric acid and bleach.

6.3.1.3 X-ray Diffraction

X-ray diffraction of the grey silver films produced after being heated in a stream of Et_2Se at 650 °C compare well with the reported pattern for rhombohedral Cr_2Se_3 (JCPDS File No. 040-1403). No secondary phase (Cr_2O_3) was observed, indicating the total selenisation of Cr_2O_3 (Figure 6.15). XRD of the films prepared with shorter selenisation times showed the distinctive patterns for hexagonal Cr_2O_3 (JCPDS File No. 006–0504) and for rhombohedral Cr_2Se_3 (JCPDS File No. 040-1403), indicating only a partial selenisation of Cr_2O_3. The evaluated lattice parameters of both phases in the composite films produced (Cr_2O_3 a = 4.929 Å, c = 13.634 Å, and Cr_2Se_3 a = 6.255 Å, c = 17.299 Å) were in good agreement with the reported ones for hexagonal Cr_2O_3 a = 4.939 Å, c = 13.627 Å, and rhombohedral Cr_2Se_3 a = 6.250 Å, c = 17.280 Å. No evidence of an other phase was observed in XRD.

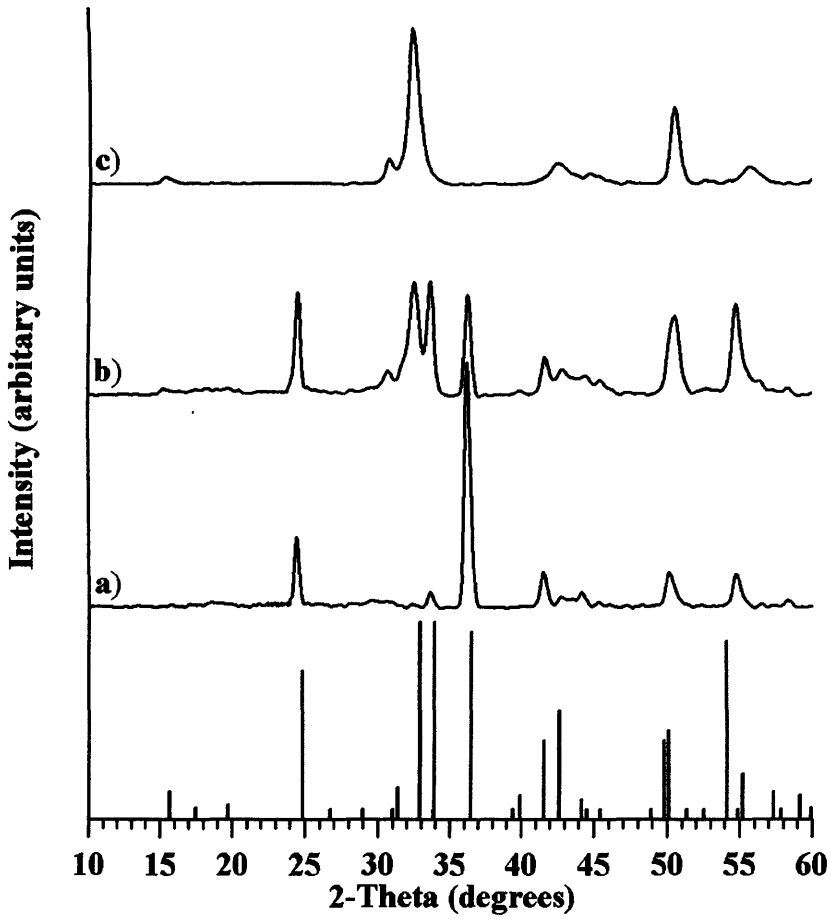

Figure 6.15 XRD pattern obtained for the films obtained before the selenisation process (a), after a 5 minutes selenisation at 650 °C (b), after a 10 minutes selenisation at 650 °C (c).

6.3.1.4 Raman Microscopy

Raman spectroscopy of the films obtained after a 5 minute selenisation showed the Cr_2O_3 Raman pattern reported in the literature with peaks at 307, 350, 524, 551 and 610 cm^{-1}. The presence of two additional broad peaks at 207 and 250 cm^{-1} was also observed (Figure 6.16). By using a lower laser intensity during the Raman analysis, which consequently was not going deeper in the film, it was possible to determine that the upper layers of the film was the source of these two additional peaks. The Raman analysis of the films obtained after a 10 minute selenisation process showed three bands at 172, 214 and 241 cm^{-1} (Figure 6.17). None of the Cr_2O_3 bands were observed.

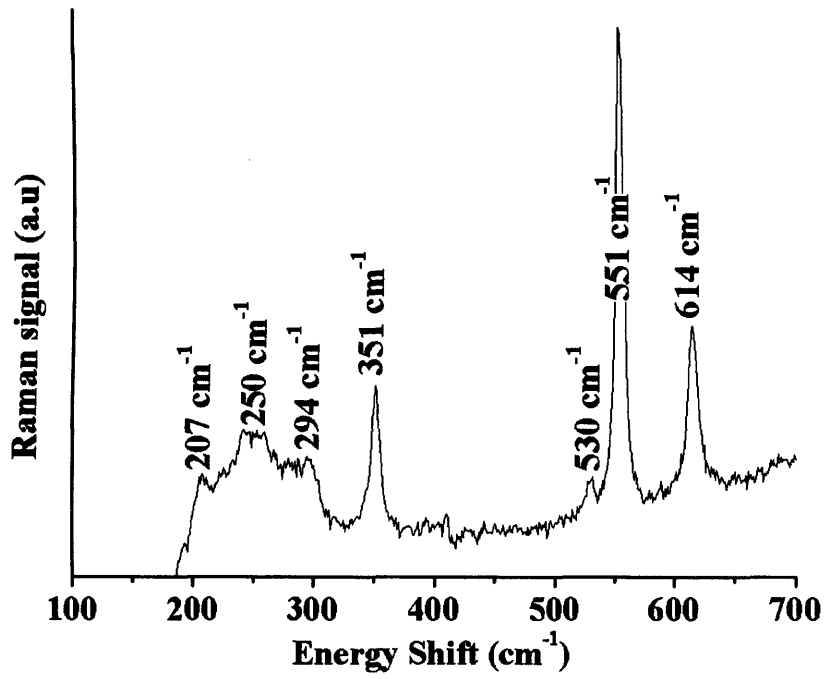

Figure 6.16 Raman pattern of the films obtained after a 5 minutes selenisation at 650 °C in a Et_2Se flow of 30 $mmol.min^{-1}$.

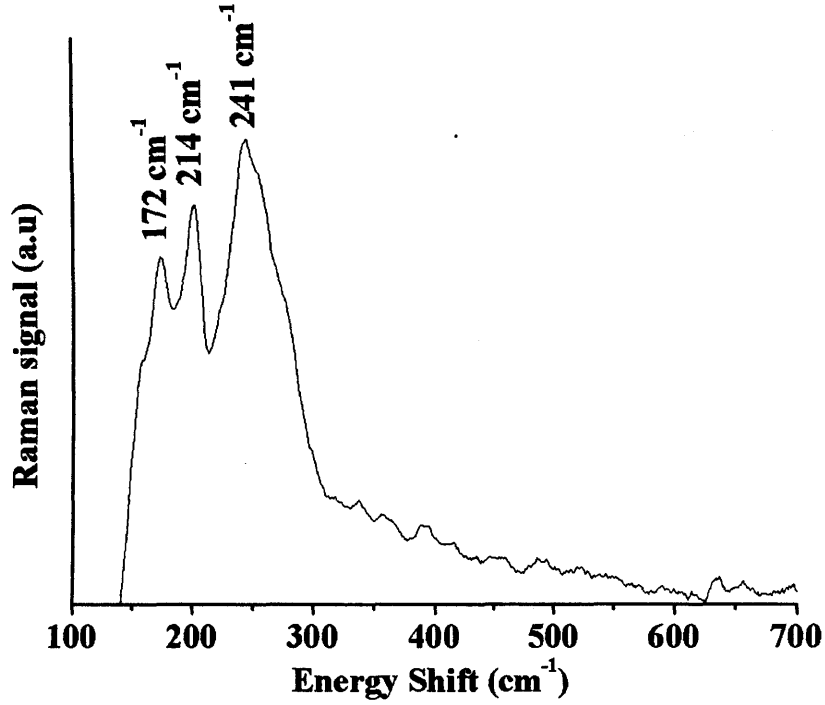

Figure 6.17 Raman pattern of the films obtained after a 10 minutes selenisation at 650 °C in a Et_2Se flow of 30 mmol.min^{-1}.

6.3.2 Discussion

The selenisation of Cr_2O_3 precursors using Et_2Se as a selenium source led to the formation of Cr_2Se_3 thin films. The films produced had a grey silver appearance and were adherent to the substrate. XRD and Raman analysis show that pure Cr_2Se_3 films were formed during the selenisation process.

6.4 Conclusion

The characterization of the films and powders formed from the APCVD or gas phase reaction of CrO_2Cl_2 and Et_2Se confirm the formation of an unknown solid solution of $Cr_2Se_{3-x}O_x$ rather than the formation of two intimately mixed phases of Cr_2O_3 and Cr_2Se_3. $Cr_2Se_{3-x}O_x$ adopts the hexagonal Cr_2O_3 structure for a stoichiometry between Cr_2O_3 and $Cr_2Se_{0.2}O_{2.8}$, and the rhombohedral Cr_2Se_3 structure for a stoichiometry varying from $Cr_2Se_{0.3}O_{2.7}$ to $Cr_2Se_{2.15}O_{0.85}$. Magnetic studies showed that all the $Cr_2Se_{3-x}O_x$ compounds formed with the rhombohedral Cr_2Se_3 structure had an antiferromagnetic ordering with a Néel temperatures lower than the expected one for

Cr_2Se_3 (ca. 43 K). Despite the formation of the new solid solution $Cr_2Se_{3-x}O_x$ over the range Cr_2O_3 to $Cr_2Se_{2.15}O_{0.85}$, the APCVD reaction of CrO_2Cl_2 and Et_2Se didn't allow the growth or formation of pure Cr_2Se_3 even for extremely high Et_2Se to CrO_2Cl_2 gas phase ratio. However, the selenisation of APCVD prepared Cr_2O_3 thin films using Et_2Se as selenium source led to the formation of adherent Cr_2Se_3 thin films.

6.5 References

[1] S. S. Batsanov, L. M. Doronina, N. V. Podberezskaya, *Zh. Struk. Khim.*, **1964**, *154*, 624.

[2] S. S. Batsanov, L. M. Doronina, *Ser. Khim.*, **1968**, *9*, 2155.

[3] V. N. Ikorskii, S. S. Batsanov, *Neorg. Mater.*, **1972**, *8*, 1858.

[4] L. M. Doronina, V. S. Filatkina, S. S. Batsanov, *Neorg. Mater.*, **1967**, *3*, 1696.

[5] V. N. Ikorskii, L. M. Doronina, S. S. Batsanov, *Zh. Struk. Khim.*, **1968**, *9*, 143.

[6] S. S. Batsanov, L. M. Doronina, *Neorg. Mater.*, **1966**, *2*, 491.

[7] V. N. Ikorskii, *Neorg. Mater.*, **1973**, *9*, 938.

[8] M. Yuzuri, T. Yusuki, *J. Magn. Magn. Mater.*, **1986**, *54*, 923.

[9] Y. Adachi, M. Yuzuri, T. Kaneko, S. Abe, *J. Magn. Magn. Mater.*, **1990**, *90*, 153.

[10] M. Yuzuri, Y. Adachi, T. Kaneko, H. Yoshida, S. Abe, *J. Magn. Magn Mater.*, **1995**, *140*, 151.

[11] M. Yuzuri, K. Segi, *Phys. B+C: Phys. Condens. Matt. + Atom., Mol. Plasma Phys.*, **1977**, 86, 891.

[12] S. Ohta, Y. Narui, Y. Sakayori, *J. Magn. Magn. Mater.*, **1997**, 170, 168.

[13] H. Fonzes-Diacon, *Compt. Rend.*, **1900**, *130* 1025.

[14] H. Fonzes-Diacon, *Compt. Rend.*, **1900**, *131*, 556.

[15] K. H. Schmidt, A. Mueller, *Spectrochim. Acta, Part A*, **1972**, *28*, 1829.

[16] K. S. Lee, Y. U. Kwon, *J. Kor. Chem. Soc.*, **1996**, *40*, 379.

[17] V. V. Tien, N. H. Dung, *Compt. Rend.*, **1981**, *293*, 933.

[18] S. Barnier, C. Julien, *Mater. Res. Bull.*, **1995**, *30*, 225.

[19] W. J. Desisto, P. R. Broussard, T. F. Ambrose, B. E. Nadgorny, M. S. Osofsky, *Appl. Phys. Lett.*, **2000**, *76*, 3789.

[20] Y. N. Cho, W. J. Desisto, *Chem. Vap. Dep.*, **2003**, *9*, 121.

[21] G. A. Shaw, I. P. Parkin, D. E. Williams, *J. Mater. Chem.*, **2003**, *13*, 2957.

[22] P. Merenda, N. Sol, *J. Cryst. Growth*, **1977**, *40*, 195.

[23] A. M. E. Hardy, Ph.D thesis, **2002**, University of London.

[24] A. F. Mota, A. J. Silvestre, P. M. Sousa, O. Conde, M. A. Rosa, M. Godinho, *Condens. Matter*, **2006**, *1*, 6.

[25] P. M. Sousa, A. J. Silvestre, N. Popovici, O. Conde, *Condens. Matter*, **2006**, *1*, 17.

[26] F. Maury, D. Oquab, R. Morancho, J. Nowak, J. Gauthier, *Proc. of the Tenth Int. Conf. on Chem. Vap. Dep.*, **1987**, 1213.

[27] H. Chbihi, *Mater. Manuf. Processes*, **1991**, *6*, 469.

[28] G. Carta, M. Natali, G. Rossetto, P. Zanella, G. Salmaso, S. Restello, V. Rigato, S. Kaciulis, A. Mezzi, *Chem. Vap. Dep.*, **2005**, *11*, 375.

[29] A. Anguelouch, A. Gupta,G. Xiao, D. W. Abraham, Y. Ji, S. Ingvarsson, C. L. Chien, *Phys. Rev. B: Condens. Matt. and Mater. Phys.*, **2001**, *64*, 180408/1.

[30] I. P. Parkin, M. N. Field, *J. Phys. IV: Proc. of the Twelfth Eur. Conf. on Chem. Vap. Dep.*, **1999**, *1*, 387.

[31] W. J. DeSisto, P. R. Broussard, T. F. Ambrose, B. E. Nadgorny, M. S. Osofsky, *Appl. Phys. Let.*, **2000**, *76*, 3789.

[32] Y-N Cho, W. J. DeSisto, *Chem. Vap. Dep.*, **2003**, *9*, 121.

[33] T. R. McGuire, E. J. Scott, F. H. Grannis, *Phys. Rev.*, **1956**, *102*, 1000.

[34] Y. Adachi, M. Yuzuri, T. Kaneko, S. Abe, H. Yoshida, *J. Phys. Soc. Jpn.*, **1994**, *63*, 369.

[35] E. Agostinelli, C. Battistoni, D. Fiorani, G. Mattogno, M. Nogues, *J. Phys. Chem. Solids*, **1989**, *50*, 269.

[36] C. D. Wagner, in *Pratical Surface Analysis Second Edition*, Vol. 1 (Eds: D.Briggs, M.P.Seah), WILEY, Salle-Sauerlander, **1990**, 606.

[37] I. Ikemoto, K. Ishii, S. Kinoshita, H. Kuroda, M. A. A. Franco, J. M. J. Thomas, *Solid State Chem.*, **1976**, *17*, 425.

[38] S. Chevalier, G. Bonnet, J. P. Larpin, *Appl. Surf. Sci.*, **2000**, *167*, 125.

[39] J. Mougin, T. LeBihan, G. Lucazeau, *J. Phys. Chem. Solids*, **2001**, *62*, 553.

[40] M. N Iliev, A. P. Litvinchuk, H. G. Lee, C. W. Chu, A. Barry, J. M. D. Coey, *Phys. Stat. Sol.*, **1999**, *215*, 643.

[41] J. E. Maslar, W. S. Hurst, T. A. Vanderrah, I. Levin, *J. Raman Spectrosc.*, **2001**, *32*, 201.

[42] S. M. Grigorovich, A. V. Novoselova, Y. M. Ukrainskii, *Neorg. Mater.*, **1975**, *11*, 2125.

[43] L. Néel, *Compt. Rend.*, **1961**, *252*, 4075.

[44] M. Kanichi, K. Tahahiko, *J. Sci., Ser. A-II*, **1965**,*28*, 47.

[45] L. Néel, *J. Phys. Soc. Jpn.*, **1962**, *17*, 676.

[46] L. Néel, *Low Temp. Phys.*, **1962**, *1961*, 411.

[47] A. Anguelouch, A. Gupta, G. Xiao, G. X. Miao, D. W. Abraham, S. Ingvarsson, Y. Ji, C. L. Chien, *J. Appl. Phys.*, **2002**, *10*, 7140.

[48] W. J. DeSisto, P. R. Broussard, T. F. Ambrose, B. E. Nadgorny, M. S. Osofsky, *Appl. Phys. Let.*, **2000**, *76*, 3789.

[49] T. Yamamoto, M. Nakamura, J. Ishizuki, T. Deguchi, S. Ando, H. Nakanishi, S. F. Chichibu, *J. Phys. Chem. Solids*, **2003**, *64*, 1855.

[50] M. Sugiyama, F. B. Dejene, A. Kinoshita, M. Fukaya, Y. Maru, T. Nakagawa, H. Nakanishi, V. Alberts, S. F. Chichibu, *J. Cryst. Growth*, **2006**, *294*, 214.

[51] S. F. Chichibu, M. Sugiyama, M. Obasmi, A. Hayakawa, T. Mizutani, H. Nakanishi, T. Negami, T. Wada, *J. Cryst. Growth*, **2002**, *243*, 404.

Chapter 7
Conclusions

In this final chapter, the results of all reactions carried out in this thesis are summarised and discussed.

7.1 APCVD of Group IV and V Selenides

7.1.1 Titanium Diselenide Films

Titanium diselenide thin films have been deposited by the APCVD reaction of $TiCl_4$ and Et_2Se_2 or $^tBu_2Se$ over a range of temperatures (Table 7.1). The APCVD reaction of $TiCl_4$ and Et_2Se_2 or $^tBu_2Se$ led to the formation of films composed of plate-like crystallites orientated parallel to the substrate. The films from either precursor gave the same XRD and Raman patterns identified as the 1T-$TiSe_2$ patterns. No change was observed in the Raman and XRD spectra of the films produced from $^tBu_2Se$, indicating that the films are relatively air stable. However, the Raman spectra of the films produced from Et_2Se_2 revealed the formation of TiO_2. The stoichiometry of the film deposited below 550 °C from either precursors was close to the one expected for $TiSe_2$. However, at substrate temperature above 550 °C the films produced were all found to be substoichiometric with an overall stoichiometry varying from $TiSe_{1.6}$ to $TiSe_{1.5}$. The use of Ph_2Se_2 with $TiCl_4$ was proved to be unsuccessful and did not deposit any films. The results identified $^tBu_2Se$ as a better precursor for the deposition of $TiSe_2$ thin films as it gave films with a better stoichiometry and quality.

Table 7.1 Summary of the APCVD reactions of $TiCl_4$ and selenide precursors.

Titanium Precursor	Selenium Precursor	Deposition temperature	Product
$TiCl_4$	Et_2Se_2	450 – 550 °C	1T-$TiSe_2$
$TiCl_4$	Et_2Se_2	550 – 600 °C	Selenium deficient $TiSe_2$
$TiCl_4$	$^tBu_2Se$	250 – 500 °C	1T-$TiSe_2$
$TiCl_4$	$^tBu_2Se$	550 – 600 °C	Selenium deficient $TiSe_2$
$TiCl_4$	Ph_2Se_2	200 – 650 °C	No film deposited

7.1.2 Vanadium Diselenide Films

The APCVD reaction of VCl_4, $VOCl_3$ or $[V(NMe_2)_4]$ and $^tBu_2Se$ was investigated over a range of temperatures (Table 7.2). The results show that the vanadium precursor used has a significant effect on the stoichiometry and quality of the films produced. Vanadium tetrachloride and vanadium oxychloride were found to be unsuitable precursors for the CVD of VSe_2 thin films. The use of VCl_4 did not deposit a thin film, while $VOCl_3$ led to vanadium rich films with significant contamination by chlorine and the co-formation of a vanadium oxide. Vanadium tetrakisdimethylamide was found to be a better precursor for the APCVD of vanadium selenide thin films. The films produced from $[V(NMe_2)_4]$ and $^tBu_2Se$ were composed of plate-like crystallites that were orientated parallel to the substrate. EDAX analysis showed a vanadium to selenium ratio close to 1 : 2. XPS, XRD and Raman analysis were also consistent with the formation of VSe_2. APCVD reaction of $[V(NMe_2)_4]$ and $^tBu_2Se$ provides a convenient route to vanadium diselenide films.

Table 7.2 Summary of the APCVD reactions of vanadium precursors with $^{t}Bu_2Se$.

Vanadium Precursor	Selenium Precursor	Deposition temperature	Product
VCl_4	$^{t}Bu_2Se$	250 – 650 °C	No film deposited
$VOCl_3$	$^{t}Bu_2Se$	250 – 650 °C	$VSe_xO_yCl_z$
$[V(NMe_2)_4]$	$^{t}Bu_2Se$	300 – 500 °C	1T-VSe_2

7.1.3 Niobium Selenide Films

The results show that the APCVD reaction of $NbCl_5$ and $^{t}Bu_2Se$ was a suitable route to the formation of niobium diselenide thin films when deposited above 550 °C. The films produced were composed of plate-like crystallites orientated perpendicular to the substrate. XPS, XRD and Raman analysis were consistent with the formation of 2H-$NbSe_2$. Below substrate temperatures of 550 °C, the films grown were all superstoichiometric, with a Nb to Se ratio between 1 : 2.4 and 1 : 2.6.

Table 7.3 Summary of the APCVD reactions of $NbCl_5$ with $^{t}Bu_2Se$.

Niobium Precursor	Selenium Precursor	Deposition temperature	Product
$NbCl_5$	$^{t}Bu_2Se$	300 – 550 °C	Selenium rich $NbSe_2$
$NbCl_5$	$^{t}Bu_2Se$	550 – 650 °C	2H-$NbSe_2$

7.2 APCVD of Group VI Selenides

7.2.1 Molybdenum Diselenide Films

Molybdenum diselenide films were deposited on glass from the APCVD reaction of $MoCl_5$ and Et_2Se or $^{t}Bu_2Se$ (Table 1.4). Above 600 °C, $MoSe_2$ thin films free of contamination were deposited from either of the selenium precursors. XPS, XRD and Raman analyses confirmed the formation of a mixture of the two polytypes 2H- & 3R-$MoSe_2$. The films produced from Et_2Se and $MoCl_5$ showed a needlelike

morphology. The needles were orientated perpendicular to the substrate and are made up of a series of clusters. While the films grown from $MoCl_5$ and $^tBu_2Se$ have a 'crazy-paving' type morphology. EDAX showed that the selenide precursor used has a significant effect on the quality of the $MoSe_2$ films formed. When ditertiarybutylselenide was used as a precursor, the stoichiometry of the films formed was found to dramatically vary along the substrate. The diethylselenide proved to be a more effective precursor for making molybdenum diselenide films. Films grown in this system gave a more uniform and complete coverage of the substrate.

Table 7.4 Summary of the APCVD reactions of $MoCl_5$ and selenium precursors.

Molybdenum Precursor	**Selenium Precursor**	**Deposition temperature**	**Product**
$MoCl_5$	$^tBu_2Se$	450 – 550 °C	$MoSe_xCl_y$
$MoCl_5$	$^tBu_2Se$	600 – 650 °C	2H- & 3R-$MoSe_2$
$MoCl_5$	Et_2Se	500 – 600 °C	$MoSe_xCl_y$
$MoCl_5$	Et_2Se	650 °C	2H- & 3R-$MoSe_2$

7.2.2 Tungsten Diselenide Films

Tungsten diselenide films have been deposited on glass substrate from the APCVD reaction of WCl_6 and Et_2Se. All the films produced, irrespective of the deposition temperature, were highly hydrophobic with values in the range 135 – 145°. Despite of the highly hydrophobic character of the films, tilting experiments show that the water droplets cling to the surface of the film. This sticky hydrophobicity of the films was linked to the morphology of the films. The fact that these can be made by CVD opens up many possibilities for patterned substrates, simply by using a masking technique.

Table 7.5 Summary of the APCVD reactions of WCl_6 and Et_2Se.

Tungsten Precursor	Selenium Precursor	Deposition temperature	Product
WCl_6	Et_2Se	500 – 650 °C	2H-WSe_2

7.3 APCVD of Tin Selenides

Tin monoselenide and tin diselenide films were deposited on glass from the APCVD reaction of and $SnCl_4$ and Et_2Se. The results show that the morphology and stoichiometry of films formed from the APCVD reaction of $SnCl_4$ with Et_2Se were strongly depend of the substrate's position and flow rates conditions used. By modification of the deposition conditions, pure SnSe, mixed SnSe - $SnSe_2$ phases or pure $SnSe_2$ thin films were produced. The CVD route developed here to $SnSe_2$ and SnSe is compatible with photovoltaic device manufacture, as such the high absorbtivity of these films could prove useful as a solar absorbtion element in a photovoltaic stack.

Table 7.6 Summary of the APCVD reactions of $SnCl_4$ and Et_2Se.

Tin Precursor	Selenium Precursor	Deposition temperature	Product
$SnCl_4$	Et_2Se	400 – 650 °C	SnSe or Mixed SnSe - $SnSe_2$ or $SnSe_2$

7.4 APCVD and Chemical Vapor Synthesis of Chromium Oxyselenides

The APCVD reaction of CrO_2Cl_2 and Et_2Se above 600 °C led to the formation of an unknown solid solution of $Cr_2Se_{3-x}O_x$. $Cr_2Se_{3-x}O_x$ adopts the hexagonal Cr_2O_3 for a stoichiometry between Cr_2O_3 and $Cr_2Se_{0.2}O_{2.8}$, and the rhombohedral Cr_2Se_3 structure for a stoichiometry varying from $Cr_2Se_{0.3}O_{2.7}$ to $Cr_2Se_{2.15}O_{0.85}$. Magnetic study showed that all the $Cr_2Se_{3-x}O_x$ compounds formed with the rhombohedral Cr_2Se_3 structure had

an antiferromagnetic ordering with a Néel temperatures lower than the expected one for Cr_2Se_3 (ca. 43 K). Despite the formation of the new solid solution $Cr_2Se_{3-x}O_x$ over the range Cr_2O_3 to $Cr_2Se_{2.15}O_{0.85}$, the APCVD reaction of CrO_2Cl_2 and Et_2Se didn't allow the growth or formation of pure Cr_2Se_3 even for extremely high Et_2Se to CrO_2Cl_2 gas phase ratio.

Table 7.7 Summary of the APCVD reactions of CrO_2Cl_2 with Et_2Se.

Chromium Precursor	Selenium Precursor	Deposition temperature	Product
CrO_2Cl_2	Et_2Se	400 – 550 °C	Cr_2O_3
CrO_2Cl_2	Et_2Se	600 – 650 °C	$Cr_2Se_{3-x}O_x$

7.5 Conclusion

The APCVD reactions of $^tBu_2Se$ with $TiCl_4$, $VOCl_3$, $[V(NMe_2)_4]$ or $NbCl_5$, respectively led to the deposition of titanium selenide, vanadium selenide and niobium selenide thin films at temperatures as low as 250 °C. The films produced showed good uniformity in composition along the substrate for all the deposition temperatures investigated. Molybdenum selenide films were also produced from the reaction of $^tBu_2Se$ with $MoCl_5$. However depositions were only noted at temperatures in excess of 450 °C. EDAX analysis of the films deposited at 600 °C showed that films with the expected stoichiometry for $MoSe_2$ were deposited on the leading edge of the substrate. However the last few centimetres of these films were found to be substoichiometric (ca. $MoSe_{1.3}$ and $MoSe_{1.4}$). These changes in the selenium concentration along the substrate are attributed to the fast depletion of the selenium precursor over time within the reactor. The $^tBu_2Se$, which starts to decompose at 150 °C, is rapidly depleted compare to $MoCl_5$ which require high deposition temperatures. This leads to a non uniformity of the stoichiometry of the films along the substrate. The use of Et_2Se was investigated as it was considered and confirmed to be a more appropriate selenium precursor with metal chloride precursors requiring higher deposition temperatures. The $MoSe_2$ thin films produced at 600 °C from Et_2Se and $MoCl_5$ showed a good uniformity in composition along the length of the substrate and across their width. The APCVD reaction of Et_2Se

with WCl_6 or $SnCl_4$ allowed to produce tungsten diselenide, tin monoselenide and diselenide films with a good uniformity.

APCVD provides a convenient route to $TiSe_2$, VSe_2, $NbSe_2$, $MoSe_2$, WSe_2, SnSe and $SnSe_2$ thin films. The films produced and described in this thesis belongs to the family of layered metal dichalcogenides (MX_2; M = Ti, V, Nb, Mo, W, Sn), except the tin monoselenide films as tin selenide has two stable oxidation state. The structure of the MX_2 compounds consists of two-dimensional covalently bound layers of the type X-M-X, which are bound to each other by weak van der Waals interactions leading to a stacking sequence X-M-X-□-X-M-X with highly anisotropic properties. The layered structure of these materials was clearly observed in most of the films produced. The $TiSe_2$, VSe_2, $NbSe_2$, WSe_2 and $SnSe_2$ thin films were composed of plate-like crystallites. The plates grown in ab-plane and were orientated perpendicularly to the substrate.

The new ternary phase $Cr_2Se_{3-x}O_x$ was synthesised by gas phase precipitation and chemical vapour deposition. Primarily used to prepare ultra fine powder, the gas phase precipitation of particles occurs when the temperature and supersaturation of reactive gas are sufficiently high. The gas phase reaction of CrO_2Cl_2 with Et_2Se above 600 °C led to the formation of stable fine particles for a gas phase ratio Et_2Se : CrO_2Cl_2 greater than 1.35 : 1 (14.7 $mmol.min^{-1}$: 10.9 $mmol.min^{-1}$). The particles formed, which were then deposited onto the heated substrate, had a stoichiometry varying from $Cr_2Se_{0.3}O_{2.7}$ to $Cr_2Se_{2.15}O_{0.85}$. For a Et_2Se to CrO_2Cl_2 ratio lower than 1 : 1, films with a stoichiometry between Cr_2O_3 and $Cr_2Se_{0.2}O_{2.8}$ were deposited on the glass substrate. $Cr_2Se_{3-x}O_x$ adopts the hexagonal Cr_2O_3 structure for a stoichiometry between Cr_2O_3 and $Cr_2Se_{0.2}O_{2.8}$, and the rhombohedral Cr_2Se_3 structure for a stoichiometry varying from $Cr_2Se_{0.3}O_{2.7}$ to Cr_2Se_3. Magnetic studies showed that all the $Cr_2Se_{3-x}O_x$ compounds formed with the rhombohedral Cr_2Se_3 structure had an antiferromagnetic ordering with a Néel temperatures lower than the expected one for Cr_2Se_3 (ca. 43 K). The gas phase precipitation and chemical vapour deposition of CrO_2Cl_2 and Et_2Se is the only route to $Cr_2Se_{3-x}O_x$.

List of Publications

N. D. Boscher, C. J. Carmalt, R. G. Palgrave, I. P. Parkin, Atmospheric pressure chemical vapour deposition of SnSe and $SnSe_2$ thin films on glass, Accepted for publication in *Thin Solid Films*, **2007**.

N. D. Boscher, C. J. Carmalt, A. Garcia Prieto, Q. A. Pankhurst, R. G. Palgrave, I. P. Parkin, Synthesis and characterisation of chromium oxyselenide ($Cr_2Se_{0.7}O_{2.3}$) formed from chemical vapour synthesis: a new antiferromagnet, *European Journal of Inorganic Chemistry*, **2007**, (29), 4579-4582.

N. D. Boscher, C. S. Blackman, C. J. Carmalt, I. P. Parkin, A. Garcia Prieto, Atmospheric pressure chemical vapour deposition of vanadium diselenide thin films, *Applied Surface Science*, **2007**, 253(14), 6041-6046.

A. Mills, M. Crow, J. Wang, I. P. Parkin, N. Boscher, Photocatalytic Oxidation of Deposited Sulfur and Gaseous Sulfur Dioxide by TiO_2 Films, *Journal of Physical Chemistry C*, **2007**, 111(14), 5520-5525.

N. D. Boscher, C. J. Carmalt, R. G. Palgrave, J. J. Gil-Tomas, I. P. Parkin, Atmospheric pressure CVD of molybdenum diselenide films on glass, *Chemical Vapor Deposition*, **2006**, 12(11), 692-698.

N. D. Boscher, C. J. Carmalt, I. P. Parkin, Atmospheric pressure chemical vapor deposition of $NbSe_2$ thin films on glass, *European Journal of Inorganic Chemistry*, **2006**, (6), 1255-1259.

N. D. Boscher, C. J. Carmalt, I. P. Parkin, Atmospheric pressure CVD of $TiSe_2$ thin films on glass, *Chemical Vapor Deposition*, **2006**, 12(1), 54-58.

N. D. Boscher, C. J. Carmalt, I. P. Parkin, Atmospheric pressure chemical vapor deposition of WSe_2 thin films on glass-highly hydrophobic sticky surfaces, *Journal of Materials Chemistry*, **2006**, 16(1), 122-127.